UNIVERSITIY OF RIJEKA
FACULTY OF CIVIL ENGINEERING

Natalija Bede

NUMERICAL AND EXPERIMENTAL STUDY OF CONCRETE FRACTURE UNDER DYNAMIC LOADING

DOCTORAL THESIS

Rijeka, 2015

UNIVERSITIY OF RIJEKA
FACULTY OF CIVIL ENGINEERING

Natalija Bede

NUMERICAL AND EXPERIMENTAL STUDY OF CONCRETE FRACTURE UNDER DYNAMIC LOADING

DOCTORAL THESIS

Supervisor: prof. dr. sc. Joško Ožbolt

Rijeka, 2015

Mentor rada: prof. dr. sc. Joško Ožbolt

Doktorski rad obranjen je dana 30. travnja 2015 na Građevinskom fakultetu Sveučilišta u Rijeci, pred povjerenstvom u sastavu:

1. Prof. dr. sc. Ivica Kožar, Sveučilište u Rijeci, Građevinski fakultet, predsjednik povjerenstva

2. Prof. dr. sc. Joško Krolo, Sveučilište u Zagrebu, Građevinski fakultet, vanjski član

3. Doc. dr. sc. Vanja Travaš, Sveučilište u Rijeci, Građevinski fakultet, član

ACKNOWLEDGEMENTS

I would like to thank my advisor, Prof. Joško Ožbolt, for offering me the opportunity to carry out this interesting research under his supervision. His support, expert guidance and insightful comments made my thesis work possible.

I would also like to thank to Uwe Mayer (MPA Stuttgart) for helping me with experimental part of my PhD thesis and his valuable suggestions. Also thanks to student Saurabh Patel and Katrin Allmendinger (MPA Stuttgart) for all their kind help and assistance with the experiments.

I am very grateful to my friends and colleagues at the University of Stuttgart for their friendship and support. Special thanks go to Josipa Bošnjak, Marina Stipetić and Filip Oršanić for providing a place to work in as well as for their good humor making the work more enjoyable. I truly appreciate their unconditional help, valuable advices and friendship. Josipa has been actively interested in my work and has always been available to advise me. I thank her for generously sharing her broad knowledge and for being patient with my questions. It has been pleasure to work with Baris Irhan very much. I appreciate his guidance in using research code CIF and numerical modeling. I enjoyed working with Akanshu Sharma who has enthusiastically shared his deep knowledge, experience or meaningful advices. I have enjoyed many useful and entertaining discussions with Daniela Ruta and Emiliano Sola during our lunch breaks.

I am grateful too for the support and advice from my dear faculty colleagues at the University of Rijeka. Special thanks to Vanja Travaš for the valuable suggestions and fun conversations. I appreciate his patience on listening to me endlessly talk about my research. An extra thank you to Ivona Gudac. Your supportive friendship and positive outlook mean a lot to me.

It has been a wonderful experience working with all of you!

My deepest gratitude goes to my parents, my sister and my friends for their faith, encouragement and unconditional support. Branko, Marina and Sandra thank you for everything.

Rijeka, April 2015 Natalija Bede

In loving memory of my father

“We don't remember days, we remember moments.”

Cesare Pavese

ABSTRACT

The behaviour of concrete structures is known to be strongly influenced by the loading rate. However, the knowledge with regards to the response of concrete subjected to dynamic loading is still incomplete. Numerical and experimental studies show that with increase of loading rate there is increase of resistance, change of failure mode, crack pattern and crack propagation velocity, while the influence of the loading (strain) rate on the tensile strength and fracture energy of concrete is not yet fully understood. Therefore, it is one of the major subjects of intensive investigation in the scientific community over many years.

The research reported in this thesis is aimed to better understand dynamic fracture behaviour of concrete and the phenomenon of progressive increase of tensile strength and fracture energy, experimentally observed at high loading rates. Both experimental and numerical approaches have been employed in order to achieve the same. The experimental investigation performed on L-specimens subjected to dynamic loading has confirmed that loading rate plays significant role in the crack propagation direction of such concrete structures. For quasi-static load, the crack tends to propagate horizontally, perpendicular to the loading direction, while with increase of the loading rate the crack propagation tends to get vertical, parallel to the loading direction. A second aim of this study is to examine the validity of explicit 3D FE code for predicting the complex phenomena related to dynamic fracture of concrete according to the results of the experimental investigations. To this end, experiments on L-shaped concrete specimens under different loading rates are numerically simulated. Additionally, to clarify the correct evaluation procedure for tensile strength and fracture energy under dynamic loading, the experiments reported in literature on dynamically impacted notched concrete beams are also numerically investigated.

The comparison between the results of experiments and numerical analyses show that presented relatively simple modeling approach based on continuum mechanics, rate dependent microplane model and standard finite elements is capable to realistically predict the performance of concrete under dynamic loading including the complex phenomena related to high loading rates such as rate dependent resistance, rate dependent failure mode, crack branching and crack velocity. Finally, it is found that progressive increase in dynamic strength and fracture energy is controlled mainly by inertial effect and it should be interpreted

as structural rather than a material property. Therefore, experimental data on dynamic fracture of concrete has to be taken with caution.

Key words: concrete fracture, dynamic load, rate sensitivity, experiments, finite elements, microplane model, failure mode, crack branching, crack velocity, tensile strength, fracture energy

SAŽETAK

Poznato je da ponašanje betonskih konstrukcija uvelike ovisi o brzini nanošenja opterećenja. Međutim, poznavanje ponašanja betona uslijed dinamičkog opterećenja i dalje je nepotpuno. Numeričke i eksperimentalne studije pokazuju da s porastom brzine opterećenja dolazi do porasta nosivosti, promjene moda sloma, promjene distribucije pukotina i brzine širenja pukotine, dok način utjecaja brzine opterećenja (deformiranja) na vlačnu čvrstoću i energiju sloma betona još uvijek nije u potpunosti razjašnjen. Prema tome, utjecaj brzine opterećenja na vlačnu čvrstoću i energiju sloma betona je jedna od glavnih tema intenzivnog istraživanja unutar akademske zajednice dugi niz godina.

U ovom radu istražuje se slom betona uslijed dinamičkog opterećenja te pojava progresivnog rasta vlačne čvrstoće i energije sloma nakon određene brzine opterećenja dobivena na temelju evaluacije eksperimentalnih podataka. U tu svrhu koristi se i eksperimentalni i numerički pristup. Eksperimentalno istraživanje provedeno na betonskim uzorcima L-oblika izloženim različitim brzinama opterećenja potvrdilo je da brzina nanošenja opterećenja znatno utječe na smjer širenja pukotine. Za kvazi-statičko opterećenje smjer širenja pukotine je horizontalan, odnosno okomit na smjer nanošenja opterećenja, dok povećanjem brzine opterećenja smjer širenja pukotine postaje vertikalan, odnosno paralelan sa smjerom nanošenja opterećenja. Drugi cilj ovog rada je verificirati računalni program temeljen na metodi konačnih elemenata za predviđanje ponašanja betona uslijed dinamičkog opterećenja i tome svojstvenih pojava na osnovu rezultata eksperimentalnog istraživanja. U tu svrhu, provedeni eksperimenti na L-uzorcima pri različitim brzinama opterećenja su numerički simulirani. Nadalje, kako bi se razjasnio točan postupak određivanja vlačne čvrstoće i energije sloma pri dinamičkom opterećenju, modelirana je slobodno oslonjena betonska greda sa zarezom izložena udarnom opterećenju čekića, a rezultati numeričke analize uspoređeni s rezultatima mjerenja dostupnim u literaturi.

Usporedbom dobivenih numeričkih rezultata s dostupnim eksperimentalnim rezultatima potvrđeno je da korišteni numerički model, temeljen na mehanici kontinuuma, mikroravninskom modelu materijala i metodi konačnih elemenata, realistično opisuje ponašanje betona uslijed dinamičkog opterećenja uključujući i složene pojave svojstvene velikim brzinama opterećenja kao što su promjena nosivosti, promjena moda sloma, pojava račvanja pukotine i promjena brzine širenja pukotine. Na temelju dobivenih rezultata dolazi se

do zaključka da je progresivni porast dinamičke vlačne čvrstoće i energije sloma, uočen kod velikih brzina opterećenja, posljedica utjecaja inercije, te se treba tumačiti kao strukturalni efekt a ne kao materijalno svojstvo betona. Prema tome, rezultate mjerenja treba procjenjivati s posebnim oprezom.

Ključne riječi: slom betona, dinamičko opterećenje, brzina opterećenja, eksperimenti, metoda konačnih elemenata, mikroravninski model, mod sloma, račvanje pukotine, brzina širenja pukotine, vlačna čvrstoća, energija sloma

CONTENTS

1. INTRODUCTION

1.1 Motivation and problem description

Concrete is the most widely used construction material worldwide due to its good strength and durability. The economy, efficiency, strength and stiffness of concrete make it an attractive material in civil as well as military engineering structures. Dynamic strengths and fracture energy of concrete are usually required in design and modeling of these structures while they are frequently exposed to dynamic loads, e.g. impact, blast loading, explosion, earthquake etc.

The behaviour of concrete structures under dynamic loading, specifically their response under high rates of loading, e.g. impact loads, has been the subject of intensive investigation for many years. In concrete structures, the behaviour under dynamic loads is complex due to significant sensitivity of concrete to strain (loading) rate. Based on reviews of experimental, analytical and numerical studies in this thesis it is shown that understanding on dynamic concrete behaviour is inconsistent. In the scientific community the influence of strain rate on the tensile strength and fracture energy is still under discussion. Up to date there is neither a standardized test nor any universally accepted procedure for measuring fracture energy and resistance under dynamic loading. The main reason that such procedure is not available comes from technical limitations in obtaining the experimental data under dynamic loading. Consequently, theoretical interpretation of the strain rate effects on concrete tensile strength and fracture energy has been lacking. While the idea of influence of loading rate on tensile strength and fracture energy of concrete is not a new one, it requires new understanding. It is generally argued on the fundamental cause of progressive increase of dynamic strength and fracture energy under high loading rates. Therefore, in order to enhance understanding of the dynamic fracture of concrete, the question that naturally arises is should the observed dynamic increase factor of tensile strength and fracture energy of concrete be attributed as inherent material property (i.e. it can be attributed to only the strain rate effect) or rather to structural effect due to inertia?

Due to the extensive use of concrete, experimental test data for concrete is quite abundant. Principally, experiments show that apparent strength and fracture energy increase with increase of strain rate and that for strain rates larger than approximately 10/s both increase progressively with increase of strain rate. Therefore, it has been generally accepted that there is an apparent increase of the dynamic strength and fracture energy when concrete is subjected to high strain (loading) rates. In addition, considering results from a large amount of experimental data under different loading rates, the dynamic increase factor of concrete strength and fracture energy is analytically determined and explicitly accounted for as a part of the various different constitutive laws used in standard computational codes. It should be noted that, in such way, structural response depends on the used constitutive model. However, such material models are capable of giving correct prediction on structural resistance and load carrying capacity, namely apparent strength, while realistic information on change in failure mode and crack pattern of a structure and/or its structural elements cannot be captured with tensor based material models.

Various experimental tests have been used to explore a wide range of strain rates (loading rates), but difficulties remain with the measurement of the data at higher rates. Moreover, due to the complexity arising from the composite nature of the concrete material, behaviour of concrete structures under dynamic loading is very difficult to understand from experiments alone. In order to overcome the limitations of experimental test, numerical methods can be helpful. Even though numerically the problem can be solved relatively easily it is essential that proposed numerical model is able to capture the dynamic behaviour realistically. The main advantage of numerical modeling is that the influence of individual parameters can be studied separately and in more detail. This provides better understanding of the relevant properties, e.g. tensile strength and fracture energy, and influence of inertia on the same. Therefore, numerical analysis has become increasingly important in understanding concrete behaviour under dynamic loading.

Numerical modeling of concrete fracture under dynamic loading, especially phenomena of crack branching or change of failure mode, is still a challenging topic for researchers. The finite element (FE) method is nowadays the most frequently used numerical method in engineering problems. In the numerical modeling, which can be of smeared or discrete type, different constitutive laws and modeling techniques are used (Rabczuk and Belytschko 2004, Ožbolt et al. 2006, Larcher 2009, Pedersen 2010). Therefore, notable effort has been made on

the study of concrete fracture under dynamic loading. However, to better understand dynamic fracture of concrete it is important to employ realistic constitutive models. For a model to be realistic, it should be able to correctly account for the interaction between inertia effect and constitutive law, and it should realistically capture phenomena such as crack branching or change of failure mode due to the increase of loading rate. Such FE model is able to predict concrete behaviour under a wide range of loading rates for a variety of different loading rates. In contrary to microplane model or discrete models, standard macroscopic plasticity or damage based models seem not to be able to predict phenomena such as crack branching without additional energy criteria. Therefore, such models cannot automatically account for the progressive increase of resistance, what means that the progressive increase must be a part of the constitutive law. The explicit definition enforces correct prediction of resistance, however, the failure mode and crack pattern will principally be incorrect. The change in failure mode and crack pattern plays an important role in the accurate prediction of dynamic response of concrete structures. Hence, one of the objectives of the work is to investigate the applicability of used computational approach based on rate dependent microplane material model for dynamic fracture of concrete.

1.2 Context of research

In the past few decades there has been a growing interest among the various researchers to understand the response of concrete structures subjected to dynamic loading (impact). Under dynamic loading, the response of structures is governed by three different effects (Ožbolt and Sharma 2012): (1) the rate dependency of the growing micro-cracks (influence of inertia at the micro-crack level), (2) the viscous behaviour of the bulk material between the cracks (creep of concrete or viscosity due to the water content) and (3) the influence of inertia, which can significantly change the state of stresses and strains of the material. For quasi-brittle materials, such as concrete, the first two effects are important for relatively low and medium strain rates. For higher strain rates (impact) the last effect dominates (Ožbolt and Sharma 2012), however, the rate dependency cannot be neglected.

This work has two main aims. First, it seeks to investigate the quasi-static and dynamic fracture properties of concrete by combining the experiments and the FE analyses. The second aim is to investigate whether recently developed explicit 3D FE code CIF (Irhan 2014) is able to realistically predict complex phenomena related to dynamic fracture of concrete. Quasi-

static analysis is carried out using 3D FE code MASA, verified by numerous exiperiments (Ožbolt et al. 2001b). Complete study of dynamic fracture behaviour of concrete is given through analysis of L-shaped specimen under high loading rate and notched beam under impact load.

The L-shaped specimen has become a popular benchmark test for the validation of numerical models for cracking of concrete under static loading. At the same time, no such test under dynamic loading conditions can be found in the literature. For that reason, it may be interesting to perform dynamic load test. Hence, the present research brings out not only numerical results for complete static and dynamic behaviour of L-shaped concrete specimen, but also experimental results as well. In order to provide experimental data, dynamic tests on L-shaped concrete specimens under different loading rates are performed at the University of Stuttgart. Based on the experimental investigation a better understanding of the concrete behaviour under dynamic loading is realized. Special attention is devoted to the loading rate dependent failure mode. Namely, it has been recently shown numerically (Ožbolt and Sharma 2012) that with increasing loading rate failure mode changes. Subsequently, evaluated experimental results are compared with numerical predictions and final conclusions are drawn out.

Although it is well known that tensile strength and fracture energy of concrete depend on strain rate, no clear consensus exists within the research community on the correct method to evaluate the fracture energy and tensile strength under dynamic loading. In drop hammer impact tests done by Zhang et al. (2009, 2010a), the evolution of dynamic fracture energy is based on the standard three-point bending test of notched beam, i.e. evaluated from the area under the reaction force-displacement curve, recommended for evaluating fracture energy from tests performed under quasi-static loading condition. Accordingly, such procedure may be very inaccurate for dynamic loading, since at high loading rates the structural inertial forces significantly contributes to reaction forces. However, to gain more insight into the problem the experiments on above mentioned dynamically impacted notched concrete beams, performed by Zhang et al. (2009, 2010a), are numerically reproduced. Therefore, to understand the correct evaluation procedure for fracture energy under dynamic loading, numerical results are evaluated, compared with experimental results and discussed in detail. Similar exercise is also performed for tensile strength. Moreover, to demonstrate the influence of inertia, rate sensitive static and dynamic analysis is carried out. Additionally, effect of

impact velocity on peak deflection, peak load, strain rate and crack velocity is determined and compared with experimental results given in Zhang et al. (2009, 2010a).

Once the results of numerical analysis are obtained to be in agreement with the results from the literature (Zhang et al. 2009, 2010a) and own experiments a broader range of parametric investigations can be accomplished. The various studies under impact loading conditions including influence of contact surface are not available in literature. Hence, it is interesting to carry out such studies. In this work, for the investigation of the influence of contact surface, response and behaviour of notched plane concrete beams loaded by impact hammer for different impact velocities, from low (order of 10^{-7} m/s) to very high (order of 10 m/s), are numerically studied. Since the contact surface of the hammer is significant for the impact problem, the influence of the contact geometry is discussed. Different shape of the striking head of the hammer produces different failure modes and crack patterns in concrete beams. The resistance of the concrete changes according to the impactor shape. In order to model impact of stiff object (hammer) with a structure (plain concrete beam), multi body finite element dynamic analysis is performed. The results of parametric study are compared in terms of several aspects including the effect of impact velocity on failure mode, crack pattern, tensile strength and fracture energy.

To resume, the failure modes, impact forces, reaction forces, crack velocities, crack mouth opening displacement (CMOD), strain rates, true and apparent tensile strength and true and apparent fracture energy of concrete under dynamic loading are discussed in the scope of the present thesis. Based on the results evaluated from experiment and numerical analysis the main conclusions are drawn.

1.3 Objectives

The main objective is to investigate dynamic fracture of concrete. The research objectives of this investigation can be summarized as follows:

1. Numerically and experimentally investigate the structural inertia effect and rate sensitivity under high loading rates (impact).

2. Verify the validity of the used 3D FE code (named Contact Impact and Fragmentation - CIF) for dynamic analysis of concrete.

3. Perform experimental investigation on the dynamic fracture of L-shaped concrete specimen to verify the numerical predictions.

4. Based on the conducted experimental and numerical investigations identify the reasons for the progressive increase of concrete tensile strength and fracture energy.

5. Perform numerical parametric study to investigate the effect of the impactor tip geometry on dynamically impacted notched plain concrete beams.

6. Improve knowledge on the dynamic fracture of concrete.

1.4 Hypothesis

For correct estimation of the true rate dependent material properties, such as tensile strength and fracture energy, inertia have to be filtered out; otherwise, for higher strain rates the material properties are significantly overestimated.

1.5 Scope and overview

The present study comprises experimental investigations and numerical modeling of concrete to better understand concrete fracture under dynamic loading. Finite element analysis provides a powerful tool that, in combination with experiments, can lead to a better understanding of the dynamic fracture of concrete. Therefore, the numerical study is conducted to investigate whether the numerical model is able to reproduce the test results correctly and, if so, to enhance understanding on the behaviour of dynamic fracture of concrete under high loading rates. In return, the test results of the experimental study provide valuable data for the verification of finite element models and for future interpretation of numerical results for dynamic fracture of concrete.

Chapter 2 presents literature relevant to dynamic fracture of concrete. The limitations and advantages or disadvantages of available test setups are discussed. A detailed summary of the

published research on tensile strength and fracture energy of concrete under different loading rates follows.

Chapter 3 presents the experimental investigation of L-shaped concrete specimens under different loading rates, with emphasis on the loading rate dependent crack propagation, crack branching and crack velocity. The details of the test specimens, test setup, instrumentation, test results and observations are described. Similarly, detail overview of the experimental analysis conducted by Zhang et al. (2009, 2010a) is given. The main objective of this experimental analysis was to study the effect of high loading (strain) rates on the material properties of the concrete on the notched beam specimens under three point bending.

Chapter 4 provides an overview of FE modeling concepts using 3D FE code MASA (static analysis) and 3D FE code CIF (dynamic analysis). Only important features of explicit 3D FE code are given, followed by brief description of the microplane material model used for concrete.

In Chapter 5 validation of finite element code follows. Results of the 3D nonlinear FE analyses of L-shaped specimens under different loading rates are reported and compared with evaluated experimental results. The comparison is done in terms of load-displacement curve, failure pattern and crack velocity. Also, experiments on dynamically impacted notched concrete beams are numerically obtained. Test results and observations are summarized and compared to numerical results in terms of crack patterns, failure modes, loads, deflections and strains. Additionally, the effect of loading rate on tensile strength and fracture energy is numerically studied.

After comparison of numerical model against experimental data, Chapter 6 addresses numerical parametric study. The objective of the parametric study is to evaluate the influence of the impactor contact geometry on fracture behaviour of dynamically impacted notched concrete beam for wide range of loading rates.

Chapter 7 provides concluding remarks of numerical and experimental investigations and suggestions for further research.

2. CONCRETE UNDER DYNAMIC LOADING

2.1 Rate dependency of concrete

Concrete is becoming increasingly used in structural applications exposed to dynamic loads. Hence, there is strong demand for a better understanding of the concrete under high loading rates. Correspondingly, the mechanical properties at high strain rates are of increasing importance in these applications.

Concrete inherently falls under the category of quasi-brittle materials characterized with significant nonlinearity in the pre-peak region and strain softening in post-peak region (see Figure 1a). For concrete like materials, the inelastic zone around a crack tip is termed as fracture process zone (FPZ) and dominated by complicated mechanism, such as microcracking, crack deflection, bridging, crack branching, and so on (Yu et al. 2010) (Figure 1b). Fracture energy and tensile strength are two material properties that describe the response of material inside the FPZ at macro-level. Size of the FPZ is assumed to be a material property. For example, for concrete its width tends to be about three maximum aggregate sizes (Bažant and Oh 1983). However, the mechanisms of deformation in FPZ region under dynamic loading are not clearly understood.

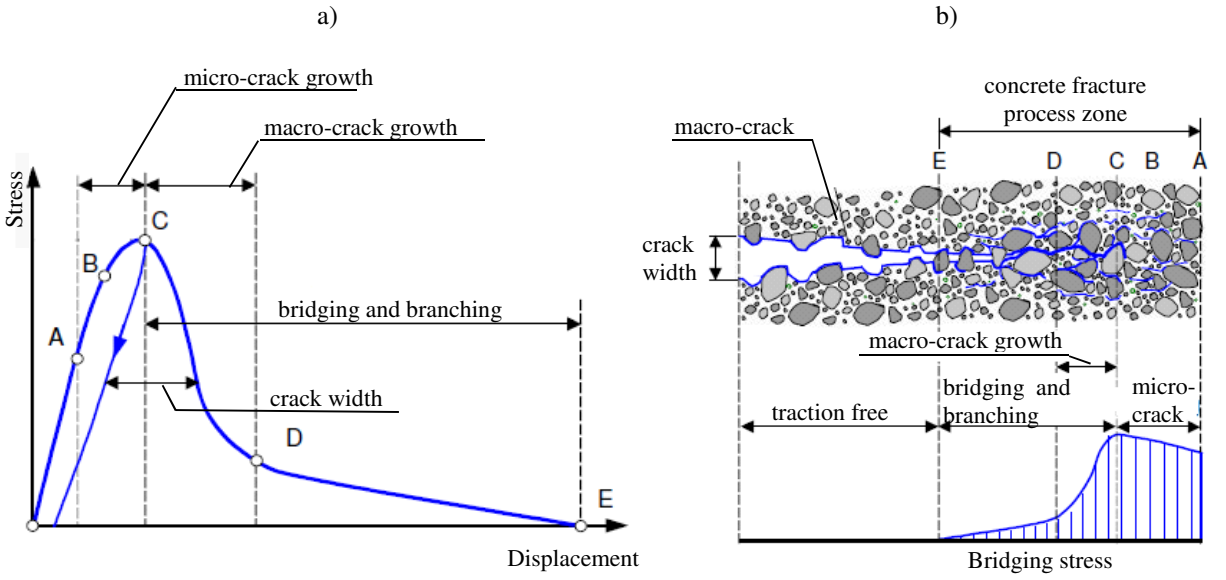

Figure 1. *a) Typical load-displacement response of a quasi-brittle material in tension and b) FPZ (Löfgren 2005).*

The response of structural components made of such quasi-brittle materials is known to be significantly influenced by the rate of loading through three different effects, see Reinhardt 1982, Weerheijm 1992, Bischoff and Perry 1995, Ožbolt and Reinhardt 2002, Ožbolt and Reinhardt 2005, Pedersen et al. 2006, Larcher 2009, Pedersen 2010 and fib 2010:

(1) through the viscous behaviour of the bulk material between the cracks (creep of concrete or viscosity due to the water content),
(2) through the rate dependency or rate sensitivity of the growing micro-cracks (influence of inertia at the micro-crack level) and
(3) through the influence of inertia effects, which can significantly change the state of stresses and strains of the material.

Depending on the type of material and loading rate, the first, second or third effect may dominate. For quasi-brittle materials like concrete, which exhibit cracking and damage phenomena, the first effect is important for relatively low loading rates (creep-fracture interaction). However, the last two effects dominate for higher loading rates (impact loading). Thus, under high loading rate (impact), two different mechanisms influence the structural behavior. First is the strain rate influence on strength, stiffness and ductility, and second, the inertia effects activated, which influence the resistance and failure mode of concrete structure. The wide range of strain rates typically expected in practice is shown in Table 1.

The experimental evidence shows that concrete exhibits the strongest influence of loading rate under tensile load (Malvar and Ross 1998), though there is also a significant influence of the loading rate on compressive strength (Bischoff and Perry 1995). Since concrete is inherently weak in tension, the response of concrete under tensile loading is key to understanding and using concrete in structural elements. In addition, understanding of complete behaviour of concrete structures/specimens under tensile loading is necessary because the material in the vicinity of the crack tip experiences tensile stress.

Table 1. *Load categories distinguished with respect to strain rate (Zelinski 1984).*

Strain rate (1/s)	Load category	Type of loading
$< 10^{-1}$	quasi-static	traffic
$10^{-1} – 10^{1}$	intermediate	aircraft impact
$10^{1} – 10^{4}$	high	hard impact
$> 10^{4}$	shock waves	

2.2 Structural response

The resistance, failure mode, crack pattern and crack velocity of concrete structures/specimens are known to be significantly influenced by the loading rate. Peak load is important parameter which reflects the loading capacity of a given structural element. In general, higher loading rates lead to higher resistance (Banthia 1987, Zhang et al. 2009, Ožbolt et al. 2013b). Moreover, with increase of loading rate failure mode also changes. However, there are only a limited number of experimental studies in which the failure mode is investigated as a function of loading rate (Vegt et al. 2007, Saatci and Vecchio 2009, Ožbolt et al. 2013b). Principally, with the increase of loading rate the failure mode changes from mode-I to mixed mode (Ožbolt et al. 2013b). For instance, this can be visualized practically as a beam failing in bending mode under static loads (ductile failure), while failing in a shear mode under high rate loads (brittle failure) (see Figure 2).

Figure 2. *Typical example of the beam shear failure caused by the impact loading from the collapsed adjacent building (source: http://nees-anchor.ceas.uwm.edu/).*

In addition, the knowledge of crack propagation velocity is essential for rational and accurate analysis of concrete structures subjected to dynamic loads. The crack velocity naturally refers to the speed in which initiated cohesive crack tip, i.e. the FPZ front, will propagate (Yu et al. 2010). Or, in other words, crack velocity is the velocity of a wave which transports energy along a surface, for instance a crack surface. Crack propagation velocity is theoretically limited to about the Rayleigh wave velocity, i.e. for normal strength concrete Rayleigh wave speed is approximately equal to 2100 m/s. However, experimental evidence (Ožbolt et al.

2013b) shows that cracks in some specific materials exhibit a branching instability before reaching the predicted limiting speed. Banthia (1987) reported that average crack velocity was only 5% of the Rayleigh wave speed of the tested HSC. The average velocity was found to be 115 m/s and the maximum velocity was around 500-600 m/s. Mindess (1995) measured crack velocity in plain concrete under impact loading by using a high-speed video camera (1000 frames per second). The results showed that the crack velocities were all in excess of 254 m/s (the limit of measurement for these tests) for the plain concrete subjected to impact velocities from 2.99 m/s to 4.72 m/s. He suggested that measured crack velocities which are different from the theoretical ones could be an indication of the amount of internal microcraking that occurs in concrete during failure. Zhang et al. (2010a) have verified the existence of low crack velocities in HSC by using strain gauges in drop weight test. It was reported that maximum crack speed reached up to 20.6% of the Rayleigh wave speed of the tested HSC, e.g. the maximum crack velocity was around 500 m/s for impact velocity of 2.64 m/s. Moreover, the rate at which crack propagates in a material seems to depend not only upon the rate of loading, but also upon the properties of the material. Wittmann (2002) pointed out that the crack velocity increases considerably with the concrete strength.

2.3 Material response

During last few decades, the effect of strain rate on the material properties of concrete, such as tensile strength and fracture energy, has been studied extensively using various testing methods. A brief overview of the effect of loading rate on relevant concrete properties is presented in the following sections.

2.3.1 Testing methods

Until today, various methods have been proposed for testing dynamic fracture of concrete specimens/structures under different loading rates. Uniaxial tensile behaviour of concrete invariably dominates the behaviour of concrete specimens as well as structural elements. Therefore, in order to understand the dynamic fracture of concrete, it is essential to understand the dynamic fracture of concrete under uniaxial tension. However, the uniaxial tensile behaviour of concrete is difficult to study experimentally even under static load, e.g. the failure always occurs locally, near the loading points, and therefore indirect methods such as Brazilian tests, three-point bending test (TPBT) and compact tension (CT) tests are often

employed. Consequently, to study the dynamic fracture behaviour of concrete and concrete structures, different types of indirect tests have been employed, like modified Charpy impact test, split Hopkinson bar test, drop weight impact test and explosive test. However, due to some limitations in experiments, i.e. problems related to measurements at high loading rates, till now, there is no standard method universally accepted how to test concrete at high strain rates.

Experimental tests with instrumented drop weight type machines are widely used for determining mechanical behaviour of concrete under dynamic loading because of its simplicity, but there are some drawbacks. For instance, with drop weight impact test maximum strain rate is limited to the low range of only 10/s. The main developers of drop weight impact machine for testing concrete under dynamic loading are Bantha and Mindess (1987). In general, the impact test consists of three main components: an impacting hammer, a drop weight guide system and a steel base plate. In this type of tests a hammer with substantial mass is raised to a certain height and then drop to the top surface of the specimen. Usually, impacting hammer height, weight and shape are adjustable. This type of machine was considered to be a suitable means of testing large concrete structures/specimens under bending impact loading (mode I fracture). Principally, impact loads differ from ordinary static loads in the very much shorter duration of loading, which in the case of impact is measured in milliseconds. Consequently, time to fracture concert is very short and the interpretation of the test results in this case may be very difficult. The strain gauges provided in the striking head generate a time-base signal which can generate the load vs. time record of the impact, which in turns is useful from the strength calculation point of view. Major problem that occurs in evolution of results is elimination of the effect of inertia. However, difficulties remain with the measurement of the data at higher rates.

More recently, the split Hopkinson pressure bar (SHPB) technique, invented by Hopkinson in 1914, is a popular way to measure the tensile strength of concrete for strain rates between 10^{-1}/s to 100/s. Even higher strain rate in the range of 20/s to 200/s can be reached with modified SHPB designed to produce spall, usually named MSHB (Schuler et al. 2006). Extensive investigations have been performed with this method by Zelinski (1982), Ross (1989), Weerheijim (1992) and Brara and Klepaczko (2007). The test setup consists of three major parts: the striking bar, the incident bar and the transmitted bar. During the test process, specimen is sandwiched between incident and transmitted bar. When a striker bar impacts the

incident bar compressive loading wave is transmitted through the bar and reflected back at the end as a tensile loading wave which than cause the fracture of concert. To calculate concrete tensile strength and fracture energy, strains at the end of the incident bar and pull back velocity at the end of concrete specimen are measured. The evaluation of experimental results of SHPB tests are based on the principle of uniaxial elastic wave propagation, under the assumption that concrete before tensile cracking is linear elastic. However, this assumption for concrete is unrealistic, since even before localization of macro crack, the pre-peak region, the entire concrete specimen is already significantly damaged (Ožbolt et al. 2013b).

2.3.2 Rate dependent tensile strength

Many experiments have been performed for the measurement of the tensile strength over a wide range of strain rates, here only a few data are reported. The strain rate dependency of the tensile strength is commonly expressed with the dynamic increase factor (DIF), the ratio of dynamic strength to the quasi-static strength.

Mellinger and Birkimer (1966) performed tests on plain concrete cylinders under impact loading with the spalling technique. Within the range of strain rates from 0.57×10^{-6}/s to 20/s the dynamic tensile strength was over 5 times its static tensile strength. In his Ph.D. Birkimer (1968) conducted impact test on plain concrete cylinders at strain rates between 2/s and 23/s. For this range of strain rates the value of DIF varied from about 2.5 to 6. The data from these tests were obtained by measurement of strain pulses on long concrete rods impacted by metallic projectiles.

Zelinski and Reinhardt (1982) used split Hopkinson bar to investigate the tensile stress-strain behaviour at stress rates up to 30 GPa/s (~1/s). They concluded that significant increase in the tensile strength of concrete at high stress rates was due to the extensive microcraking in the whole volume of the stressed specimens. Also, it is reported that in the case of very high loading, since much energy was introduced into the system in a short time, cracks are forced to develop along the shorter paths of higher resistance, through stronger matrix zones and also through some aggregates.

Rossi et al. (1994) also carried out tests using Hopkins bar. The author reported DIF of 1.4 in dry concrete and DIF of 2.1 in wet concrete, respectively. The authors concluded that the

effect of loading rate on the behaviour of concrete in uniaxial tensile testing is due to the presence of free water in the concrete, at least for loading rates up to 80 GPa/s.

Brara et al. (2001) tested several concrete specimens using Hopkinson bar principle combined with the spalling phenomenon. Again the tensile strength was evaluated via velocity of the ejected parts of specimens, using again the one-dimensional wave analysis. In the case of wet specimens, for strain rates up to 120/s (~5000 GPa) the tensile strength increases greatly by a factor 13 compared to the static strength. In the case of dry specimens they measured a strength increase up to a factor of 8.5 at a strain rate of about 100/s.

Schuler et al. (2006) conducted spall tests on concrete cylinders at high strain rates between 10/s and 100/s. For this range of strain rates a DIF for tensile strength between 4 and 5.5 was observed.

Weerheijm and Van Doormel (2007) performed Hopkinson spall bar tests in order to study dynamic tensile strength of concrete. A DIF value of 5.3 was obtained at the maximum loading rate of about 1000 GPa/s (~22.5/s).

Finally, a valuable review of several results from tension experiments is given by Schuler et al. (2006) as shown in Figure 3a. The experimentally observed values for DIF in tension are available in many empirical relations given in the literature. However, in CEB-FIP Model code (2010) is presented the most comprehensive model for the relation between tensile strength under static and dynamic loading (impact), namely DIF. Figure 3b shows the model results DIF in dynamic tension together with the test data (on log-log scale). Since test data have been obtained by means of different test setups, specimen dimensions and material properties, large scatter in the results is present. However, from Figure 3 it is evident that all data show the same trend and that tensile strength under high loading rate differ significantly when compared to static loading. The behaviour is bilinear with the limit of approximately 1/s -10/s, i.e. the first part shows a linear dependency of the DIF with strain rate and the second steep increase of the DIF with strain rate. For that reason it has been generally accepted that there is an apparent increase of the dynamic strength when concrete is subjected to high strain rates and that for strain rates larger of approximately 10/s this increase is progressive. From a physical point of view, for lower strain rates the rate dependency in tension is related to the viscosity due to water content, whereas for higher strain rates there are very limited or more

often contradictory interpretations for progressive increase of strength. Hence, the question that is still under discussion is what are the reasons for such progressive increase? It is not yet clear whether the progressive increase of experimentally measured resistance can be attributed only to material strength or also to other effects, e.g. inertial effects Thus, more research has to be done for further explanations of the rate effect observed experimentally.

a) b)

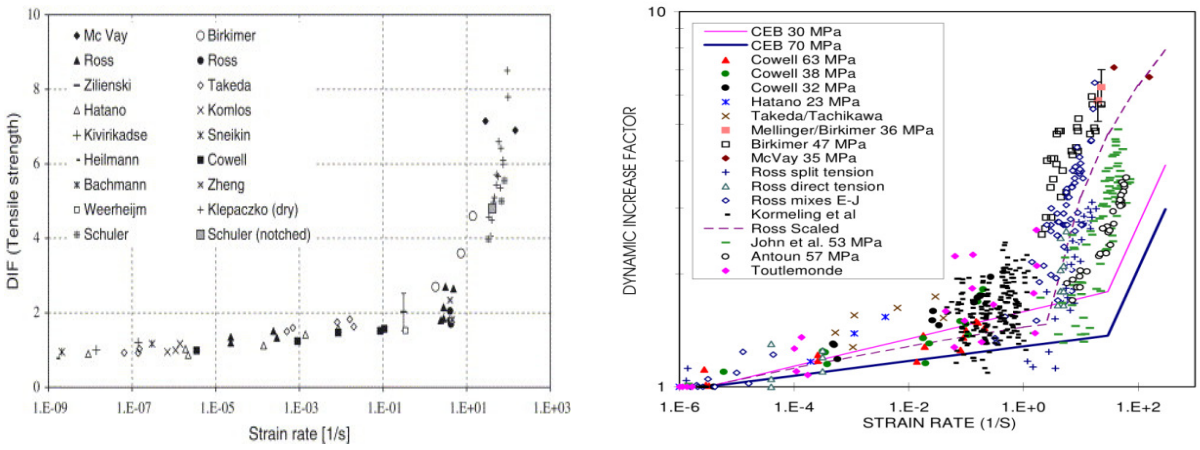

Figure 3. *Dynamic increase factor (DIF) for tensile strength a) test data (Schuler et al. 2006) and b) CEB versus test data (Malvar et al. 1998).*

2.3.3 Rate dependent fracture energy

Compared with the extensive studies on the tensile strength over a wide range of strain rates, much less information is available on the fracture energy. Due to the lack of experimental test data, no information is available on fracture energy under loading rate in CEB-FIP Model code (2010).

Some researchers concluded that fracture energy is constant and independent of the loading rate. For instance, impact tensile tests on notched and unnotched specimens with split Hopkinson bar performed by van Doormaal et al. (1994) showed that the dynamic fracture energy is approximately the same as the static fracture energy up to loading rate of approximately 15 GPa. In addition, it is reported that the higher fracture energies obtained in dynamic loading experiments in comparison to quasi-static values are exclusively due to structural effects, for example inertia and geometry.

Schuler et al. (2006) measured fracture energy at high strain rates between 10/s and 100/s with spalling tests. A DIF for fracture energy, i.e. the ratio of dynamic to quasi-static fracture energy, of approximately 3 was observed at crack opening velocity of 1.7 m/s (see Figure 4a).

Weerheijm and Van Doormel (2007) measured fracture energy with a split Hopkinson bar. For the fracture energy at strain rates up to 1000 GPa/s maximum enhancement factor of 2.5 is observed.

Vegt et al. (2009) studied the influence of the loading rate on the failure mechanisms and on the mechanical properties of cylindrical concrete specimens using SHB and MSHB technique. The tested specimens were subjected to quasi-static, medium (~50 GPa/s) and high-loading rate (>1000 GPa/s). It was reported that fracture energy is constant in the range from static up to 50 GP/s. However, for loading rates beyond 50 GPa/s fracture energy increase dramatically and DIF equals 12.5 for loading rate of 1700 GPa/s.

Ruiz et al. (2009) also investigated the loading rate effect on the fracture properties of concrete using drop weight impact machine. The loading rate was varied from a quasi-static level to a dynamic level, from 10^{-4} mm/s to 10^{3} mm/s. The results show that both the fracture energy and the peak load increase with increases in loading rates. In addition, it was reported that all tested specimens fall due to bending (mode I). An overview of data from the literature is provided in Figure 4b. The maximum DIF for the peak load is 7.14 whiles for fracture energy is even more pronounced than that on the peak load and equal to 38.23. They supported this result with argument that the fracture energy is more sensitive to micro-cracks than the peak load under high loading rates.

a) b)

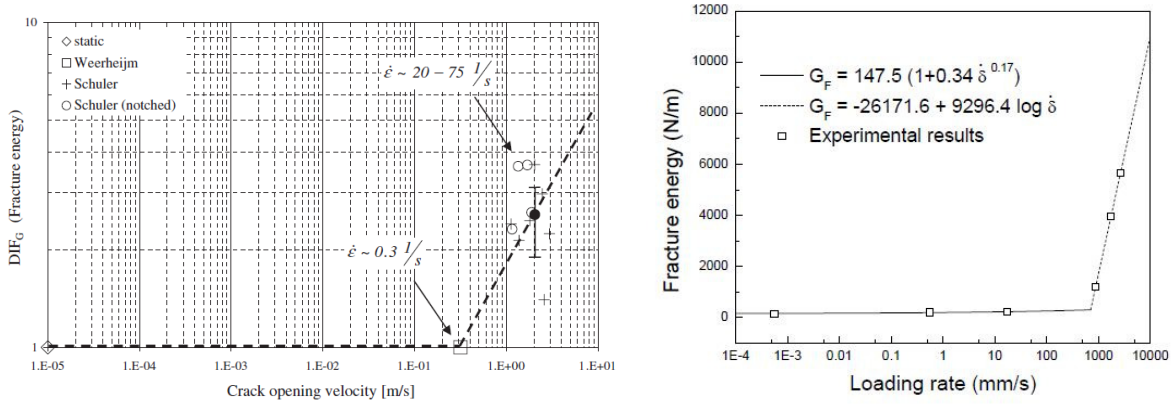

Figure 4. *a) Relation between dynamic increase factor (DIF) for fracture energy and crack opening velocity (Schuler et al. 2006) and b) rate dependent fracture energy (Zhang et al. 2009).*

2.4 Numerical modeling

Many researchers have proposed various numerical models to predict response of concrete under dynamic loading. However, in order to predict dynamic response properly, a realistic material model (constitutive relationship) for concrete is needed. In most of these studies different constitutive relations were employed, for example, plasticity, microcrack planes, viscous hardening, cohesive model, viscoplasticity, rate dependent damage, consistency viscoplastic model etc. Furthermore, most of these studies usually investigate only the differences between mechanical behaviour of the concrete under static and dynamic loading such as tensile strength and fracture energy. All these models use some simplified formulation for DIF, which is calculated based on experimentally measured results, and directly incorporate into the constitutive law of material to fit better test results. In addition, some of the above mentioned models cover only a limited range of loading rates while the other are applicable for more general types of loading (Travaš 2009, Irhan 2014). However, depending on the model, different hypothesis have been proposed to explain the reasons for progressive increase of experimentally measured resistance. Hence, the results of several studies are presented as follows.

For example, Barpi (2004) reported that viscosity is a key reason for the increase of DIF. He proposed a viscoplasticity based model that incorporated a viscosity parameter as a function of strain rate. Similarly, Hentz et al. (2004) concluded that the dynamic tensile strength based on spalling tests represented the material intrinsic behaviour of concrete.

Complete study on strain rate effect has been given by Cotsovos and Pavlović (2008a, 2008b, 2008c). By using a quasi-static constitutive model as well as static material strength, authors performed non-linear finite element analysis to study the behaviour and failure of concrete specimens under dynamic load and found that their results from numerical simulations were consistent with the published experimental data. Based on their results they concluded that the effect of strain rate on the specimens behaviour reflects the effect of inertia (represents a structural effect) instead of intrinsic material property. Therefore, the use of experimental data from dynamic tests to model constitutive behaviour of concrete under dynamic loads is questionable (Cotsovos and Pavlović 2008a). Cotsovos and Pavlovic (2008) suggested that under dynamic tests the concrete specimen must be viewed as a structure since its behaviour is directly linked to the inertia effect of its mass and the boundary conditions. However,

currently there is only limited number of studies in which the failure mode is investigated as a function of loading rate (Sukontasukkul and Mindess 2003, Ožbolt and Reinhardt 2005, Ožbolt et al. 2006, Travaš et al. 2009, Ožbolt et al. 2013b).

Most recently, a complete study on dynamic fracture of concrete was made also by Ožbolt et al. (2006, 2013b, 2014) using microplane constitutive model. It was demonstrated that the progressively increasing resistance of structural elements relying on tensile strength of concrete, such as pull-out of anchor bolt from concrete block (Ožbolt et al. 2006), compact tension specimen (Ožbolt et al. 2013b) and direct tension (Ožbolt et al. 2014), is related primarily to inertia effects. If in the analysis of these problems only rate sensitive constitutive law is used but inertia is not activated (rate sensitive static analysis), then no progressive increase in resistance was observed, which confirms that such increase is due to inertia. Moreover, if the inertial effects are ignored, the failure mode remains independent of the loading rate, which is unrealistic.

Depending on the test setup and measurement technique, the progressive increase can be explained either by inertia invoked by material softening or by the fact that in the evaluation of experimentally measured data, damage of concrete is ignored. In the case of compact tension specimen (Ožbolt et al. 2013b) it was confirmed that the progressive increase of resistance is due to the inertia generated at the tip of the macro crack, which causes crack branching and leads to progressive increase of resistance. Moreover, it was shown that the true tensile strength and fracture energy increase approximately linear in semi-log scale with increasing strain rate. The linear increase is controlled by the constitutive law (inertia at micro scale and influence of viscosity) whereas the progressive increase comes automatically from dynamic finite element analysis. The same conclusion was obtained by Cusatis (2011) based on the 3D finite element analysis using discrete finite elements. Furthermore, as discussed by Ožbolt et al. (2014), assumption of elastic behaviour prior to fracture is not realistic for concrete, since even before localization of macro crack, the entire concrete specimen is already significantly damaged. Therefore, to evaluate experimental measurements objectively, damage should be somehow accounted for. The assumption of elastic behaviour prior to fracture is valid only for elasto-brittle material, e.g. glass (Ožbolt et al. 2014). It is emphasized that if damage is ignored, the effect of damage induced inertia is not filtered out from the results of experimental measurements and apparent instead of true strength of concrete is measured.

Lu and Li (2011) conducted numerical study based on a micro-mechanism model. They concluded from their study that micro-crack inertia is one of the mechanisms responsible for the strain rate sensitivity of the tensile strength of concrete like materials and that the observed increase of tensile strength with strain rate from dynamic tensile test can be largely attributed to the inertia effects of micro cracks.

2.5 Summary and conclusions

Concrete is a very strain rate sensitive material, especially in tension. During last few decades, a large amount of experimental and numerical studies have been done to investigate dynamic fracture of concrete subjected to high loading rates. These studies usually investigate the differences between tensile strength and fracture energy under static and dynamic loading and suggest some simple relations to predict behaviour of concrete under high loading rates. Most of these investigations suggest that concrete exhibit apparent increases of strength (higher resistance) and toughness (more fracture energy) under dynamic loads. The reasons for this phenomenon are not yet well understood, although a number of different hypotheses have been proposed.

A various experimental testing techniques and specimen types have been used during the past to study dynamic fracture of concrete. The evolution of most experimental results shows that up to the strain rates of about 1/s to 10/s, DIF of tensile strength approximately increases linearly in semi log scale and after reaching this threshold the strength increase becomes progressive. Although the reason for this increase is not clearly understood, it is now widely accepted to be a material property. However, recent numerical studies call into question this existing and widely accepted view.

In addition, the primary objective of all presently available experiments was to investigate the behaviour of concrete at the material level, namely dynamic tensile strength and fracture energy, rather than at the structural level. There are only a few reports about failure mode and are mostly related to the failures due to bending. Accordingly, relatively little is known about physical process of crack propagation during dynamic loading. Thus, further research on dynamic fracture of concrete is required.

On the other side, in computational codes different constitutive models were used to reproduce the dynamic behaviour of concrete. Most of these constitutive models are based on simple equations obtained by fitting test results under static and dynamic loading. Because of this, such standard macroscopic material models (e.g. plasticity or damage based models) are capable of giving correct prediction on apparent strength. As such, none of these models are able to capture information on change in failure mode or phenomena of crack branching realistically. However, the proper response prediction is only possible when the material behaviour of concrete and failure mechanism at high loading rates is known and understood (Veget et al. 2009). To this date, only a relatively small number of publications with reliable model for simulating failure of concrete at high loading rates characterized by complex phenomena are available (Ožbolt et al. 2013b). Thus, much more work has to be done to clarify dynamic fracture mechanism of concrete.

3. EXPERIMENTAL STUDY

3.1 Introduction

In the past few decades, various researches have undertaken significant effort to understand the concrete fracture under dynamic loading. To this end, numerous experimental studies under dynamic loading are performed by employing different test setups, for instance drop hammer test, splitting test etc., as well as different measurement methods, since currently there is no standardized testing procedure (see Chapter 2). The main focus of performed tests has been to study only specifically chosen parameters, such as fracture energy and tensile strength, as a function of loading (strain) rate. Principally, results obtained from those experiments show progressive increase of tensile strength and fracture energy, especially for strain rates higher than 10/s. However, the reasons for progressive increase of the same are not yet clearly understood. Moreover, the results of experimental study can be grossly misleading if they are not interpreted with the certain caution. The elimination of inertial effects is one of the main problems and therefore tremendous care must be used in interpreting the data. Consequently, complexity of dynamic tests and inherent difficulties at measurements lead to wide variations of experimental data, which often results in contradictory conclusions. Obviously, new tests should be devised for the proper identification of the concrete behaviour under dynamic loading.

Furthermore, the dynamic response of concrete materials is not only involved with strength but also accompanied with the cracking features, which can be varied through different loading rates (John and Shah 1990). Therefore, these parameters should not be separated out to understand the phenomenon of progressive increase of tensile strength occurring at high loading rates. Hence, in order to understand the dynamic mechanical properties of concrete, such as fracture energy and tensile strength, it is essential to understand the complete dynamic fracture behaviour, in particular failure mode and crack patterns. However, only very limited studies aimed at understanding the complete fracture of concrete and influence of dynamic loading on the failure mode, see for example Ožbolt et al. (2013b). It was therefore deemed essential to perform further experimental investigation on the fracture behaviour of concrete under dynamic loading. For that purpose L-shaped concrete specimens are employed.

3.2 L-shaped concrete specimen under high loading rate

L-shaped specimen has become a popular benchmark test for the validation of material models and phenomenon of mesh sensitivity (Winkler et al. 2001, Ožbolt et al. 2002) under static loading. Due to geometrical specificity L-specimens are of interest from the viewpoint of crack propagation and fracture of concrete. Although it is a relatively simple test setup, the fracture behaviour of L-shaped specimens under static loading is rarely but available in literature (Winkler et al. 2001). On the other hand, there are currently no available experimental data which discuss dynamic behaviour of L-shaped concrete specimens. For that reason, in addition to static load test it may be desirable to perform dynamic load test.

The main aim of present experimental study was to develop a valid test setup to gain better insight into the complete mechanism of concrete fracture under dynamic loading. Next, to better understand the inertial effects during testing of L- shaped concrete specimens, a special attention is devoted on the change of crack propagation. Therefore, the main intention is to demonstrate the loading rate dependent failure mode, crack velocity, phenomena of crack branching and to verify the computational model.

3.2.1 Numerical predictions (Ožbolt and Sharma 2012)

Even though many researchers performed different types of dynamic tests on concrete, very few data are available with respect to loading rate effect on crack propagation, crack velocity and crack branching phenomenon. Ožbolt and Sharma (2012) numerically studied the influence of displacement (loading) rate on the crack propagation of L-specimen. The numerical study was performed for L-specimen tested by Winkler et al. (2001), see Figure 5a. Simple 2D model under assumption of plane strain conditions is used in numerical study in order to minimize the computation time. Firstly, the specimen was analyzed under static load to validate the results of analysis against results of experiment. The numerical predictions are found to be in good agreement with experimental observations (see Figure 5). In the next step, the same model was subjected to high loading rate to investigate the influence of loading rate on failure mode and crack propagation in the specimen. By changing loading rate from quasi static to higher rates of loading, direction of crack propagation changes tremendously, i.e. for static loading there is one horizontal crack that is approximately perpendicular to the loading direction. On contrary, with increase of loading rate the crack becomes more inclined and closer to the loading zone (see Figure 6). It is reported that structural inertia effect is

responsible for the change in crack propagation, i.e. with increase of loading rate crack propagates from horizontal direction to vertical. Hence, an experiment was conducted to confirm the numerical predictions.

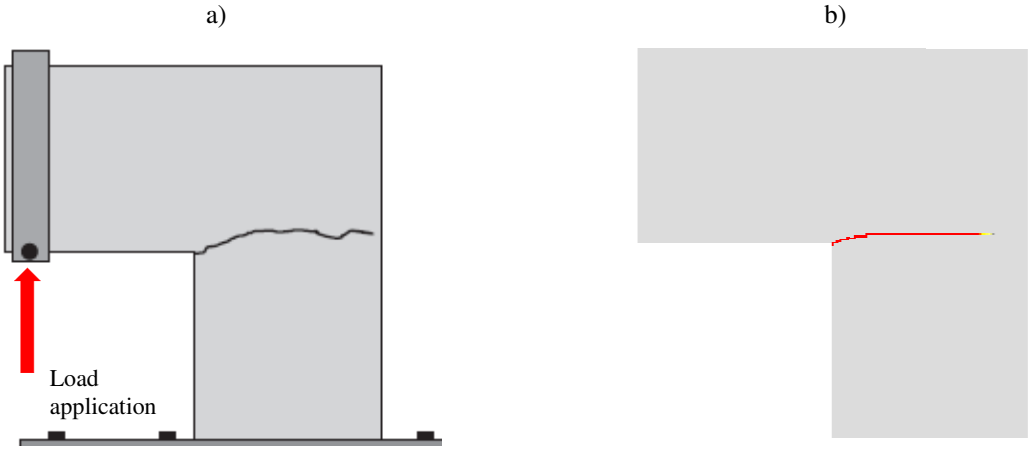

Figure 5. *Failure pattern and crack propagation for the L-shaped concrete specimen under static load a) experimental result (Winkler et al. 2001) and b) numerical result (Ožbolt and Sharma 2012).*

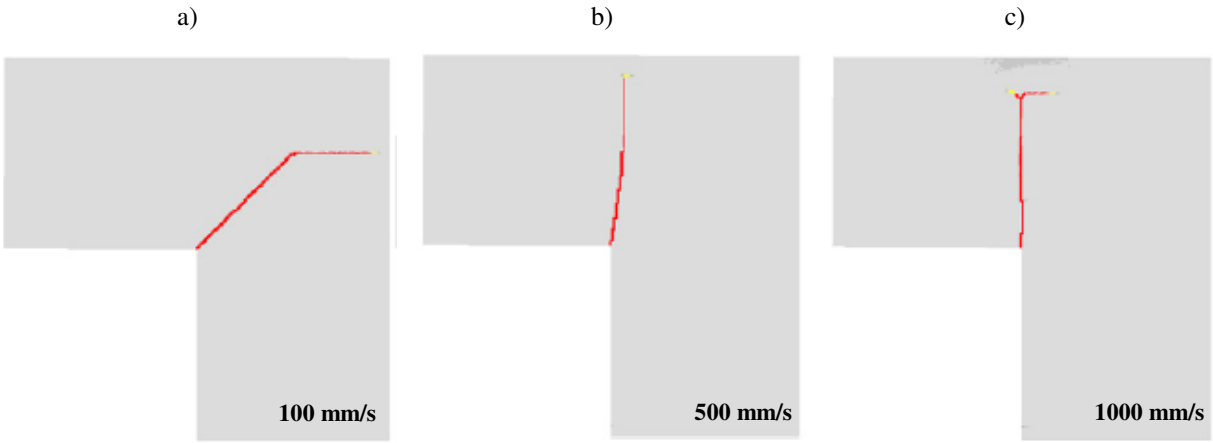

Figure 6. *Failure pattern and crack propagation for the L-shaped concrete specimen under dynamic load for the following displacement rates a) 100 mm/s, b) 500 mm/s and c) 1000 mm/s (Ožbolt and Sharma 2012).*

3.2.2 Experimental procedure

Prior testing, additional numerical simulations are carried out providing essential information for testing procedure, such as design parameters of the test setup, calibration of measuring instrumentation, constraint conditions and loading point positions.

A series of quasi-static and dynamic loading tests has been performed on L-shaped concrete specimens at the Institute for Building Materials of Stuttgart, MPA Stuttgart, in order to investigate the concrete fracture under high loading rates and to verify the predictions of recent numerical study (Ožbolt and Sharma 2012). The special notation is given on rate dependent failure mode, crack velocity and possible crack branching phenomena. In the following section details related to the specimen geometry, material properties, instrumentation of test specimens, loading arrangement and measuring instrumentation are described. Subsequently, results of experiments are presented and discussed.

3.2.2.1 Material properties and specimen geometry

For the experimental work L-shaped concrete specimens were cast. During casting, great care was devoted to ensure that the specimen had flat and smooth surfaces to avoid technical difficulties related to fixing of the specimen on testing machine. The essential advantage of this shape of geometry is its ability to change failure mode for relatively small range of loading. The dimensions given in Winkler et al. (2001) are found to be to heavy and awkward to handle, therefore thickness is reduced from 100 mm to 50 mm. Here adopted dimensions of the tested L-shaped concrete specimens for present experimental study are shown in Figure 7.

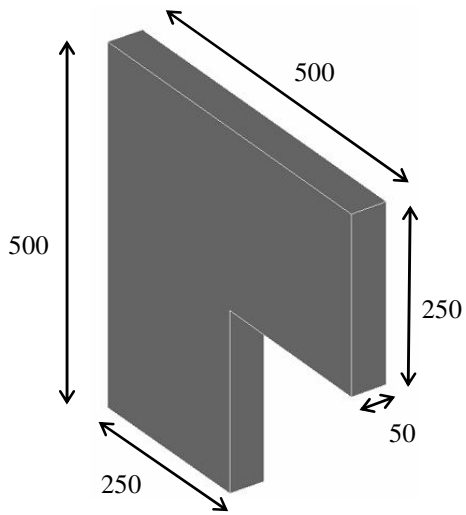

Figure 7. *Geometry and dimensions of the L-shaped concrete specimen (all in mm).*

Considering the dimensions of the concrete specimens, the maximum coarse aggregate size was chosen as 8 mm. The concrete specimens are cured 7 days under constant temperature of 20°C and relative humidity (RH) of 100%. Subsequently the specimen is approximately three weeks exposed to RH of 60%. The age of concrete at the time of testing was approximately 4

months. Before testing, the uniaxial compressive strength and the splitting tensile strength were obtained from cubes with dimensions of 150 mm, following the procedures recommended by DIN-EN-12490. Six cubes were cast, three for compressive test and three for splitting test. Two concrete mixes were tested. For both mixtures concrete class is determined as C50/60 in reference to DIN-EN-206-1. For each concrete mix, a total of 10 specimens were cast, all in a single batch. The average material properties for each concrete mixture as determined from control tests are summarized in Table 2. Prior the testing, front surface of specimen is colored in white to ensure good visibility of cracks.

Table 2. *Average mechanical properties of experimental concrete mixtures.*

Batch	Density ρ_c (kg/m^3)	Tensile splitting strength $f_{t,sp}$ (MPa)	Compressive strength f_c (MPa)
1	2205	3.5	51.4
2	2214	3.5	56.4

3.2.2.2 Test setup

Here, a detail description of new test setup for investigation of concrete fracture under dynamic loading is presented. An INSTRON servo-hydraulic high speed tensile testing machine, located at MPA Stuttgart, was used to apply different loading rates on the L-shaped concrete specimens up to failure. The testing machine has load capacities of maximum 100 kN and loading velocity up to 20 m/s. The machine is mainly used to carry on various kind of tests for metal like materials (e.g. steel). In order to use it for testing of concrete under dynamic loading, certain modifications had to be done. Thus, modifying part of the testing machine, corresponding test setup was arranged and employed.

For the present investigation special supporting plate and side plate, made of mild steel, were designed and manufactured. The details of the plates are shown in Figure 8a, 8b and 8c. The purpose of these plates was to fix relatively large concrete specimen. The supporting plate was directly attached to the base plate of the testing machine (pedestal) to ensure a rigid base (see Figure 8a). This part was not moved during testing. The outer surface of side plate, area of size 250 × 100 mm, was glued to the corresponding surfaces of the concrete specimen using an epoxy adhesive and placed on the top surface of supporting plate (see Figure 8b). The epoxy was left to dry for a minimum period of time recommended by the producer. Before testing, in order to fix the concrete specimen, the bottom of side plate was bolted to

the supporting plate (see Figure 8c). In this position the specimen was ready for testing. The photo of the test setup arrangement together with the L-shaped concrete specimen is shown in Figure 8d.

Dynamic loading on the specimen was provided by means of machine actuator (loading piston). All tests were performed in displacement control. This was achieved with different programmed actuator displacements rates in the direction opposite of gravity. The imposed loading point displacement rates were varied from 0.25 mm/s up to 5 m/s. Due to safety reasons the tests were not performed for higher loading (displacement) rates. A steel cylinder was attached to the striking end of the loading piston to apply the load along the inner horizontal face of the tested concrete specimen (see Figure 9a). Two different steel cylinders were used, one with diameter contact area of 20 mm and other one 45 mm. The detail of steel cylinders used in investigation is shown in Figure 9b. Steel cylinder of 45 mm in diameter was employed to avoid localized damage area in the vicinity of the loading point observed for cylinder with smaller contact surface at higher loading rates. The main tests were done with the use of 20 mm diameter steel cylinder. Before the loading piston hit the specimen, the aluminum plate was placed on the top of the striking cylinder. Purpose of using the aluminum plate is to prevent damage and to distribute the load more uniformly to the cross section of the L-specimen. Dimension of aluminum plate was always approximately same as diameter of steel cylinder which is used.

Two types of test were performed, broadly classified as dynamic tests at high displacement rates and quasi-static at low displacement rates, all with the same testing machine. In total 20 experiments are carried out, but only 12 are presented here. Careful attention has been given to ensure protection for machine and instrumentation against any possible damage during testing. It is important to note that for this kind of tests it is difficult to obtain a perfect repetition of the results because of technical difficulties with arrangement of specimens, e.g. the eccentricity of the load which has a significant influence on the result of impact tests. However, the aim of the study was not to make a series of repetition but to confirm or disconfirm the numerical predictions and finally to improve the knowledge on dynamic fracture of concrete.

a)

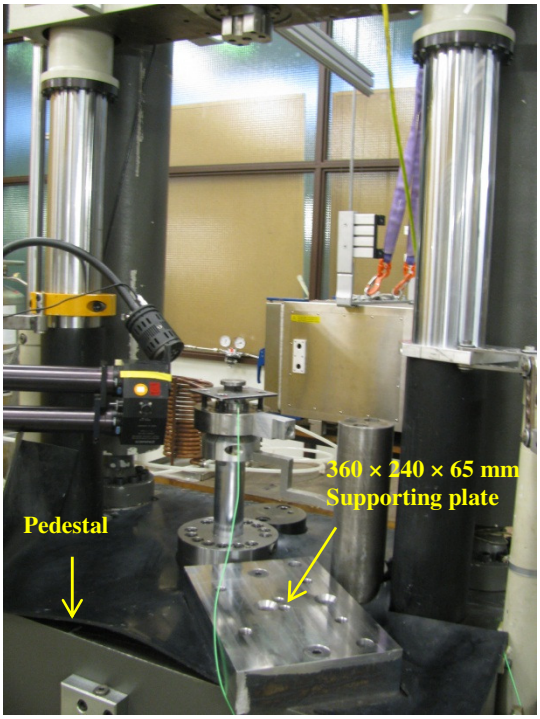

b)

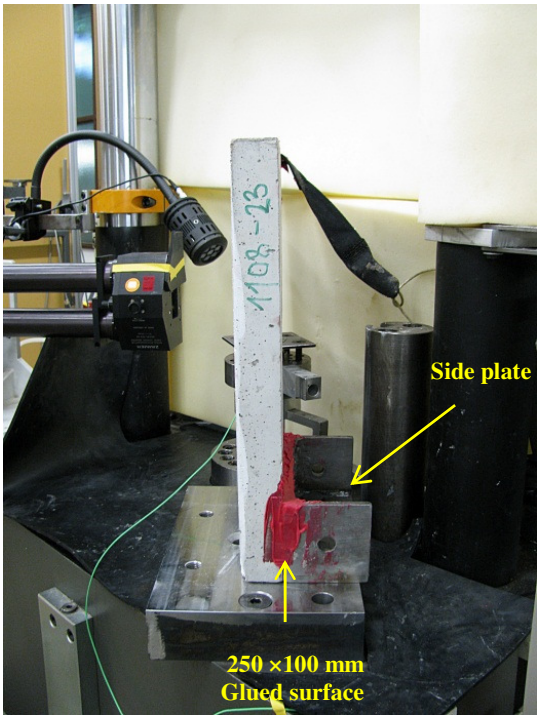

c)

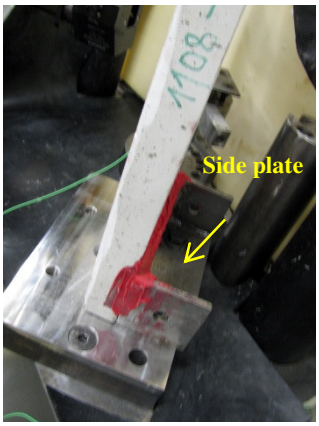

d)

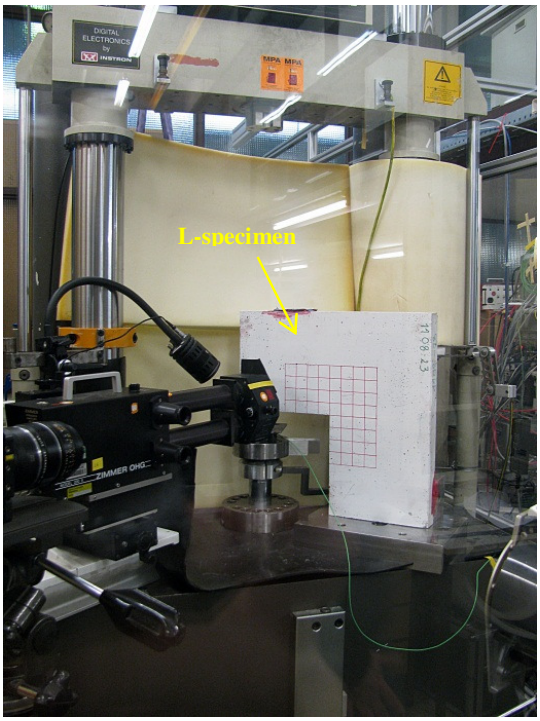

Figure 8. *Photo of a) detail of supporting plate, b), c) detail of side plate and d) test setup.*

a) b)

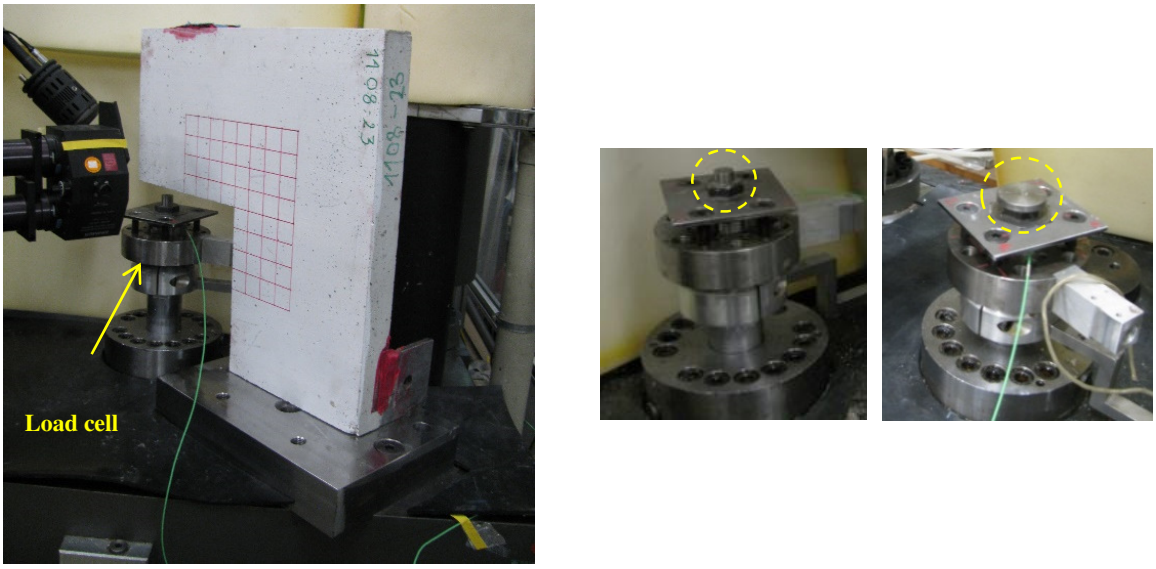

Figure 9. *Photo of a) load cell arrangement and b) detail of striking end of load cell: steel cylinder with diameter contact area 2R = 20 mm (left) and 2R = 45 mm (right).*

3.2.2.3 Measuring equipment

A detailed view of the measuring equipment is given in Figure 10. The load cell built into inner part of the loading piston (machine actuator) was used to measure applied loads. KISTLER piezoelectric force sensor Type 9061A used to determine the dynamic forces is capable of measuring loads range from 0 kN up to 200 kN (Figure 10a). The load cell was connected to a charge amplifier with a highly insulating special cable.

The vertical displacement is measured in relation to point of the load application by means of optical extensometer Zimmer OHG 200 X-5 No. 246 (Figure 10b). Figure 9a depicts the relationship between the applied load, optical extensometer and point where vertical displacement is measured. Optical extensometer was placed about 210 mm away from front surface of tested specimen for safety reasons (Figure 9a). The vertical displacement was monitored just above the point of load application, about 30 mm away from the left vertical edge on the front surface of tested specimen.

In addition, the failure mode and crack patterns were observed and examined. A FASTCAM-APX RS high-speed video camera (HSC) with a maximum of 30000 frames per second was used to record the fracture process (Figure 10c). Only the cracks at the front surface of the concrete specimen, in the zone of cracking with area of measurement = 120 x 120 mm were recorded. The zone where the cracks are expected to propagate is denoted with a 30 x 30 mm

uniform mesh size, visible in Figure 8d. From the record of crack propagation, crack velocity was estimated. To record the wider area of concrete specimen during test, additional video camera is used (Figure 10d).

a) b)

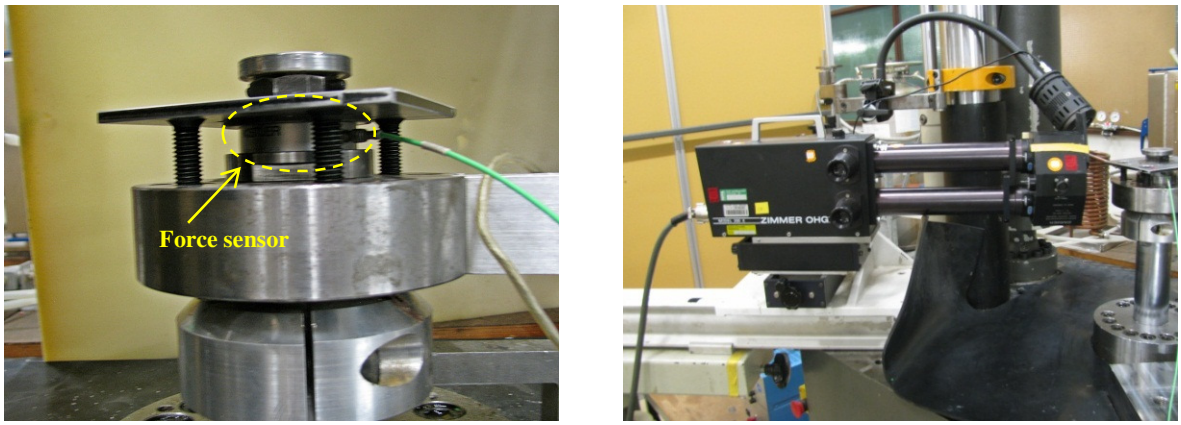

c) d)

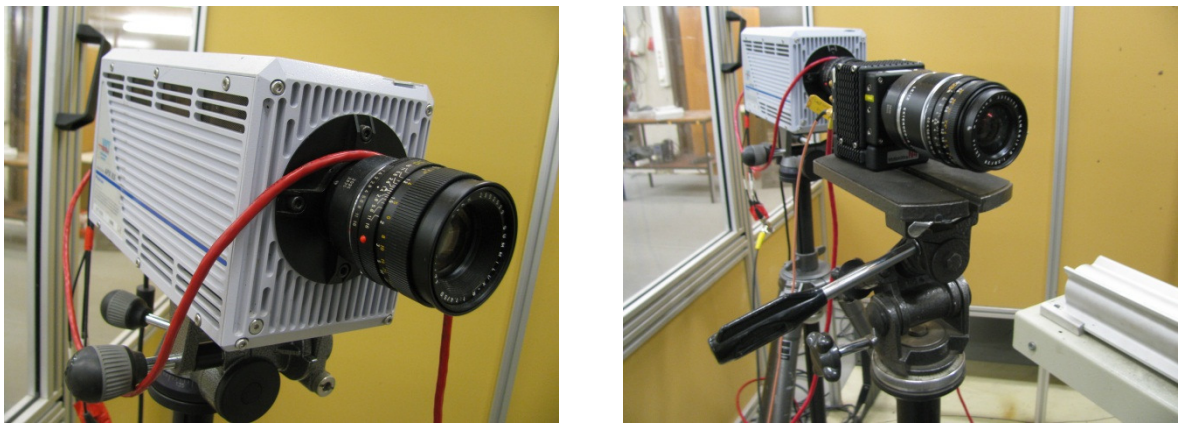

Figure 10. *Photo of measuring equipment a) load cell, b) optical extensometer, c) high-speed video camera and d) video camera.*

3.2.3 Results and discussion

The L-shaped concrete specimens were tested with different displacement (loading) rates. A total of 12 experimental results obtained from performed tests are analyzed. Projected displacements rates set at the machine actuator, actual displacement rates measured on the tested specimens and corresponding peak loads are summarized in Table 3. Actual displacement rates are given as maximum displacement rates where maximum displacement rate is defined as a tangent on the displacement history output curve at time at which maximum load is reached.

The measured load-displacement curves for representative test results are illustrated in Figure 11. As explain above, the displacement is measured in relation to point of load application on the front surface of the specimen, 30 mm away from left vertical edge. From Figure 11 it is obvious that peak load increases with increase of displacement rate, as expected. The maximum load of approximately 130 kN was obtained from the Test No. 12, which was with the fastest loading rate of approximately 2400 mm/s. Figure 12 shows plot of peak loads obtained for the specimen against loading point displacement rates in semi-logarithmic plot. Note that after approximately of 100 mm/s peak load is increasing progressively.

Table 3. *Summary of experimental results.*

		Displacement rate (mm/s)		
Test No.	Specimen No.	Machine	Specimen (maximal)	Peak load (kN)
1	23	0.25	0.25	4.00
2	15	100	82	4.88
3	18	500	350	13.96
4	13	1000	740	22.30
5	25	2000	1200	48.54
6	17	2500	1300	56.16
7	16	2500	1150	51.95
8	24	3000	1000	56.93
9	28	4000	1100	56.35
10	20	1000	710	35.74
11	27	3000	1500	66.41
12	19	4500	2400	127.73

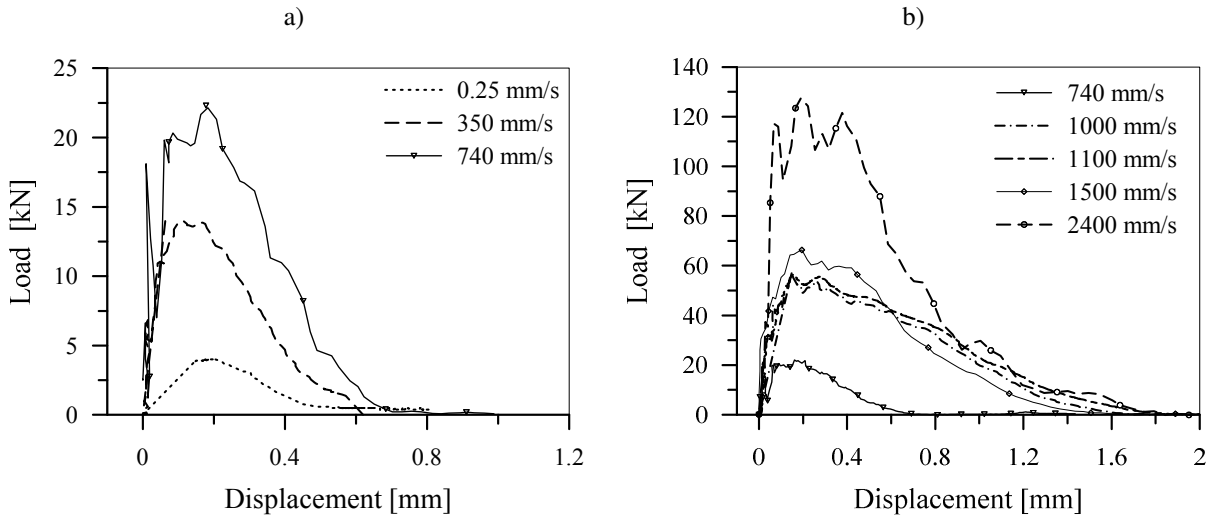

Figure 11. *Experimentally measured load-displacement response a) for displacement rates up to 740 mm/s and b) for displacement rates from 740 mm/s up to 2400 mm/s.*

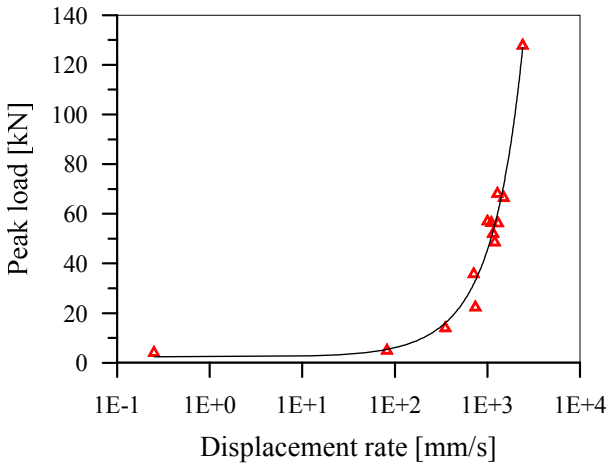

Figure 12. *Peak load obtained for different displacement rates.*

In Figure 13 are shown typical crack patterns observed for different displacement rates. It can be noted there is a marked difference in the failure patterns and crack propagation between the low and higher displacement rates. Hence, it is interesting to observe how the crack propagation changes with the change of displacement rate. From Figure 13 it is obvious that crack always begins at the same point (junction point) and propagates forward into the specimen, however angle and direction of crack propagation are different. Note that term junction point is used for point of crack initiation. When displacement rate is low, close to quasi-static, the crack propagates in horizontal direction, almost perpendicular to the loading direction (see Figure 13a). In contrary, with further increase of the displacement rate crack initiation and propagation direction tends to become more vertical, almost parallel to the loading direction (see Figures 13g to 13l). Consequently, it is confirmed that the crack path is loading rate dependent, i.e. the crack propagation direction gradually changes from almost horizontal for static case to vertical for high displacement rates. Furthermore, in most cases with higher displacement rates numerous small cracks, crack branching, crack bridging and crack deflection can be detected, as can be seen more clearly in Figure 14. Multiple branching phenomena can be seen in Figure 13l. Such a phenomenon was also observed earlier with the compact tension specimen (Ožbolt et al. 2013b).

Figure 13 shows that cracking propagation angle increases with increase of loading rate. In the case for quasi-static and displacement rates lower of approximately 100 mm/s crack propagates almost horizontal. For the displacement rates between approximately 100 mm/s and 700 mm/s the crack initiates at 45° direction afterwards it progress in horizontal direction. Subsequently, at the displacement rate of approximately 750 mm/s the crack initiates and propagates at angle of 45° (see Figure 13e). Next, at 1000 mm/s the crack becomes more vertical and even more, crack branches. The two new cracks travel on either side of specimen whereas one crack going vertically while the second crack propagate parallel with the static crack propagation direction (horizontal). Here, it turns out that for given concrete properties and geometry of specimen a single crack is observed for loading rates less than approximately 1.0 m/s. For displacement rates equal or higher than approximately 1.0 m/s crack branching is observed as well as multiple branching for approximately of 2.5 m/s.

The typical crack velocities evaluated from the experiments are shown in Figure 14 (views of the cracked region via HSC). As mentioned above, the crack velocity is determined from the evaluation of photos obtain from high resolution camera. However, it should be noted that the precision of the estimation of crack velocity is limited by the resolution of the camera. For example, at the highest loading rate equal to 2400 mm/s, test No. 19, from crack initiation till crack branching it takes only 0.2 ms. Hence, just 6 photos was possible to make. The critical crack width was assumed to be 0.1 mm. It was measured from the available camera resolution and the corresponding measured frame window (area of measurement = 120 x 120 mm). Note that for specimen No. 25 the onset of branching was outside the measured frame window (Figure 14h). The highest crack velocity is observed before crack branching and it was found to be of around 650 m/s (see Figure 14). It is interesting to observe that only for specimen No. 19 (see Figure 14k) crack branching starts simultaneously and afterwards both cracks travel with the same speed. On the other hand, for specimens No. 24, No. 16 and No. 17 after crack branching occurs, vertical crack first appear and then second crack starts to propagate along horizontal direction. Hence, in most cases, after crack branching, horizontal crack propagates much slower than the vertical crack. Generally, in either case, it can be concluded that after propagating crack split into two or more branches, new cracks propagate more slowly than before branching.

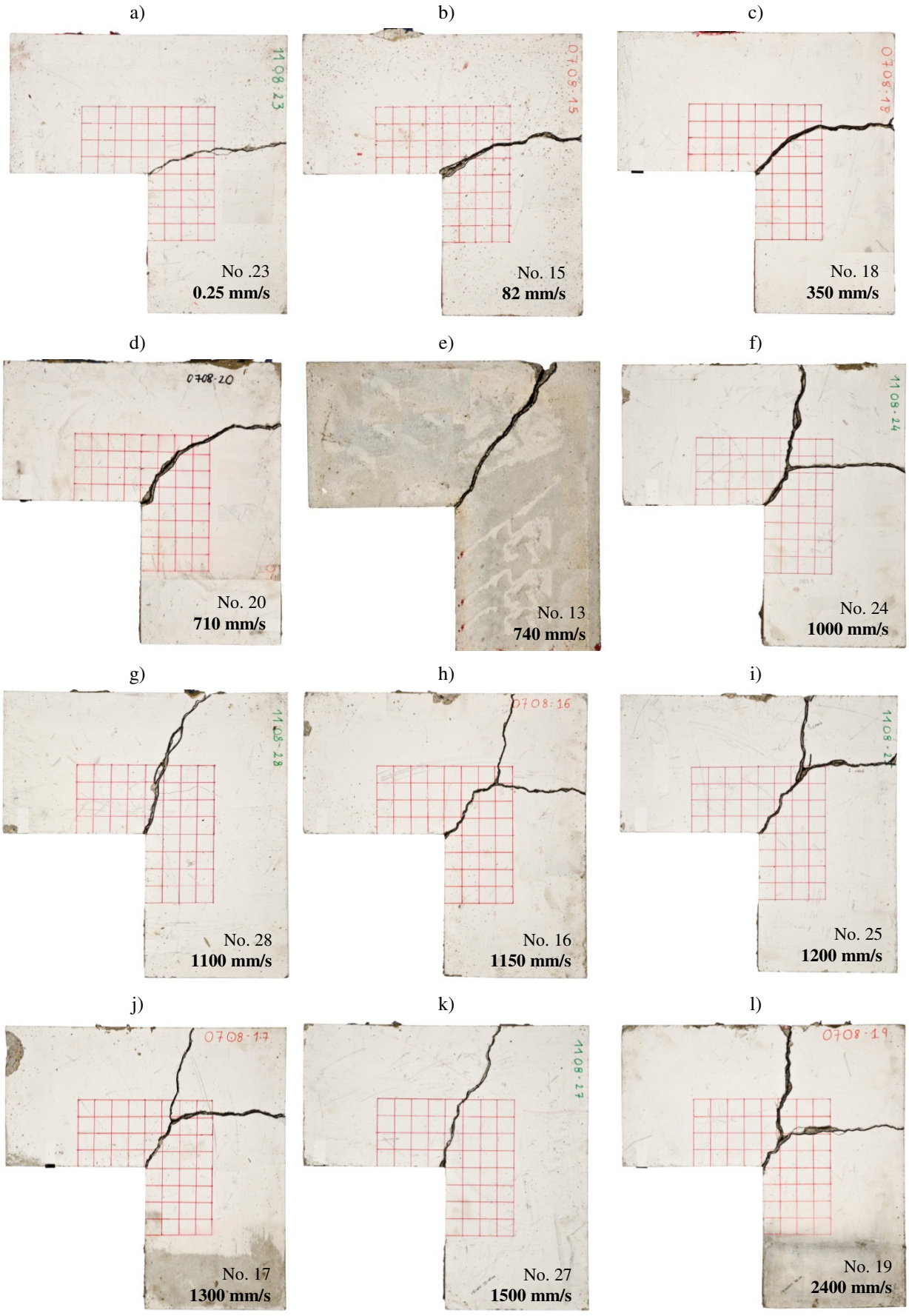

Figure 13. *Experimentally observed crack patterns for different displacement rates.*

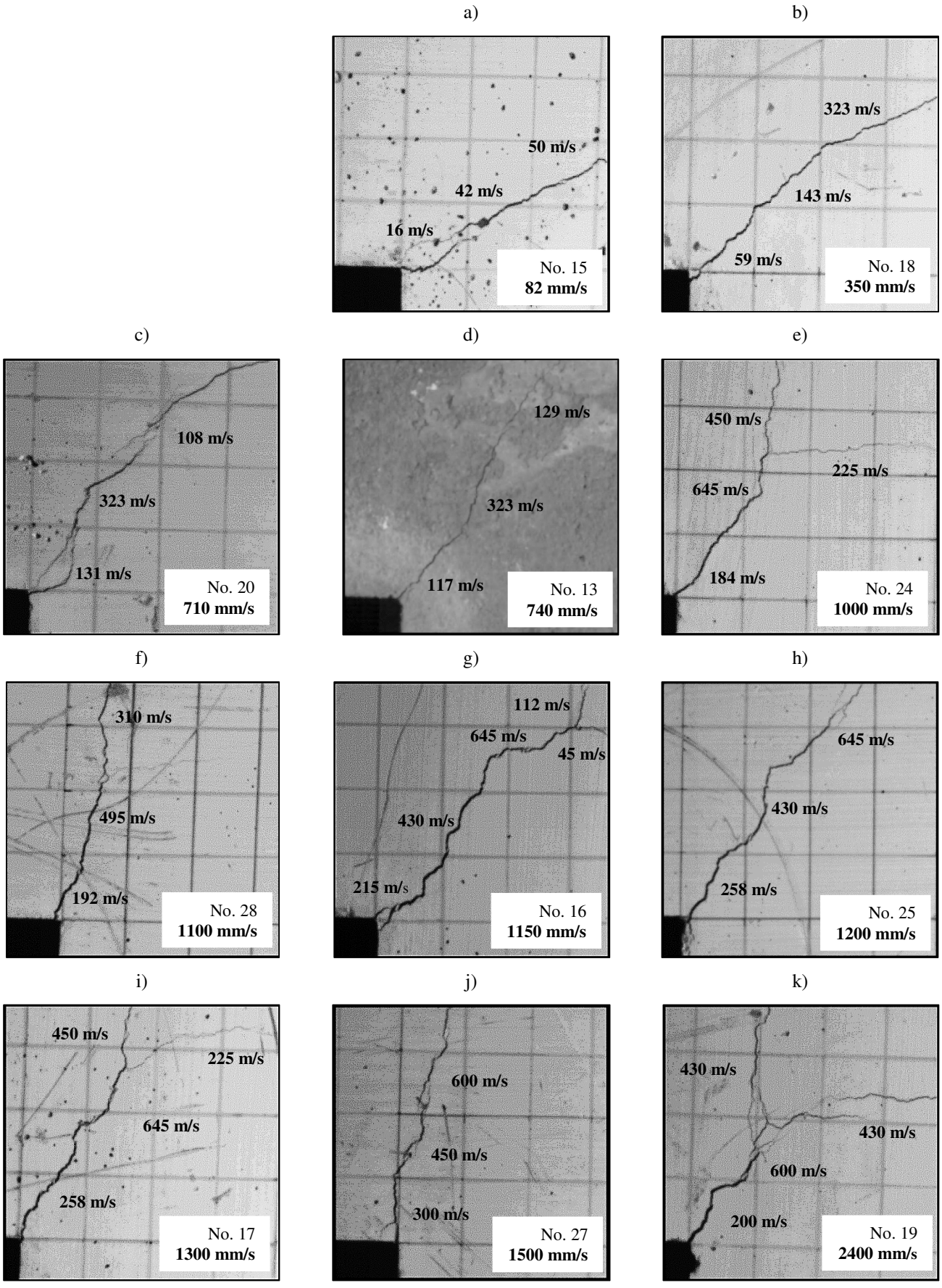

Figure 14. *Experimentally observed crack velocities for performed tests at different displacement rates.*

3.2.4 Conclusions

In the present experimental study the influence of the different loading point displacement rates on the fracture behaviour of concrete was investigated. Most of experimental investigations are focused only on certain material properties, such as rate dependent tensile strength and fracture energy. In contrast, there are very little information regarding the mechanism of concrete fracture due to dynamic loading. Therefore, the purpose of the experimental study was to determine the loading rate effect on the dynamic fracture behaviour of concrete in general, with particular emphasis on the rate dependent failure mode and crack velocity.

The used test setup is relatively simple and straight forward. The L-shaped concrete specimen is found to be a very interesting specimen to study effects of loading rate on dynamic fracture of concrete, particularly rate dependent failure mode. All of the tests were performed with the same testing machine. Loading was applied by prescribed displacement. The displacement rate of tested specimens ranged from 0.25 mm/s to 2400 mm/s. In summary, significant difference is found for low and high displacement rates.

From experimental results it is clear that peak load is rate dependent. The peak load varies from approximately 4 kN for quasi-static loading to 130 kN for displacement rate of 2400 mm/s. Hence, for relatively low displacement rates the peak load increases proportionally with increase of displacement rate and for higher displacement rates, higher than 100 mm/s, the peak load increases progressively. Furthermore, the experimental results also indicate that the loading rate has remarkable influence on the failure mode and crack propagation. In general, there is a tendency that with the increase of loading rates the failure mode changes from horizontal to vertical. For relatively low loading rates there is only one crack that is approximately perpendicular to the loading direction, however, with increase of displacement rate the crack becomes more inclined with respect to the loading direction. Besides, it is demonstrated that the number of cracks depends on the loading rate. When loading rate reaches approximately 1000 mm/s there is a crack branching and for even higher loading rates around 2400 mm/s multiple crack branching is observed. The results show that crack velocity also depends on the rate dependent failure pattern. According to this study the maximum crack velocity is around 650 m/s. The maximum crack velocity is measured just before crack branching and once the crack branches the velocity drops down. Finally, based on the

conclusions of the conducted experimental study it is confirmed that the experimental results confirm the predictions discussed in Ožbolt and Sharma (2012).

3.3 Notched plain concrete beam under impact load (Zhang et al. 2009, 2010a)

3.3.1 Introduction

In material science, drop hammer experiments are frequently used to study the behaviour of concrete under impact load. Recent experiments on pre-notched concrete beams were performed by Zhang et al. (2009, 2010a) using hydraulic and drop hammer test machines. The main aim of these experiments was to evaluate fracture energy of concrete under dynamic loading (impact) (Zhang et al. 2009). Additionally, information related to peak strains, average strain rates and crack propagation velocity are given in Zhang et al. (2010a). More detail on this experimental study can be found in their publications (Zhang et al. 2009, 2010a, 2010b). Here, only a brief description of the tests and their results is presented.

3.3.2 Experimental procedure

3.3.2.1 Material properties and specimen geometry

Material properties of high strength concretes (HSC) used in the experiments are summarized in Table 4 (Zhang et al. 2009, 2010a). The classification of concrete is C100/115 in reference to EN 206-1. The same experiments were performed on two similar high strength concrete mixtures. The dimensions of the tested beams were 100 x 100 x 400 mm (widith x depth x length) and the initial notch-depth ratio was 0.5. The span was fixed at 300 mm during the tests.

Table 4. *Mechanical properties of HSC.*

	Zhang et al. (2009)	Zhang et al. (2010a)
Young's modulus, E_c (GPa)	43.3	31.0
Poisson's ratio (assumed value), ν_c	0.18	0.18
Mass density, ρ_c (kg/m^3)	2400	2368
Tensile strength, f_t (MPa)	6.3	5.4
Compressive strength, f_c (MPa)	127.0	102.7
Fracture energy, G_F (J/m^2)	148	141

3.3.2.2 Test setup

The test setup and specimen geometry are depicted in Figure 15. The beams were simply supported with two rigid steel cylinders fixed at a span of 300 mm. Impact load was applied by dropping weight hammer of 120.6 kg on the top surface of the beam at the mid-span. The

striking head of the hammer was formed in a semi-cylindrical shape. During impact the hammer strikes the beam surface only with its apex. Five different loading rates were applied. At low loading rates (5.50×10^{-4} and 1.74×10^{1} mm/s) tests were performed under displacement control (quasi-static), while the high loading rates (8.81×10^{2}, 1.76×10^{3} and 2.64×10^{3} mm/s) were achieved by dropping the hammer from different heights (40, 160 and 360 mm).

a) b)

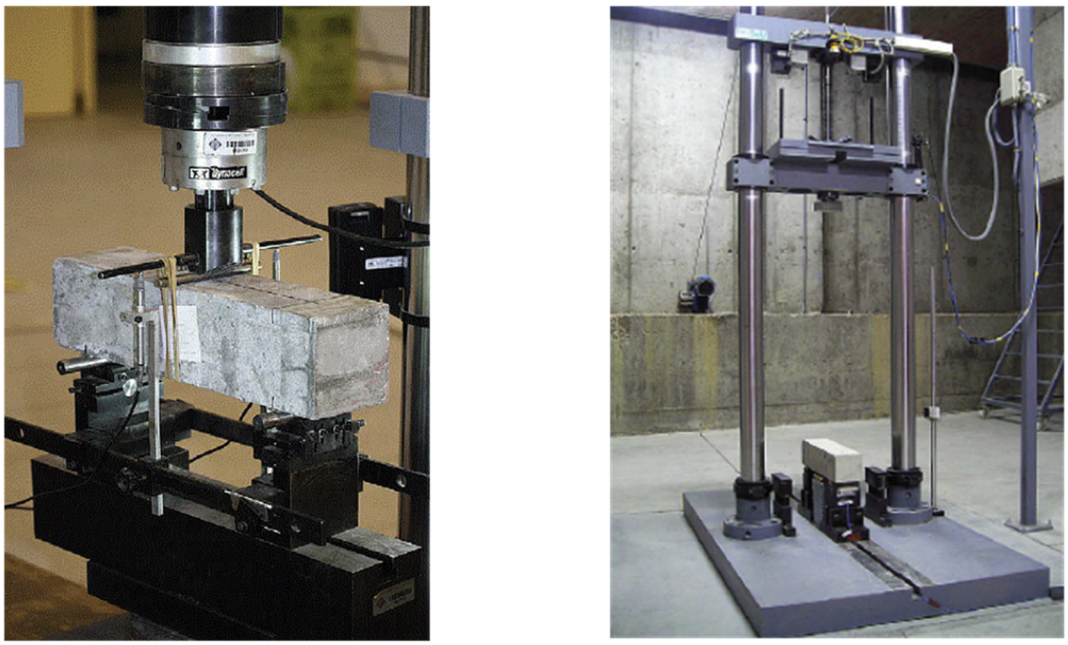

Figure 15. *a) Photo of experimental setup for three point bending tests on beams and b) photo of the drop weight impact machine (Zhang et al. 2009).*

3.3.2.3 Measuring equipment

The impact force between the hammer tup and the specimen is measured by a piezoelectric force sensor, with the measurement range up to 177.92 kN. The reaction force between the support and the specimen is determined by another two force sensors that can measure up to 89 kN. It was assumed that hammer displacement is equal to beam deformation. Based on that argument, the accelerometer was attached to the impact hammer and used to measure acceleration and displacement. Four strain gauges bonded on the front surface of the beam were used to measure the crack velocity. A more detailed description of instrumentation can be found in references (Zhang et al. 2009, 2010a).

3.3.3 Results and discussion

The loading rate effect on the peak load and fracture energy of the HSC at loading rates between 10^{-4} mm/s and 10^{3} mm/s has been studied. The tests from low to medium loading rates (up to 10 mm/s) were performed using hydraulic testing machine, while for the tests performed under high loading rates (impact velocities), a drop hammer test machine was utilized (Zhang et al. 2009, 2010a).

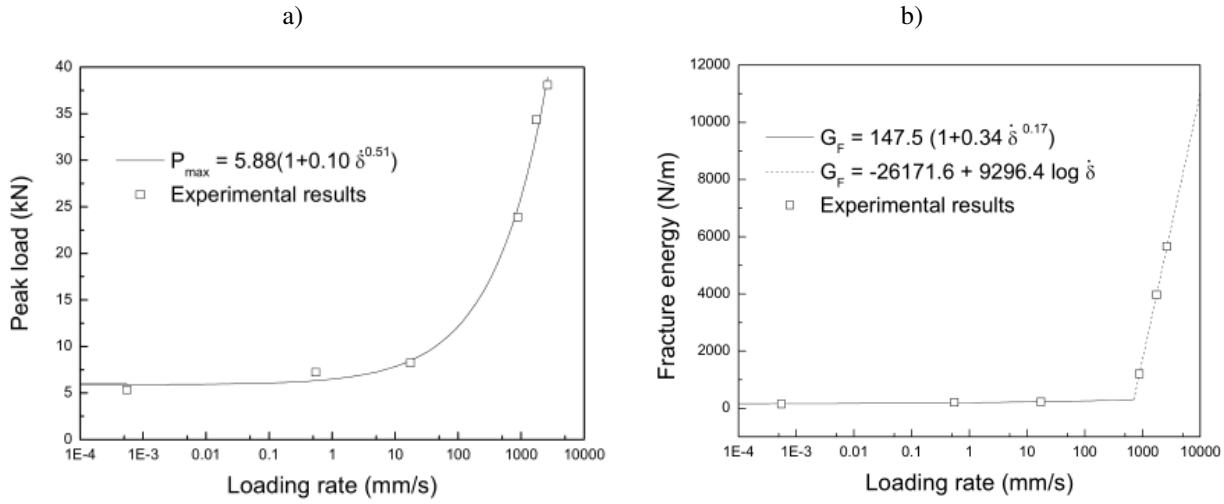

Figure 16. *Loading rate dependence of a) peak load and b) fracture energy (Zhang et al. 2009).*

It was reported that under dynamic loading, there is neither a standard nor any generally accepted procedure for measuring fracture energy. However, the authors evaluated fracture energy from the area under the reaction forces-displacement curve, where the reaction force is evaluated by adding the values from both support data points. Hence, the fracture energy was evaluated using the following expression (Zhang et al. 2009):

$$G_F = \frac{W_{\exp} + W_{num}}{B(D-a)} \tag{1}$$

where, W_{exp} is the area under the experimental load-displacement curve, W_{num} is the unmeasured energy due to the unbroken portion of ligament at the end of test, B is the width of specimen, D is the depth of the specimen and a is the notch depth, recommended by Elices et al. (1992, 1997), Guinea et al. (1992) and Planas et al. (1992). The results show that both the fracture energy and the peak load increase with increases in the loading rates, however, under low loading rates, such tendency is slight, while under high loading rates it is

significant (see Figure 16). Based on this results it is reported that the dynamic increase factor of the peak load is 7.14 and for the fracture energy much greater, 38.23.

3.3.4 Conclusions

Zhang et al. (2009, 2010a) performed tests on notched beams under three point bending. The impact velocity was varied from low (order of 10^{-4} mm/s) to medium (order of 10 mm/s) and to high (order of 10^{3} mm/s). For the tests performed under high loading rates (impact velocities), a drop hammer test machine was utilized (Zhang et al. 2009, 2010a). Based on the results of these experiments the fracture energy under dynamic load was attempted to be evaluated.

It was reported that under dynamic loading, there is neither a standard nor any generally accepted procedure for measuring fracture energy. Nevertheless, the authors evaluated fracture energy based on the area under the reaction forces-displacement curve (Zhang et al. 2009). The results of evaluation of the tests show a sudden rise in the fracture energy as a function of loading rate beyond a certain critical value of loading rate. Similar observations were made for reaction (resistance) as a function of loading rate. It should be noted, however, that such procedure is applicable for evaluating fracture energy from tests performed under quasi-static loading condition, while it needs to be clarify whether such evaluation of fracture energy is also valid for dynamic loading, since at higher loading rates (impact) structural inertia significantly contributes to reaction forces, even if the material is linear elastic. Furthermore, the reasons for this sudden and progressive increase in fracture energy and tensile strength are not clearly understood. Thus, it is important to clarify and to understand the reasons for such sudden jumps in the fracture energy and resistance, which are considered as inherent material properties. Principally, the contribution of structural inertia should not be accounted for while evaluating tensile strength and fracture energy because they are material and not structural property. Therefore, to bring more light in to this problem, the experiments performed by Zhang et al. (2009, 2010a) are numerically replicated.

4. MODELING CONCRET UNDER DYNAMIC LOADING

4.1 Numerical framework

As discussed previously, the resistance and the failure mode of concrete structures/specimens are known to be significantly influenced by the loading rate (Malvar and Ross 1998, Bischoff and Perry 1995). There are principally three different effects, which have to be accounted for (Ožbolt et al. 2014): (1) the rate dependency of the growing micro-cracks (influence of inertia at the micro-crack level), (2) the viscous behaviour of the bulk material between the cracks (creep of concrete or viscosity due to the water content) and (3) the influence of inertia, which can significantly change the state of stresses and strains of the material. When modeling concrete in the framework of meso- or macro-continuum, the first two effects can be accounted for by the constitutive law while the third effect should be automatically accounted for through dynamic analysis where the constitutive law interacts with inertia. In other words, the rate sensitive material resistance comes from the pre-peak rate dependent response (viscosity and rate dependent growth of micro-cracks) whereas the contribution of structural inertia comes from inertia forces that are activated as a consequence of softening that takes place in the fracture process zone (Ožbolt et al. 2013a). In addition, it should be pointed out that there are different aspects of inertia that need to be considered. For instance, (i) structural inertia, which is present even in case of elastic analysis, (ii) inertia activated due to the material softening (e.g. lateral compressive forces in uniaxial compression tests), or (iii) inertia at the crack tip that is responsible for crack branching.

For the model to be realistic, it should be able to correctly account for the interaction between inertia and constitutive law in order to account for phenomena such as crack branching or change of failure mode due to the increase of loading rate. Standard macroscopic plasticity or damage based models have a limitation to predict, for instance, crack branching phenomena without additional energy criteria. Such models can not automatically account for the progressive increase of resistance, and therefore the progressive increase must be included as a part of the constitutive law itself. Consequently, the resistance may be correctly predicted, however, the failure mode and crack pattern might be incorrect.

It is important for the correct prediction of the resistance and failure modes that the contribution of inertia is considered explicitly through dynamic analysis and not through the adjustments in the constitutive law. At the same time, the constitutive law must interact correctly with the dynamic analysis. As stated before, for quasi-brittle materials, such as concrete, the first two effects are important for relatively low and medium strain rates. For higher strain rates (impact) the influence of inertia dominates, however, the rate dependency cannot be neglected. Further detailed discussion can be referred to Ožbolt et al. (2014).

4.2 Finite element program

In this work, both static and dynamic numerical FE analysis is performed. In order to investigate rate dependent behaviour of concrete explicit 3D finite element code developed by Irhan (2014) is employed. The code is formulated in the framework of continuum mechanics following basic principles of irreversible thermodynamics. As a constitutive law, the rate dependent microplane model for concrete based on relaxed kinematical constraint (Ožbolt et al. 2001a) is used. Material model is extended to account for large displacements and deformations (Irhan 2014). Large deformation frictional contact problem is solved by predictor-corrector type algorithm in which kinematical contact constraints are enforced by a Lagrange multiplier penalty method. To obtain results objective with respect to the element size, crack band approach is employed as a regularization method (Bažant and Oh 1983, Ožbolt and Bažant 1996).

Finite element meshes (pre-processing) and results preview (post-processing) were conducted using commercial program package FEMAP. In static and dynamic analysis, the numerical spatial discretization is performed by the linear tetrahedral finite elements. A short description of fundamental concepts and features of 3D FE code for nonlinear multi-body dynamic analysis of concrete (Irhan 2014) is given. For more details see Irhan (2014).

4.2.1 Transient finite element analysis

The static FE analysis is performed using an implicit 3D FE code, which is based on the incremental secant stiffness approach (Belytschko et al. 2001). In the 3D transient multi body dynamic FE analysis, the system of unknown displacements in each time step Δt is calculated by solving the following system of equations (Voigt notation):

$$\mathbf{M}\ddot{\mathbf{u}}(t)+\mathbf{C}\dot{\mathbf{u}}(t)+\mathbf{G}^{T}(u,t)\,\boldsymbol{\lambda}+{}^{int}\mathbf{f}(t)={}^{ext}\mathbf{f}(t) \tag{2a}$$

with: ${}^{con}\mathbf{f}(t)=\mathbf{G}^{T}(u,t)\,\boldsymbol{\lambda}$

$$\mathbf{G}(u,t)\{\mathbf{u}+\mathbf{X}\}=\mathbf{0} \tag{2b}$$

where **M** = mass matrix, **C** = damping matrix, $\ddot{\mathbf{u}}$ = nodal accelerations, $\dot{\mathbf{u}}$ = nodal velocities, $\mathbf{u}$ = nodal displacements, ${}^{int}\mathbf{f}(t)$ = internal nodal forces, ${}^{ext}\mathbf{f}(t)$ = external nodal forces, ${}^{con}\mathbf{f}(t)$ = contact nodal forces, **X** is the material coordinate vector, **G** is the element contact displacement constrain matrix and $\boldsymbol{\lambda}$ is the vector of unknown Lagrange multipliers (Belytschko et al. 2001).

The system of equations (2) is solved using an explicit direct integration scheme (Belytschko et al. 2001). The external nodal forces are known nodal loads. The internal nodal forces are unknown and they are calculated by the integration of the stresses over the finite elements. In the FE code used in the numerical study the mass and damping matrices are assumed to be diagonal.

4.2.2 Contact detection and resolution

If the weak (integral) form of balance equation for linear momentum is discretized with finite elements, time-continuous space-discrete dynamic nodal equilibrium equations (Eq. 2a) can be written as (Irhan 2014):

$$m_I\mathbf{a}_I={}^{ext}\mathbf{f}_I-\left[{}^{int}\mathbf{f}_I+{}^{con}\mathbf{f}_I\right] \qquad (I=1\ldots nnd) \tag{3}$$

where m_I, $\mathbf{a}_I$, ${}^{ext}\mathbf{f}_I$, ${}^{int}\mathbf{f}_I$, ${}^{con}\mathbf{f}_I$ are, respectively, lumped mass, acceleration, external force, internal force and contact force associated with generic global node *I, nnd* denotes total number of nodes. Next we consider time-discrete version of Eq. (3) and rewrite it for a typical time step t^k corresponding to a known state as:

$$m_I\mathbf{a}_I^k={}^{tot}\mathbf{f}_I^k \tag{4}$$

with

$$ {}^{tot}\mathbf{f}_I^k := {}^{ext}\mathbf{f}_I^k - {}^{int}\mathbf{f}_I^k - {}^{con}\mathbf{f}_I^k \tag{5} $$

where ${}^{tot}\mathbf{f}_I^k$ = total nodal forces.

Using second order central differences, nodal acceleration can be approximated as:

$$ \mathbf{a}_I^k \cong \frac{\Delta\mathbf{x}_I^k - \Delta\mathbf{x}_I^{k-1}}{\Delta t^2} \tag{6} $$

Combining Eq. (4) and Eq. (6), an explicit expression for position update is obtained as:

$$ \Delta\mathbf{x}_I^k = \frac{\Delta t^2}{m_I} {}^{tot}\mathbf{f}_I^k + \Delta\mathbf{x}_I^{k-1} \text{ where } \mathbf{x}_I^{k+1} = \mathbf{x}_I^k + \Delta\mathbf{x}_I^k \tag{7} $$

In the presence of contact interactions, unfortunately, position update cannot be performed in single step because contact forces are not known beforehand. One can remedy such a situation by setting up a predictor-corrector type algorithm. In the algorithm, $\Delta\mathbf{x}_I^k$ is first additively decomposed as:

$$ \Delta\mathbf{x}_I^k = {}_p\Delta\mathbf{x}_I^k + {}_c\Delta\mathbf{x}_I^k \tag{8} $$

where ${}_p\Delta\mathbf{x}_I^k$, ${}_c\Delta\mathbf{x}_I^k$ are, respectively, predictor (known) and corrector (unknown) position increments.

In the predictor step node-level update is performed assuming that no contact takes place within the current time increment. Therefore for node *I* we have:

$$ {}^{tot}_{p}\mathbf{f}_I^k = {}^{ext}\mathbf{f}_I^k - {}^{int}\mathbf{f}_I^k \tag{9a} $$

$$ {}^{con}\mathbf{f}_I^k \overset{!}{=} \mathbf{0} \tag{9b} $$

where ${}^{tot}_{p}\mathbf{f}_I^k$ is total predictor force acting on node *I*. From Eq. (7), predictor position increment and predictor position itself are obtained as:

$$ {}_{p}\Delta\mathbf{x}_I^k = \frac{\Delta t^2}{m_I} {}^{tot}_{p}\mathbf{f}_I^k + \Delta\mathbf{x}_I^{k-1} \text{ where } {}_{p}\mathbf{x}_I^{k+1} = \mathbf{x}_I^k + {}_{p}\Delta\mathbf{x}_I^k \tag{10} $$

Next, based on predictor position given by Eq. (10), a global contact search is performed and it is checked if there are some nodes for which impenetrability constraint is violated. If there is violation, one has to take another step and compute corrector position increment ${}_{c}\Delta\mathbf{x}_I^k$ due to unknown contact force ${}^{con}\mathbf{f}_I^k$. For the moment assume that it is possible to compute contact force using the predictor positions of contributing nodes in some way. With ${}^{con}\mathbf{f}_I^k$ at hand, corrector position increment can be computed from Eq. (7) as:

$$ {}_{c}\Delta\mathbf{x}_I^k = -\frac{\Delta t^2}{m_I} {}^{con}\mathbf{f}_I^k \tag{11} $$

Contact problem is formulated on an auxiliary discretization constructed based on node-to-surface contact finite elements (Wriggers 2006, İrhan 2014). Then, in most general form, nodal contact force can be expressed as:

$$ {}^{con}\mathbf{f}_I^k = \sum_{e=1}^{nel} {}^{con}_{e}\mathbf{f}_I^k \tag{12} $$

In Eq. (12), ${}^{con}_{e}\mathbf{f}_I^k$ is the contribution of *e*-th contact finite element connected to node *I* and *nel* denotes total number of contact finite elements connected to node *I*. If Lagrange multiplier method is employed for constraint enforcement, contact force ${}^{con}_{e}\mathbf{f}_I^k$ has the form:

$$ {}^{con}_{e}\mathbf{f}_I^k = \alpha_I \boldsymbol{\lambda}_e \tag{13} $$

In Eq. (13), weighting factor α_I is equal to 1.0 if node *I* is associated with penetrated slave particle, otherwise it is a function of local coordinates corresponding to partner master particle

located on master surface associated with penetrated slave particle, $\boldsymbol{\lambda}_e$ is the contact force (Lagrange multiplier) transmitted over *e*-th contact finite element connected to node *I*. $\boldsymbol{\lambda}_e$ can be computed by exploiting kinematical contact constraints for element *e* in normal and tangential directions. Using Eq. (11) and Eq. (13), corrector position increment due to element *e* turns out to be:

$$ {}^{e}_{c}\Delta\mathbf{x}^{k}_{I} = -\Delta t^{2}\gamma_{I}\boldsymbol{\lambda}_{e} \text{ with } \gamma_{I} := \frac{\alpha_{I}}{m_{I}} \tag{14} $$

Using predicted positions of the nodes connected, predictor gap vector for element *e* can be written as:

$$ {}^{e}_{p}\mathbf{g} = \sum_{j=1}^{4} \alpha_{J(j)} \; {}_{p}\mathbf{x}^{k+1}_{J(j)} \tag{15} $$

By employing Eq. (15), corrector gap vector is written as:

$$ {}^{e}_{c}\mathbf{g} = \sum_{j=1}^{4} \alpha_{J(j)} \; {}^{e}_{c}\Delta\mathbf{x}^{k}_{J(j)} \tag{16} $$

With the insertion of Eq. (14) into Eq. (16), it is obtained that:

$$ {}^{e}_{c}\mathbf{g} = -\Delta t^{2}\theta\,\boldsymbol{\lambda}_{e} \tag{17} $$

with

$$ \theta := \sum_{j=1}^{4} \alpha_{J(j)}\,\gamma_{J(j)} = \sum_{j=1}^{4} \alpha^{2}_{J(j)} / m_{J(j)} $$

Note that for $j = i$ we have $J(j) = I$. If partner master particle on master surface is located based on trajectory of penetrated slave particle, kinematical contact constraints in normal and tangential directions for that element can be formulated purely based on gap vector, i.e.

$$ {}^{e}\mathbf{g} = {}^{e}_{p}\mathbf{g} + {}^{e}_{c}\mathbf{g} = \mathbf{0} \tag{18} $$

If, instead, partner master particle is located based on conventional closest-point projection algorithm, resulting gap vector does not have any tangential component by construction. Therefore in such a case kinematical contact constraint in tangential direction must be formulated based on gap rate ${}^{e}\dot{\mathbf{g}}$.

Substituting Eq. (17) into Eq. (18), contact force is then obtained as:

$$ \boldsymbol{\lambda}_{e} = \frac{1}{\Delta t^{2}\theta}\, {}^{e}_{p}\mathbf{g} \tag{19} $$

In tangential contact direction material behaviour is assumed to be governed by non-smooth non-associative Mohr-Coulomb type frictional model. Therefore tangential component of the contact traction given by Eq. (19) must be corrected if there is a slip. The form given by Eq. (19) gives us the possibility to smooth out material behaviour in tangential direction and employ return mapping algorithm, based on stick predictor slip corrector steps, to perform constitutive update. With the insertion of Eq. (19) into Eq. (14) corrector position increment due to element *e* takes the final form as:

$$ {}^{e}_{c}\Delta\mathbf{x}^{k}_{I} = -\frac{\gamma_{I}}{\theta}\, {}^{e}_{p}\mathbf{g} \tag{20} $$

As can be grabbed from Eq. (20), integration coefficient Δt^2, consistent with central difference approximation employed, drops out during back-substitution. This cancellation reveals the fact that integration coefficient does affect the magnitude of contact force but actually has no role in the computation of position increments. Therefore its value does not change overall global pure mechanical response of the system in case of both stick and slip.

If the master surfaces belonging to contact finite elements are not connected to each other, the global contact problem reduces down to local contact problem at element level. Therefore with contact algorithm discussed above contact constraints can be resolved at element level and exactly satisfied without any problem. On the other hand, if there are some surfaces

connected to each other, one has to first assemble contact forces at common nodes, as given by Eq. (12), and then compute the corrector position increments accordingly from Eq. (11). However with such an update corresponding position increment will be the summation coming from all neighbor contact finite elements. It is obvious that in such a case exact fulfillment of contact constraints within neighbor elements is not possible. Therefore an iterative solution method has to be employed. For this purpose a robust procedure based on elemental updates in the form of Gauss-Seidel iteration has been developed (Carpenter et al. 1991, İrhan 2014). Note that after converged state is reached, there still remains some amount of residual penetration within each connected contact element. This, of course, contradicts with the nature of Lagrange multiplier method employed for the solution of contact problem. In addition, from Eq. (19), it comes out that contact force is expressed as a function of gap vector, i.e. one can derive an expression for penalty parameter for each contact element separately such that contact constraints are exactly satisfied for those which are not connected. Therefore it is better to call method of constraint enforcement described out here as penalty with varying parameters instead of Lagrange multiplier (İrhan 2014).

4.3 Material constitutive model

4.3.1 General

Over the past few years many researchers have put significant effort to model concrete like materials for general stress-strain histories. Currently available models for concrete can be broadly classified as: (1) macroscopic modes, in which the material behaviour is considered to be an average response of rather complex microstructural stress transfer mechanism and (2) microscopic models, where the micromechanics of deformations is described by stress-strain relations on the microlevel (Ožbolt et al. 2001a). From a physical point of view, microscopic models are more promising but they are computationally extremely demanding. On the other hand, the macroscopic phenomenological model may not be applicable over the whole range of deformation histories and stress states. However, at the macroscale the model should be able to correctly describe micro-structural phenomena such as cohesion, friction, aggregate interlocking and interaction of microckracks. The microplane model offers such a modeling technique.

4.3.2 Microplane material model

In the microplane model the material response is calculated based on the monitoring of stresses and strains in different predefined directions. Integrating microplane stresses in a thermodynamically consistent way, it is possible to calculate macroscopic stress tensor from a known macroscopic strain tensor. The constitutive framework is similar to discrete type of the models (e.g. random particle model) with the difference that the model is formulated in the framework of continuum. The physical concept behind the microplane model was discussed at the beginning of last century by Mohr (1900) and Taylor (1938).

The here employed microplane model is based on the so-called relaxed kinematic constraint concept (Ožbolt et al. 2001a). In the model, material is characterized by the uniaxial relation between stress and strain components on planes of various orientations, called microplanes. The microplanes may be imagined to represent damage planes or weak planes in the microstructure, such as those that exist at the contact between aggregate and the cement matrix (Ožbolt et al. 2001a).

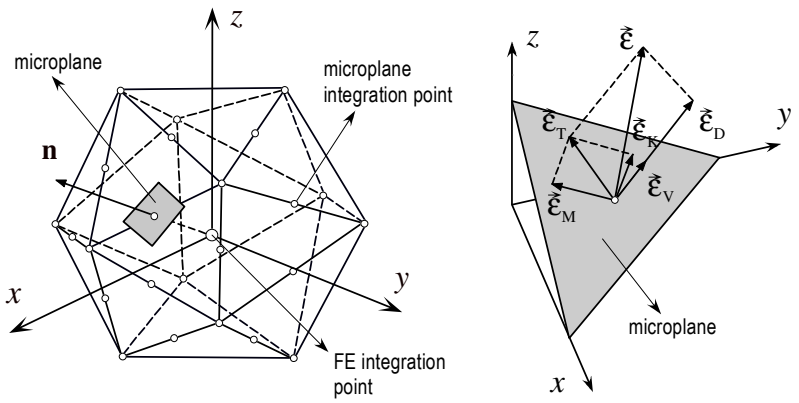

Figure 17. *Decomposition of the macroscopic strain vector into microplane strain components-normal (volumetric and deviatoric) and shear.*

Each microplane is defined by its unit normal vector components n_i (Figure 17). Microplane strains are assumed to be the projections of macroscopic strain tensor ε_{ij} (kinematic constraint). On the microplane are considered normal (σ_N, ε_N) and two shear stress-strain components (σ_M, σ_K, ε_M, ε_K). To realistically model concrete, the normal microplane stress and strain components have to be decomposed into volumetric and deviatoric parts ($\sigma_N = \sigma_V+\sigma_D$, $\varepsilon_N = \varepsilon_V+\varepsilon_D$). Unlike to most microplane formulations for concrete, which are based

on the kinematic constrain approach, to prevent unrealistic model response for dominant tensile load, for strong localization of strains kinematic constrain is relaxed (Ožbolt et al. 2001a). Based on the micro-macro work conjugancy of volumetric-deviatoric split and using in advance defined microplane stress-strain constitutive laws, the macroscopic stress tensor is calculated as an integral over all possible, in advance defined, microplane orientations (indicial notation):

$$\sigma_{ij} = \sigma_V \delta_{ij} + \frac{3}{2\pi}\int_S \left[\sigma_D \left(n_i n_j - \frac{\delta_{ij}}{3} \right) + \frac{\sigma_K}{2}\left(k_i n_j + k_j n_i\right) + \frac{\sigma_M}{2}\left(m_i n_j + m_j n_i\right) \right] dS \tag{21}$$

where S denotes the surface of the unit radius sphere and δ_{ij} denotes Kronecker delta and k_i and m_i are direction of shear microplane components. The integration is performed by numerical integration using 21 integration points (symmetric part of the sphere, see Figure 17). To account for large strains and large displacements, Green-Lagrange finite strain tensor is used. As a stress tensor co-rotational Cauchy stress tensor is employed. Detailed discussion of the features and various aspects related to the finite strain formulation of the microplane model are beyond the scope of the present work. More details may be obtained from Bažant et al. (2000) and Ožbolt et al. (2001a).

4.3.3 Microplane material model with rate sensitivity

The rate dependency in the here presented version of the microplane model for concrete (Ožbolt et al. 2001a) accounts for two effects: (i) the rate dependency related to the formation (propagation) of the micro-cracks, which is the effect of inertia forces at the level of the micro-crack tip, and (ii) the rate dependency due to the viscosity of concrete (bulk material) between the micro-cracks. Note that the influence of inertia at the macro scale (e.g. inertia at the macro crack tip or structural inertia) on the rate dependency is not a part of the constitutive law. This effect is automatically accounted for in dynamic analysis in which the constitutive law interacts with forces due to structural inertia.

In the present model, the rate dependent behaviour of concrete is modeled based on the rate process theory, similar to the concept proposed by Mihashi and Wittmann (1980). It is assumed that the micro-cracks start to grow immediately after the application of load. The initial stiffness, which is in experiments always measured as secant stiffness, is assumed to be

controlled by the rate of growing micro-cracks. Since in the model the out-coming strength is proportional to the initial stiffness, an increase in initial stiffness, because of higher strain rate, also causes an increase in strength.

The rate of strain $\dot{\varepsilon}$ in a continuum with a number of parallel cohesive cracks, which can be imagined to represent macroscopic strain softening, can be expressed as

$$\dot{\varepsilon} = \frac{\dot{w}}{s_{cr}} + \frac{\dot{\sigma}}{E} \approx \frac{\dot{w}}{s_{cr}} \tag{22}$$

where ε = average macroscopic strain normal to the direction of parallel cracks, s_{cr} = spacing of the parallel cracks, E = effective Young's modulus of bulk material and $\dot{\sigma} / E$ is the elastic strain ratio which can be, compared to the crack opening ratio $\dot{w}$, neglected. After introducing a few reasonable simplifications into the concept that is based on the energy activation theory (Krausz et al. 1988), the influence of the rate effect on the rate stress-strain relation $\sigma^0(\varepsilon)$ can be can be calculated according to

$$\sigma(\varepsilon) = \sigma^0(\varepsilon)\left[1 + C_2 \ln(\frac{2\dot{\varepsilon}}{C_1})\right] \tag{23}$$

where σ = stress at dynamic load, σ^0 = stress at static load, $\dot{\varepsilon}$ = strain rate, C_1 and C_2 are constants determined from experiments (Bažant et al. 2000a).

In the microplane model macroscopic response is obtained by integrating normal and shear microplane stresses over all microplanes. The rate independent microplane stress components $\sigma^0{}_M(\varepsilon_M)$ (M = stands for microplane volumetric, deviatoric and shear components, respectively) are calculated from the known microplane strains ε_M using pre-defined microplane uniaxial stress-strain constitutive relations (Ožbolt et al. 2001a). The strain rate independent model parameters are: Young's modulus, Poisson's ratio, uniaxial compressive and tensile strengths and fracture energy. These macroscopic properties are related to internal microplane parameters (Ožbolt et al. 2001a). It seems reasonable to assume that the rate effect on each microplane component is of the same type as given by (21). Consequently, the rate dependency for each microplane component reads (Ožbolt et al. 2006):

$$\sigma_M(\varepsilon_M) = \sigma_M^0(\varepsilon_M)\left[1 + c_2 \ln(\frac{2\dot{\gamma}}{c_1})\right] \text{ with } \dot{\gamma} = \sqrt{\frac{1}{2}\dot{\varepsilon}_{ij}\dot{\varepsilon}_{ij}} \quad c_1 = \frac{c_0}{s_{cr}} \tag{24}$$

where c_0 and c_2 are material rate constants, which have to be calibrated by fitting test data, ε_{ij} = components of the macroscopic strain rate tensor (indicial notation). From Eq. (24) is obvious that the rate magnitude is not measured on the individual microplanes, which would be not objective, but on the macro-scale. Furthermore, Eq. (24) applies to all microplane components except to volumetric compression, which is assumed to be rate insensitive. This is because for volumetric compression there is no crack development, i.e. the material is compacted.

The model parameters from (24) are calibrated (Ožbolt et al. 2006) based on the uniaxial compressive tests performed by Dilger et al. (1984). The tests have been carried out for three loading rates: 0.2/s, 3.33×10^{-3} /s and 3.33×10^{-5}/s. Assuming average crack spacing of s_{cr} = 100 mm, the following values are obtained from the calibration procedure: $c_0 = 0.0004$ and $c_2 = 0.032$. Using these parameters, the rate dependent uniaxial compressive stress-strain curves are plotted for three different loading rates in Figure 18a. In the same figure, the test results are also shown. Figure 18b shows the model response in the case of a sudden increase and decrease of the strain rate for the compression softening. Similar behaviour was observed in the experiments (Bažant et al. 2000a). The influence of strain rate on the uniaxial compressive strength and initial Young's modulus is shown in Figure 19. In both Figures, the static strength and the static Young's modulus correspond to the strain rate of 10^{-5}/s for which the average test value of the ratio between dynamic and static strengths is equal to one. As can be seen, for medium strain rates up to approximately 1/s the microplane model prediction agrees well with the average trend observed in the experiments.

As mentioned above, the influence of structural inertia on the rate sensitive response is not a part of the constitutive model. By a number of numerical studies (Ožbolt et al. 2005, 2006, 2012, 2013b, 2014) it was demonstrated that inertia effect, which cause a kind of homogenization of the material, is accounted for automatically in dynamic analysis through the interaction between inertia forces (stresses) and constitutive law. The effect is here illustrated on the example of concrete cylinder of normal strength concrete (Young's modulus

E_c = 35000 MPa, Poisson's ratio ν = 0.18, tensile strength f_t = 2.25 MPa, uniaxial compressive strength f_c = 23 MPa and concrete fracture energy G_F = 0.08 N/mm; cylinder diameter D = 50 mm and height H = 100 mm) loaded by different strain rates. To demonstrate the influence of inertia, rate sensitive static and dynamic analysis were carried out. The relation between the relative compressive strength (resistance) and strain rate is plotted in Figure 20. The results of the rate dependent static analysis show almost linear increase of relative strength as a function of strain rate (log-log scale). The outcome of rate sensitive dynamic analysis for medium strain rates shows the same tendency. However, similar as in the experiments (Bischoff and Perry 1991), after reaching strain rate of about 10/s the increase of resistance becomes progressive. Obviously, the results clearly show that inertia forces are responsible for the progressive increases obtained in the dynamic analysis. For comparison a curve proposed by CEB (1988) is also shown. As can be seen, the agreement between test data, CEB prediction formula and numerical results is very good.

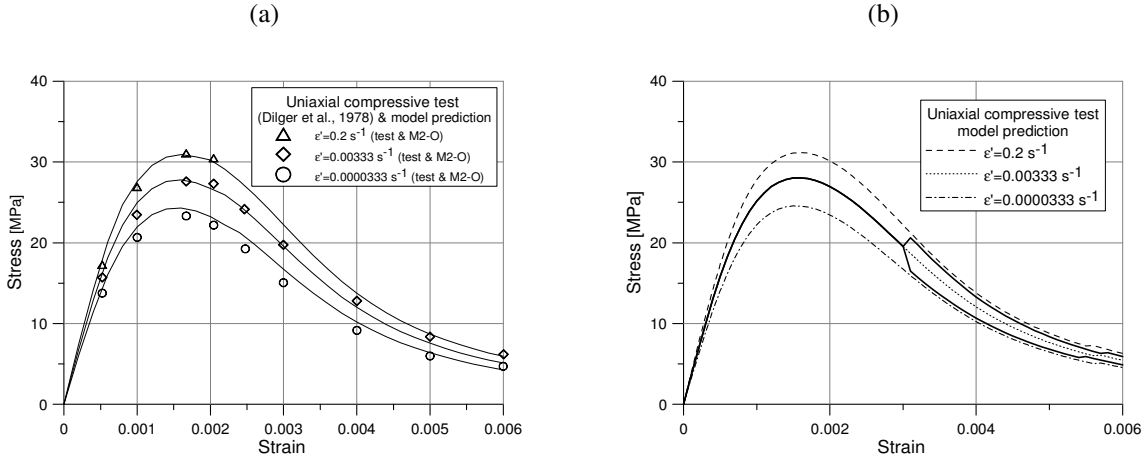

Figure 18. *Uniaxial compressive test (Ožbolt et al. 2006) (a) model prediction and test data (Dilger et al. 1978) and (b) model prediction – increase and decrease of the loading rate in the softening region.*

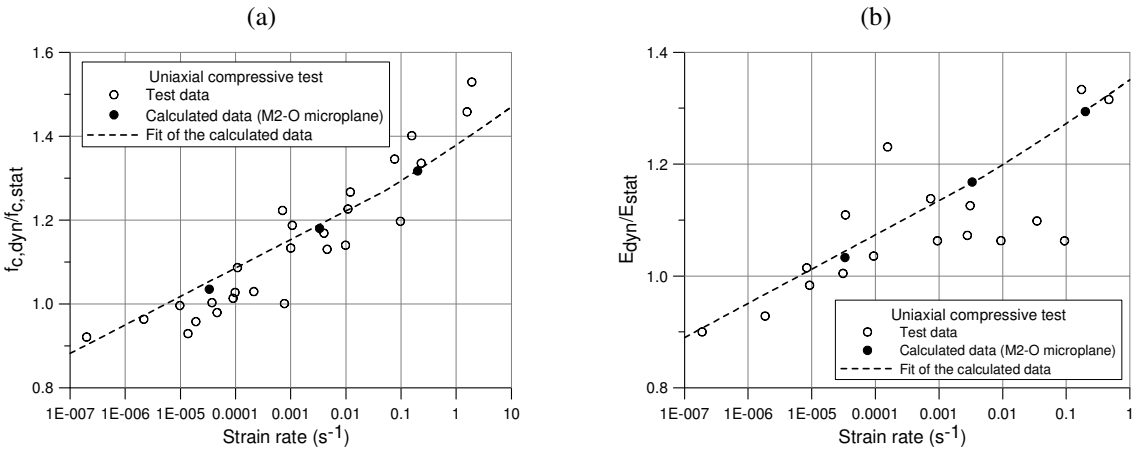

Figure 19. *Uniaxial compressive test (Ožbolt et al. 2006) (a) rate dependent compressive strength–test data and model prediction and (b) rate dependent initial Young's modulus - test data and model prediction.*

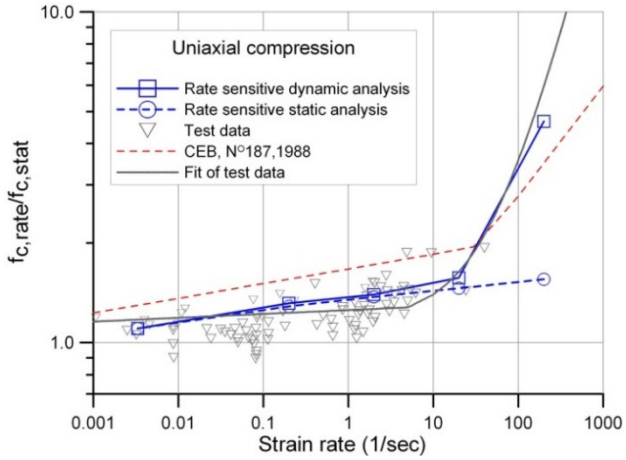

Figure 20. *Relative compressive strength as a function of strain rate (Ožbolt et al. 2006).*

5. NUMERICAL EXPERIMENTS

In this chapter the capability of recently developed explicit 3D FE code CIF (Irhan 2014) to model the fracture behaviour of concrete under dynamic loading is studied. Rate sensitive microplane model (Ožbolt et al. 2001a) has been employed as the material model, while the effect of inertia is accounted for by explicit dynamic analysis. For quasi-static loading conditions the analysis is carried out using 3D FE code MASA (Ožbolt et al. 2001a). The correlation between experimental and numerical results is given through the experiments described in Chapter 3. Finally, after the verification process, material strength and fracture energy at high loading rates are briefly discussed. At the end, summary and conclusions are drawn out.

5.1 L-shaped concrete specimen under high loading rate

To better understand the results of the experimental tests and to verify the 3D FE code (Irhan 2014), the results of numerical analyses are compared with data obtained from experiments on L-specimens subjected to different loading rates. All details regarding the experiment, i.e. setup, testing procedure and results are provided in Chapter 3. The comparison of numerical results against experiment is performed in terms of load-displacement curves, load-time history curves, crack patterns and crack velocity propagation. The reliable numerical simulation of the failure patterns plays an important role in the accurate prediction of dynamic response of concrete structures. Hence, it is important to see if the same failure mode is obtained in the numerical analysis as in the experiment. In order to fully understand the effect of loading rate on concrete fracture as well as to gain more insight into the behaviour at the material level, the influence of some relevant parameters that are difficult to observe experimentally, are studied by employing numerical model. The numerically investigated parameters are: strain rate, crack opening rate, rate dependent fracture energy and rate dependent tensile strength.

5.1.1 Finite element model

The geometry, boundary conditions, loading and finite element mesh of the specimen model are depicted in Figure 21. The geometry, boundary conditions and loading are same as in the

experiment. The spatial discretization is performed by four node solid finite elements. To simulate the real restraints as in the experimental test, the bottom nodes on the back surface of the L-specimen, area of size 250 x 100 mm, are restrained from movement in all directions (three translations) (Figure 21). Also, same as in the experiment, the load is applied in a displacement control fashion. Furthermore, in simulations the load is distributed over the same cross sectional area as observed in tests. A typical displacement-time curve as recorded in test (see Figure 22) is approximated, and employed in simulations, by giving the displacement (loading) rates at the bottom surface of the vertical edge of the specimen as shown in Figure 21b.

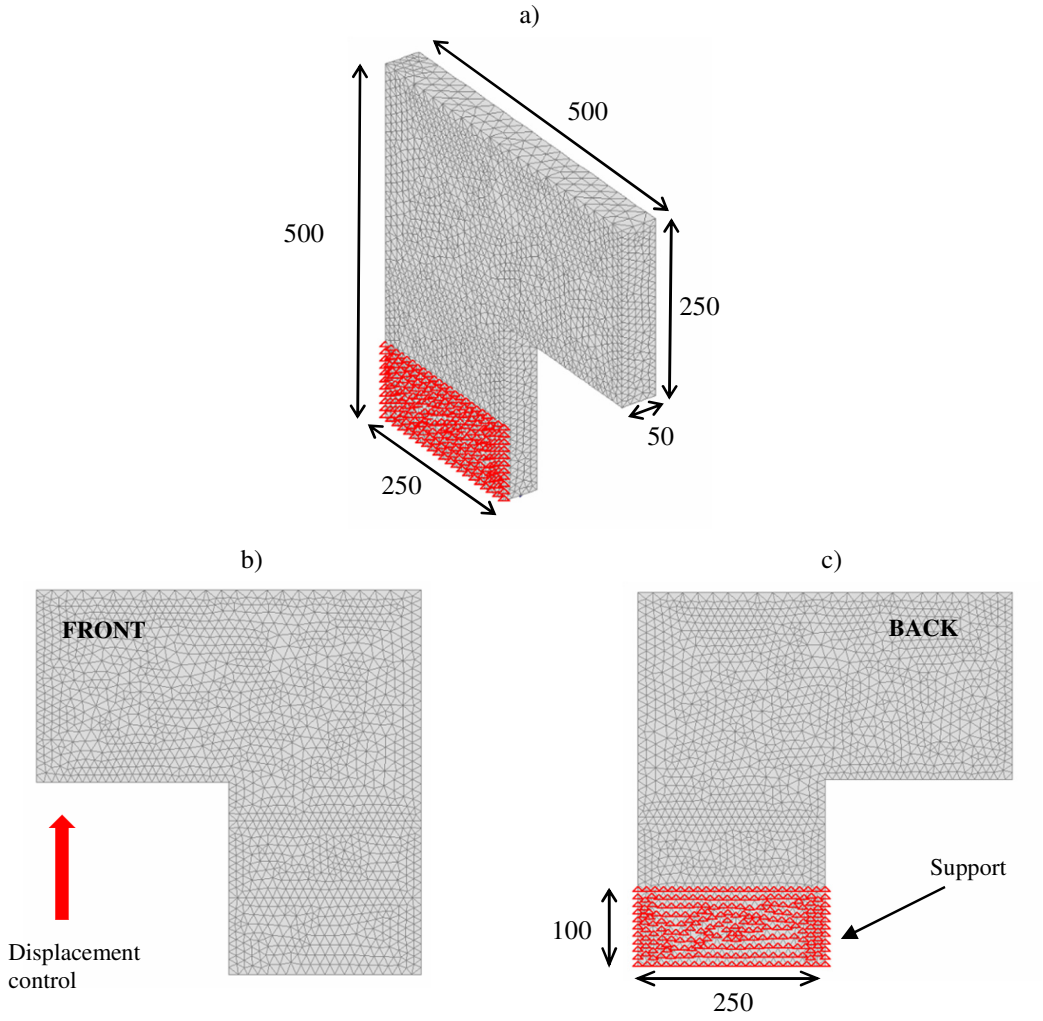

Figure 21. *Geometry (all in mm), finite element mesh, loading (displacement control) and boundary conditions.*

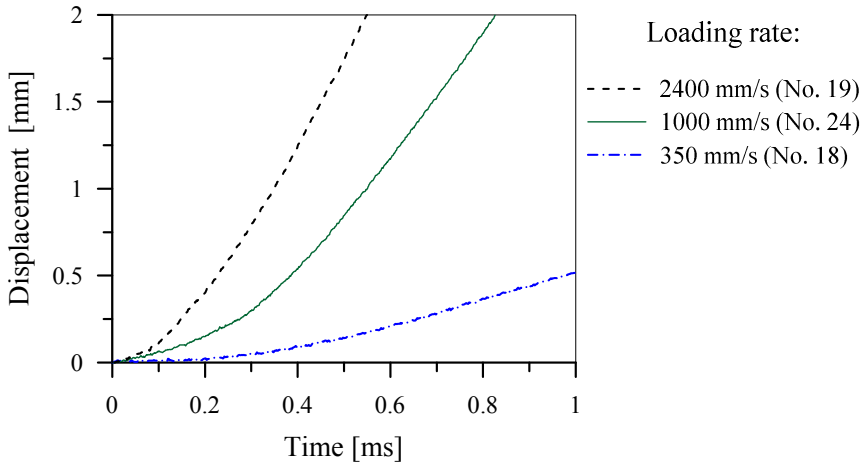

Figure 22. *Typical displacement-time response as reported from experiments for different loading rates.*

The overview of concrete properties used in the finite element study is summarized in Table 5. The material fracture properties are estimated from the experimentally measured data using equations given in literature (Karihaloo 1995). From the 12 performed tests, 7 different displacement rates are used in numerical analyses. The experimental data are chosen such that they cover the range of displacement rates studied in test (2.5×10^{-1} mm/s through 2.4×10^{3} mm/s). The specimen was first analyzed employing quasi-static loading conditions. This is assumed to be comparable to specimen loaded with a displacement rate of 2.5×10^{-1} mm/s. Subsequently, dynamic analysis is carried out with the following displacement rates: 8.2×10, 3.5×10^{2}, 7.4×10^{2}, 1×10^{3}, 1.5×10^{3} and 2.4×10^{3} mm/s.

Table 5. *Overview of the material properties used in numerical analysis.*

Young's modulus, E_c (GPa)	32.2
Poisson's ratio (assumed value), v_c	0.18
Mass density, ρ_c (kg/m^3)	2210
Tensile strength, f_t (MPa)	3.12
Compressive strength, f_c (MPa)	46.25
Fracture energy, G_F (J/m^2)	58.56

5.1.2 Calibration of numerical model

Although the results of numerical simulations performed recently by Ožbolt and Sharma (2012) have shown to give good predictions of the crack patterns, i.e. with increase of loading rate the crack propagation direction is changing from horizontal to vertical, comparing the tests results and results of numerical predications it is quite clear that there is a need for

parametric study in order to calibrate the numerical model. However, keeping in mind that relatively simple 2D model (1 row of elements) under assumption of plane strain condition was used in numerical prediction (Ožbolt and Sharma 2012) it can be stated that the used numerical model capture the crack patterns with reasonable accuracy.

Generally, damping plays an important role in the accurate prediction of dynamic response of concrete structures. As discussed by Travaš (2009), the response of real structures to external forces is always accompanied by a certain amount of energy dissipation manifested through the damping behaviour of structure oscillations. However, for high energy impact loadings the presence of viscous damping forces can be ignored due to low amplitude of oscillations. Accordingly, the influence of viscous damping is studied and discussed. To this end, set of numerical simulations have been performed to study the sensitivity of numerical results with respect to damping value. In the proposed numerical simulations following damping values are studied: 0/s (no damping), 100/s, 1000/s, and 10000/s. Here, in order to calibrate the numerical model by experiments, investigation is done for the specimen No. 13 with loading rate of 740 mm/s. The crack patterns computed employing four above mentioned damping values are shown in Figure 23. They can be compared with the experimentally observed crack pattern shown in Figure 13e (740 mm/s). The crack (dark zone) is presented in terms of principle tensile strains larger than critical strain where critical strain is calculated as critical crack opening (w_{cr} = 0.1 mm) divided by the average element size (h = 10 mm). Hence, the critical strain is obtained as 0.01 (smeared crack approach).

Figure 24 shows a comparison of the load, measured in the test, with the respective computed values. Obviously, results obtained from numerical simulations are very sensitive to the damping value. With too high damping the value of maximum load is overestimated. The deviation of the computed crack path from the experimental one is also reflected by the overestimation of the load. For that reason the crack propagation in model with to high damping value seems to be unrealistic. On the other hand, damping values smaller than approximately 1000/s do not significantly influence load time response neither crack pattern, i.e. results show convergence with decrease of damping value. Namely, based on this study it can be concluded that for viscous damping smaller than 1000/s numerical model gives reliable predictions of the load and crack pattern. Even if the viscous damping is ignored, no change in overall response is observed. In the present model, the viscous damping is chosen to be 100/s and all simulations in the following section are performed using this value.

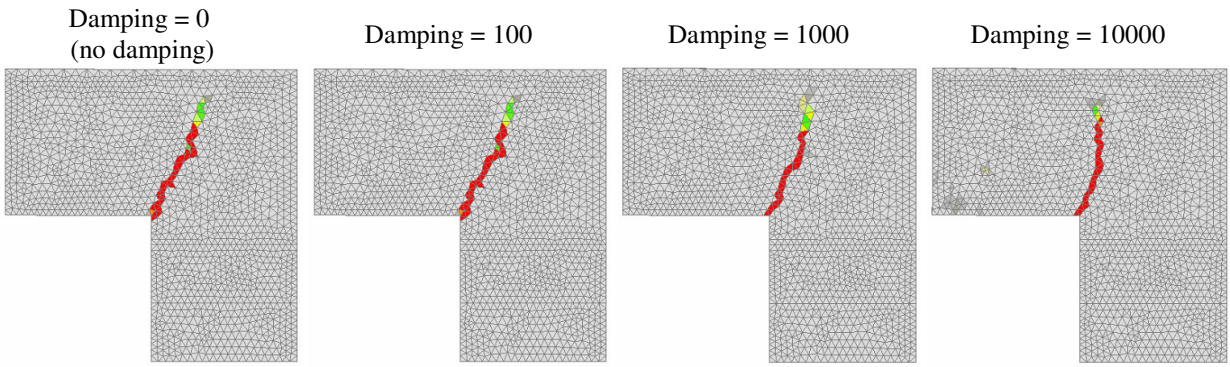

Figure 23. *Crack propagation obtained from the FE simulations for different values of viscous damping (in 1/s) for 740 mm/s (specimen No. 13).*

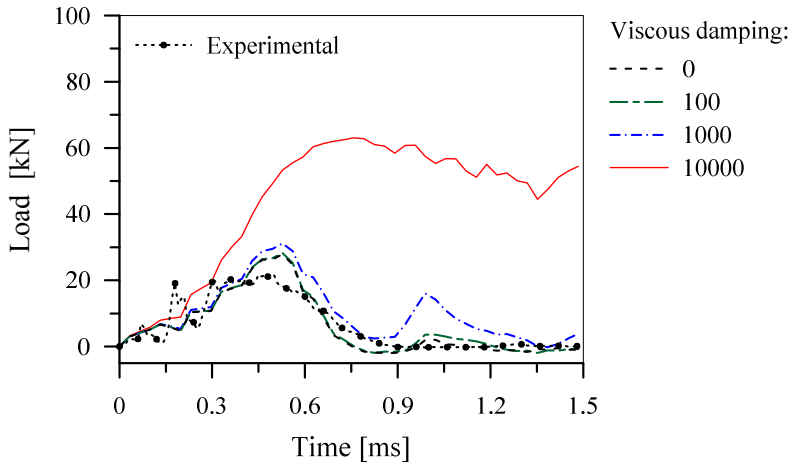

Figure 24. *Influence of viscous damping on the load time history against experiment for 740 mm/s (specimen No. 13).*

5.1.3 Results and discussion

5.1.3.1 Effect of loading rate on failure mode and crack velocity

Figure 25 shows crack patterns obtained from the finite element analysis and crack patterns from experiment for different displacement rates in the range from static to approximately 2400 mm/s. Obviously, results of numerical simulations are consistent with the results obtained from the experiment. As already discussed before, the direction of crack propagation is loading rate dependent. As the loading rate increases, the direction of the critical principal tensile stresses change due to the presence of inertia, see Ožbolt et al. (2013b). For quasi-static and relative low loading rates there is only one crack which is nearly horizontal, perpendicular to the loading direction, however, with increase of loading rate the crack

becomes more inclined, parallel to the loading direction. A as can be seen from Figure 25, in most cases with high loading rates there is also crack branching observed. The first crack branching, for both experiment and numerical results, is obtained for loading rate of 1000 mm/s. Such a phenomenon was also observed earlier with the compact tension specimen (Ožbolt et al. 2013b).

In addition, in Figure 26 are shown predicted and experimentally obtained crack patterns with corresponding crack velocities for different displacement rates. Crack velocity is calculated by dividing the distance between two observed finite elements (integration points) with the time interval in which the critical crack opening (w_{cr} = 0.1 mm) is reached. A very good agreement between the experimental and numerical results can be observed. The results indicate that the crack velocity depends on loading rate. In general, crack velocity increases with increase of displacement rate and after crack reaches critical speed of propagation there is crack branching (Ožbolt et al. 2011, Ožbolt et al. 2013b) and velocity decrease. For the here used properties of concrete, experimentally obtained maximum crack speed is around 650 m/s, while in numerical analysis is equal to 750 m/s.

a) 0.25 mm/s static

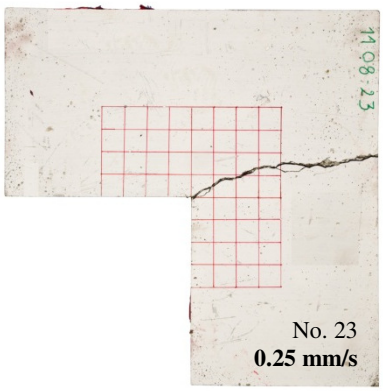

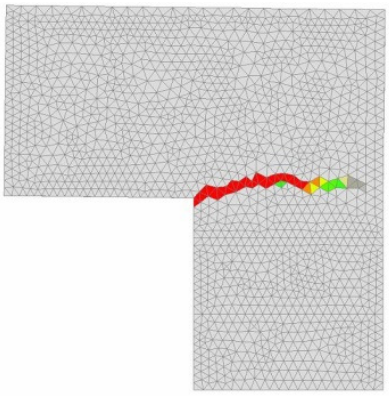

b) 350 mm/s

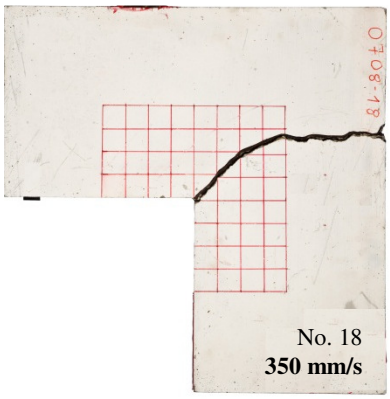

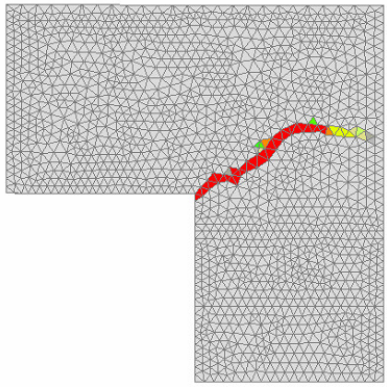

c) 740 mm/s

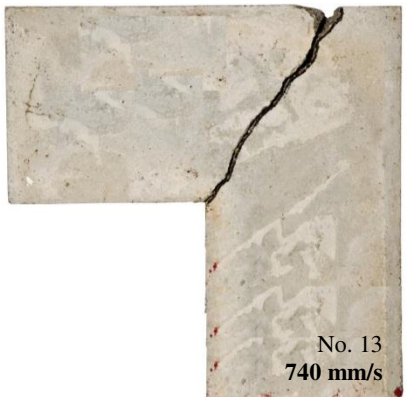

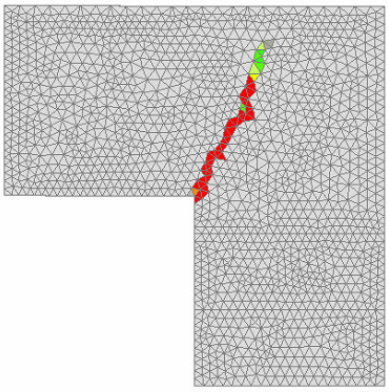

d) 1000 mm/s

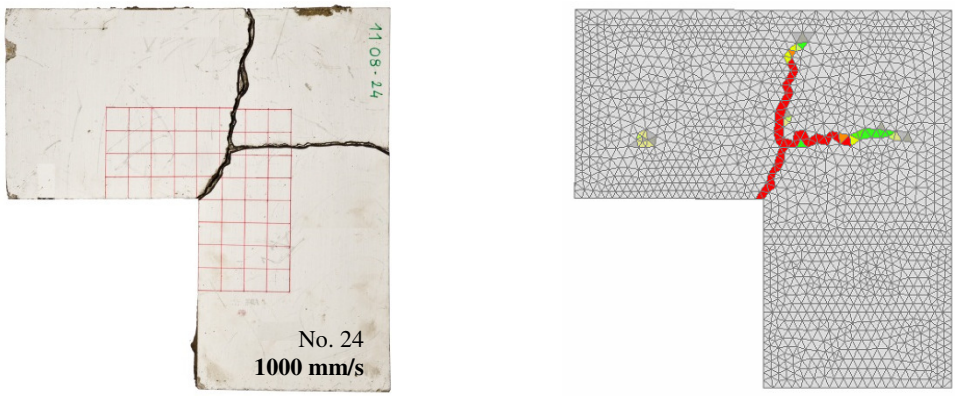

e) 2400 mm/s

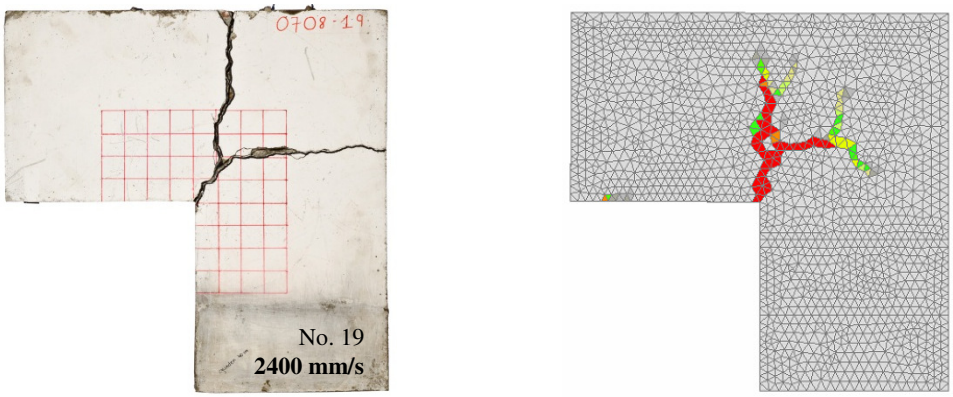

Figure 25. *Experimentally (left) and numerically (right) observed crack patterns for different loading rates: a), b), c), d) and e).*

a) 350 mm/s

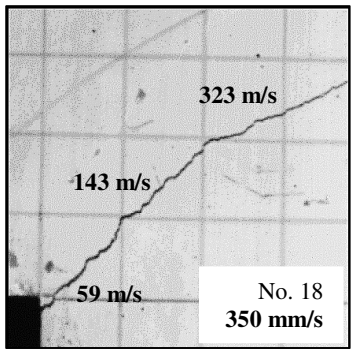

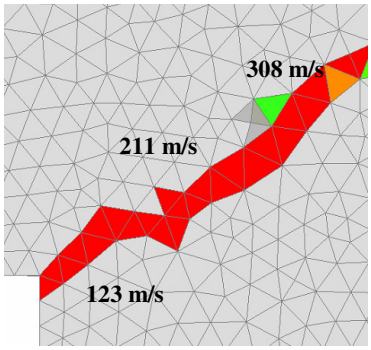

b) 740 mm/s

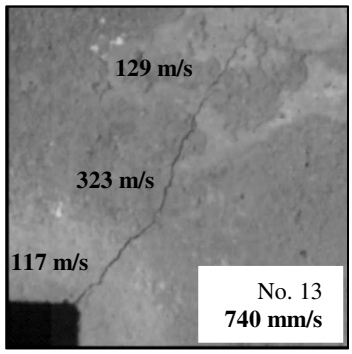

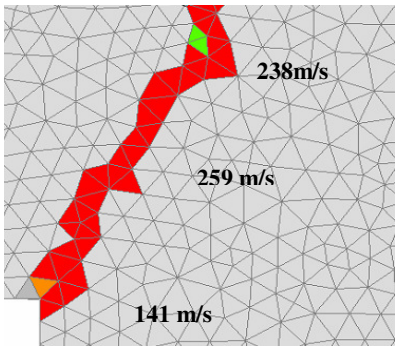

c) 1000 mm/s

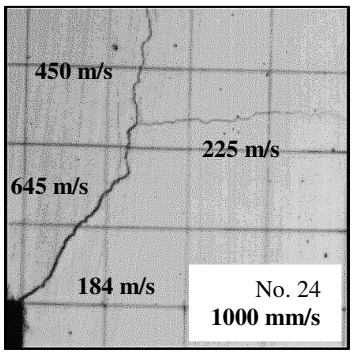

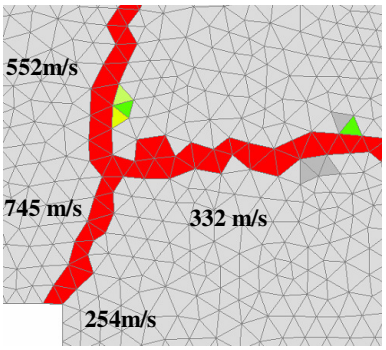

d) 2400 mm/s

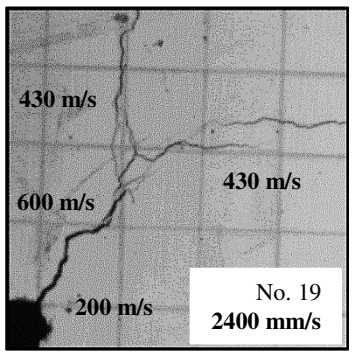

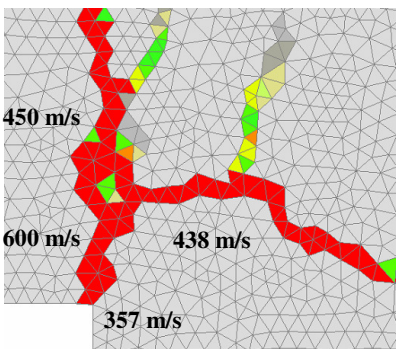

Figure 26. *Experimentally (left) and numerically (right) observed crack velocities for different loading rates: a), b), c) and d).*

5.1.3.2 Effect of loading rate on peak load

The results for seven representative tests and the corresponding numerical counterparts are summarized in Table 6. Also, the comparison of the measured and computed value of peak load against the corresponding value of applied loading (displacement) rate is shown graphically in Figure 27, in semi-logarithmic plot. Evidently, the numerical results follow the trend impose by experiment. The trend in both cases shows that the peak load increases with the increase of displacement rate, as expected. This increase becomes more pronounced when the displacement rate is greater than 100 mm/s while for displacement rates of approximately 1000 mm/s and higher this increase is progressive. It is important to note that increase coincides with moment when crack propagation is changing direction from horizontal and tends to become vertical. Finally, progressive increase of peak load is observed when the crack propagates almost vertical. Besides change of crack propagation direction, for higher strain rates there is crack branching and large amount of micro cracks. These suggest that the progressive increase of load is related to inertial effects activated due to cracking of concrete.

In addition, load-displacement (Figure 28) and load-time (Figure 29) curves obtained experimentally are correlated with numerical results. Same as in experiment, displacement is measured in node located on the front surface just above the applied load, 30 mm away from the vertical edge. In general, a surprisingly good agreement between the experimental and numerical results at different loading rates can be observed.

Table 6. *Summary of numerical and experimental results for peak load at different loading rates.*

Specimen No.	Loading rate (mm/s)	Peak load (kN)	
		Experimental results	Numerical results
/	static	/	3.57
23	2.50E-01	4.00	/
15	8.2E+01	4.88	7.46
18	3.5E+02	13.96	16.19
13	7.4E+02	22.30	25.40
24	1.0E+03	56.93	56.80
27	1.5E+03	66.41	75.50
19	2.4E+03	127.00	139.00

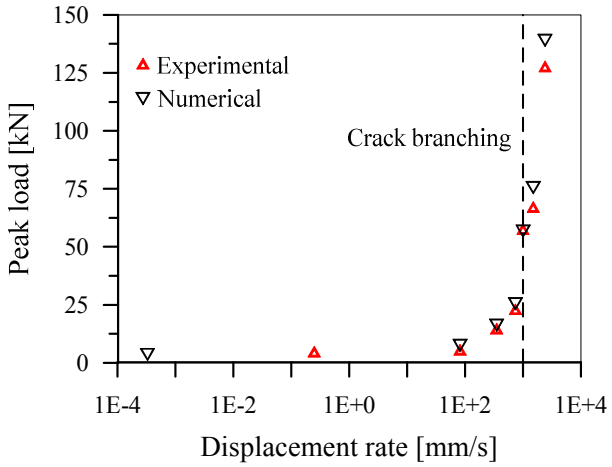

Figure 27. *Comparison between numerical and experimental results for peak load at different loading (displacement) rates.*

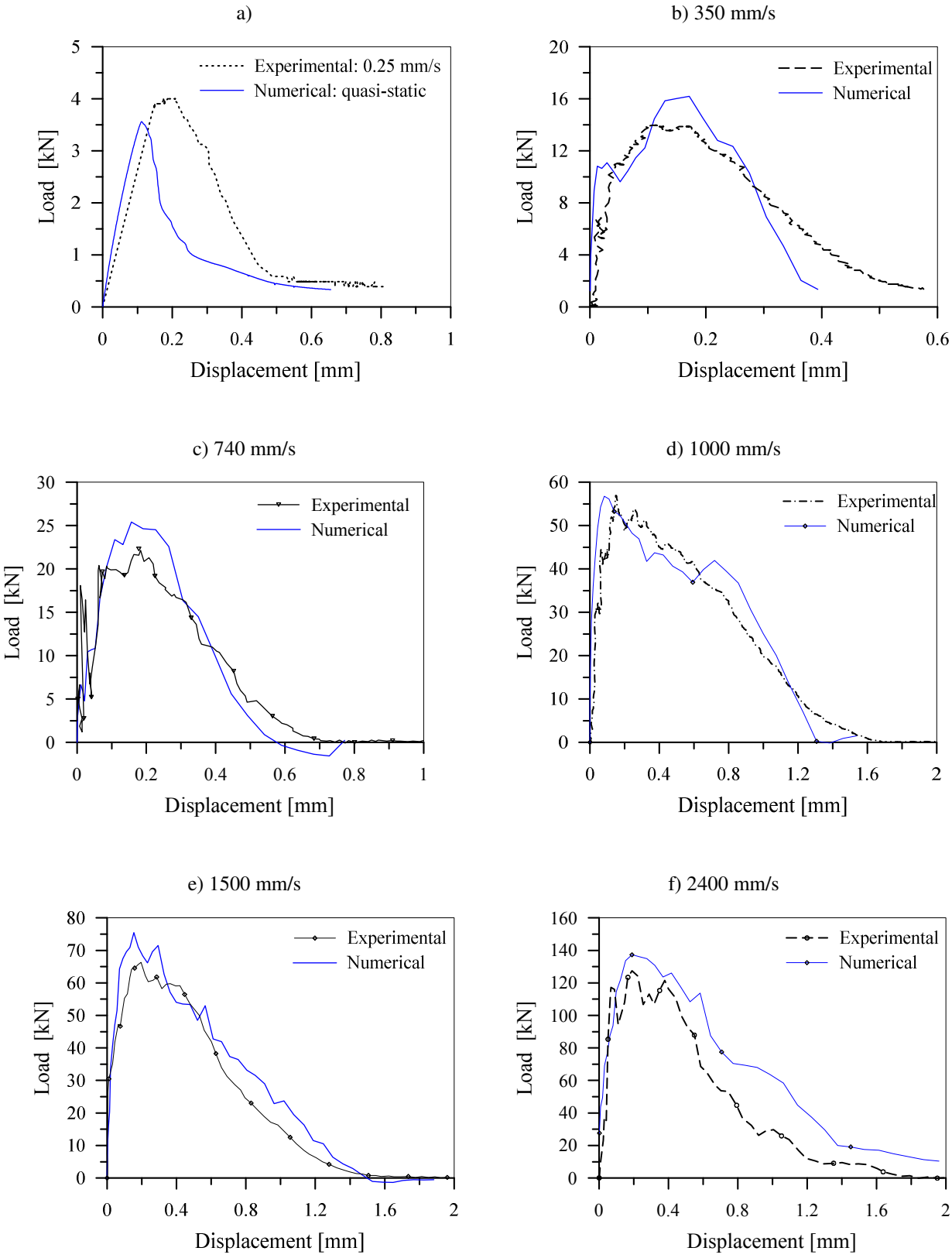

Figure 28. *Comparison of experimentally observed and numerically predicted load-displacement response for different displacement rates.*

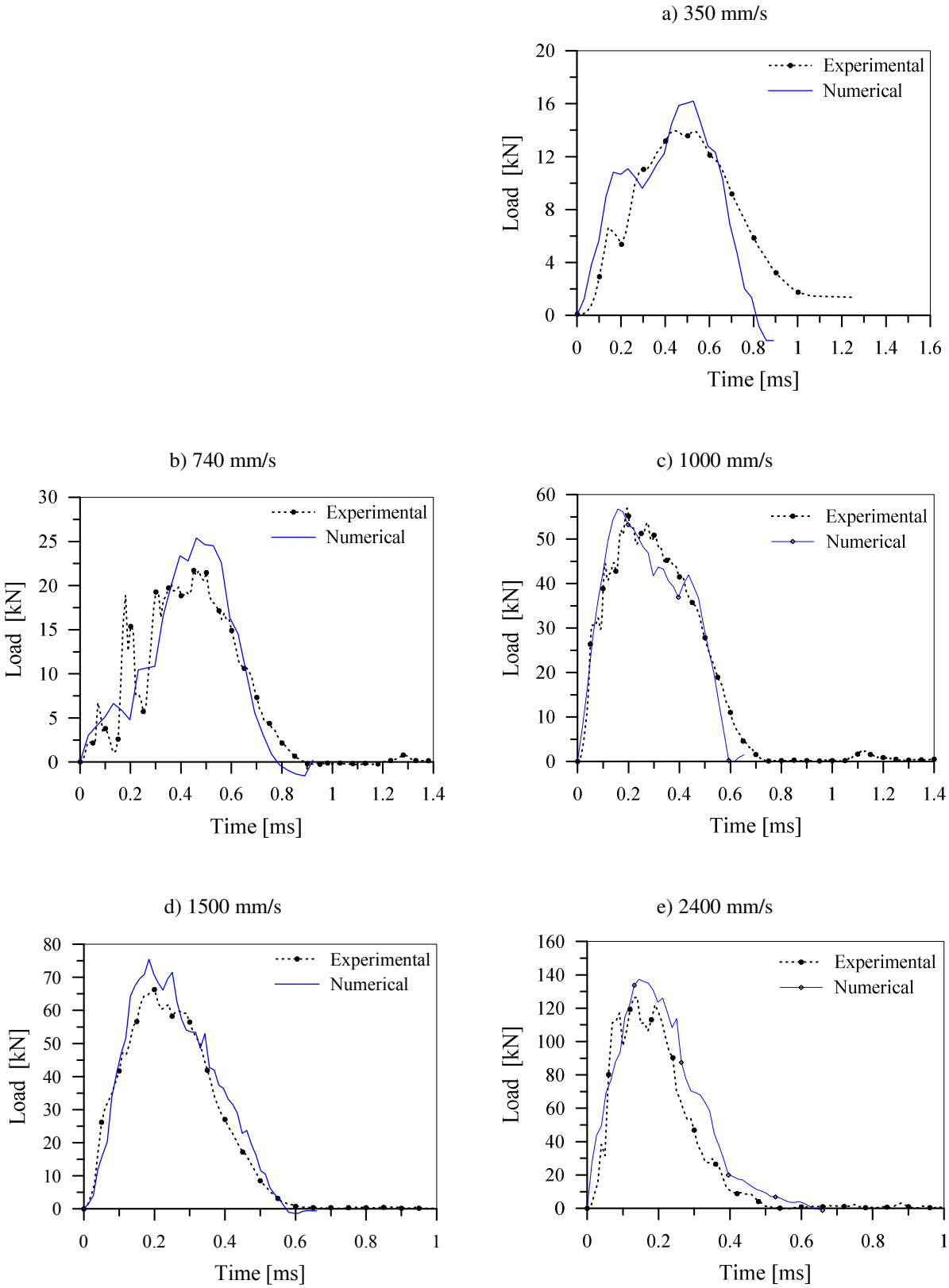

Figure 29. *Comparison of experimentally observed and numerically predicted load-time history for different displacement rates.*

5.1.3.3 Rate dependent tensile strength and fracture energy

Although experiments are necessary and helpful in understanding general behaviour of concrete under high loading rates, there are still lots of limitations with measurement of inherent material properties, for instance rate dependent tensile strength and rate dependent fracture energy, as well as strain rate and the rate of crack opening. Also, experimental techniques are unable to identify the reasons for changes exhibited in the structural response which are essential for understanding behaviour of concrete structures under dynamic loading. In order to overcome limitations of experiments and to gain a better understanding on the structural response, the influence of the loading rate on the above mentioned parameters is estimated employing numerical model. In this study a very good agreement between the experimental and numerical data in terms of load-deflection response, failure mode and crack velocity is observed. This confirms that the employed numerical procedure is able to simulate the overall experimental response of concrete exposed to relatively high displacement rates realistically. In the following treatment of the subject the above mentioned features of concrete are briefly reviewed.

In Figure 30 are plotted maximal principal strains and corresponding maximal principal stresses as a function of time for different loading rates in the typical finite element where crack initiates (junction point). All calculations are performed in the first cracked finite element located at the onset of crack initiation. The strain rate $d\varepsilon/dt$ is evaluated as a tangent to the principal strain-history curve (Figure 30a and 30c) at the time step just before reaching the peak stress (tensile strength). The crack opening velocity dw/dt is calculated from the strain rate after localization of crack, $dw/dt = (d\varepsilon/dt)\, h$, where h is the width of the crack band (equivalent element size) in the sense of the crack band approach (Bažant and Oh 1983). In addition, the rate dependent tensile strength (peak stress) and fracture energy are calculated from these curves. Overview of all numerically investigated parameters and corresponding results is given in Table 7. Clearly, both strain rate and crack opening rate, increase with increase in loading rate. However, crack opening rate shows the same order of magnitude as loading rate while strain rate increases much slower. Again, this can be attributed to the influence of structural inertia. Finally, values of tensile strength and fracture energy evaluated for single finite element and listed in Table 7 are almost constant for observed range of loading rates. Note that fracture energy and tensile strength evaluated for quasi-static loading at the typical finite element are slightly lower than obtained directly from the uniaxial tensile

constitutive law. The reason is probably due to the 3D effect at the location of crack initiation which leads to the three-dimensional stress state.

The computed rate sensitivities of the tensile strength and fracture energy are shown graphically in Figure 31 and Figure 32. DIF for tensile strength as a function of loading rate is depicted in Figure 31a and as a function of strain rate in Figure 32a, respectively (plotted in semi-log scale). As can be seen, the strength increases linearly in semi-log scale with increase of loading/strain rate and approximately follows the rate dependent constitutive law (Ožbolt et al. 2001a, Ožbolt et al. 2006). This was expected since true material strength depends only on the constitutive law (Ožbolt et al. 2001a). Figure 32 plots the DIF for fracture energy as a function of loading rate and strain rate. Opposite to tensile strength, DIF on fracture energy does not follow the rate dependent fracture energy from constitutive law. Similar observations were made on CTS (Ožbolt et al. 2013b) as well as MSHB test (Ožbolt et al 2014). It can be that in case of higher strain rate the part of the energy is consumed by damage that takes place before the crack is localized or this can be attributed to the 3D effects.

Table 7. *Overview of numerically obtained results.*

Loading rate (mm/s)	Strain rate (1/s)	Crack opening rate (m/s)	Tensile strength f_t (MPa)	Fracture energy G_F (J/m^2)
static	/	/	2.73 (3.12*)	49.25 (58.00*)
8.2E+01	0.83	0.08	3.83	77.58
3.5E+02	6.57	0.50	3.86	85.17
7.4E+02	7.33	0.93	3.89	86.56
1.0E+03	10.60	1.56	3.87	56.66
1.5E+03	13.10	1.92	3.90	59.79
2.4E+03	14.31	3.33	3.90	60.24

*uniaxial tensile constitutive law

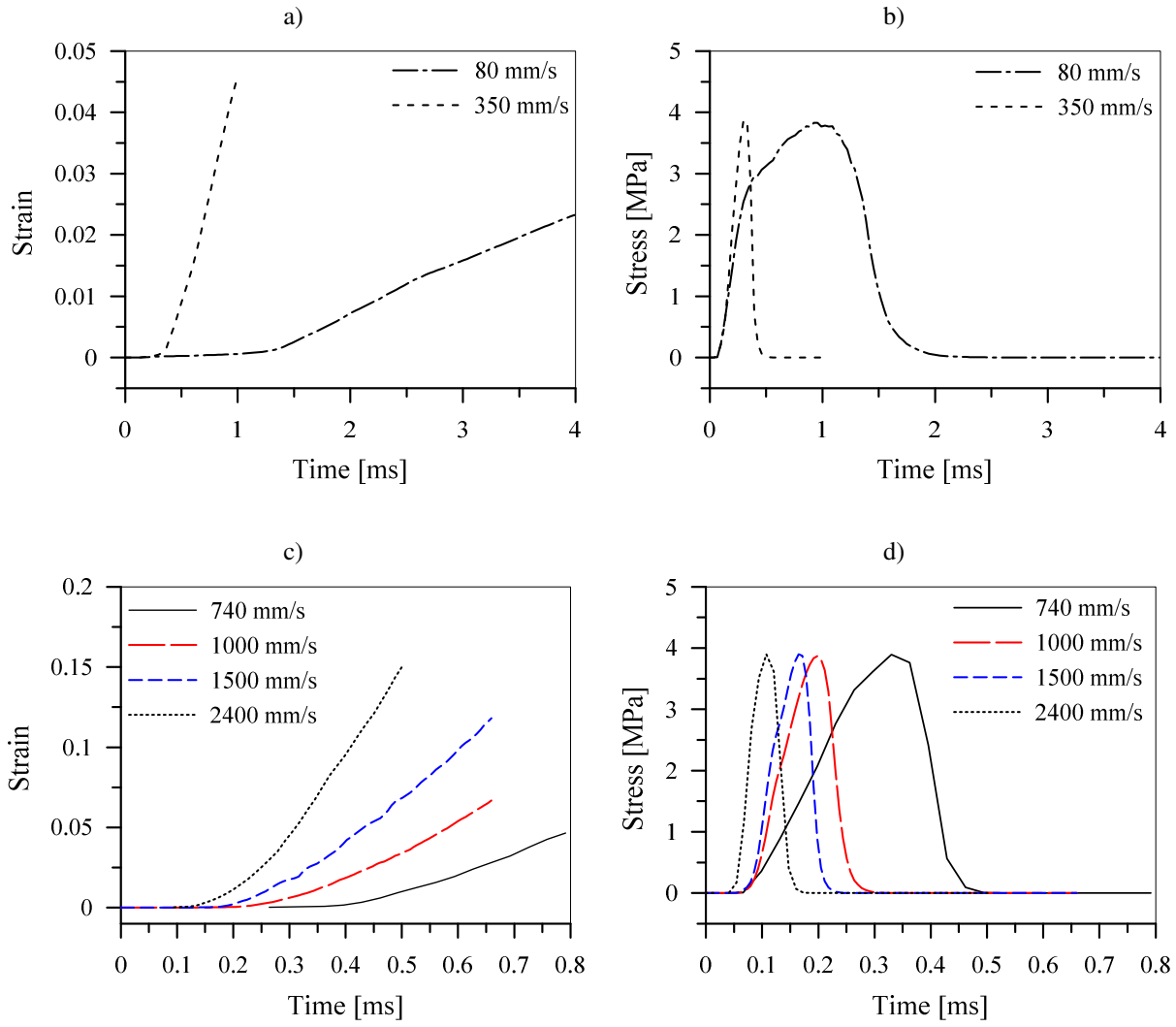

Figure 30. *Numerically obtained maximal principal strain and stress histories in the finite element where crack is initiated.*

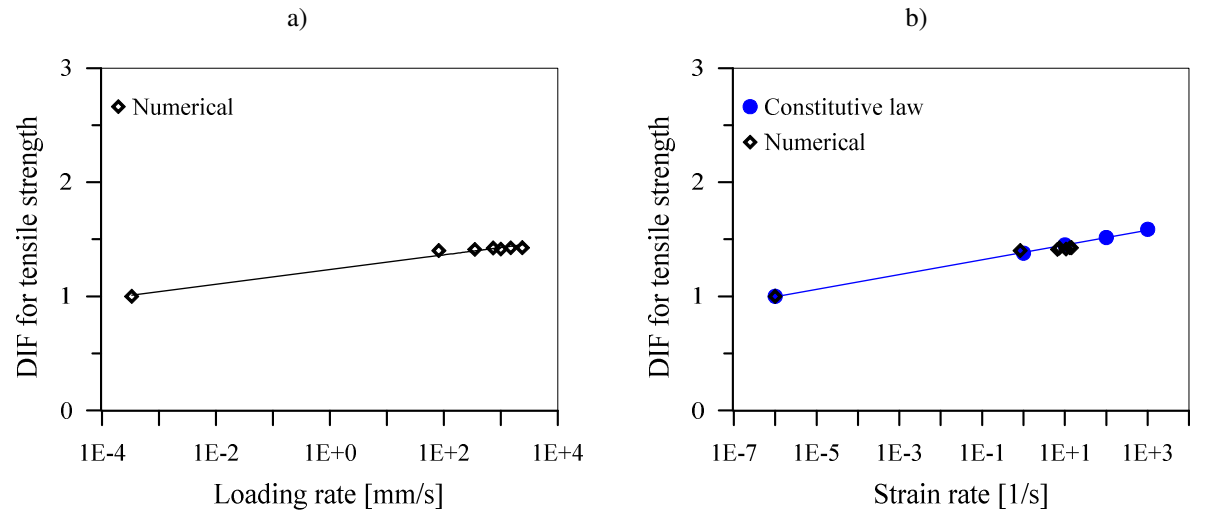

Figure 31. *Numerically obtained DIF for tensile strength as a function of a) loading rate and b) strain rate.*

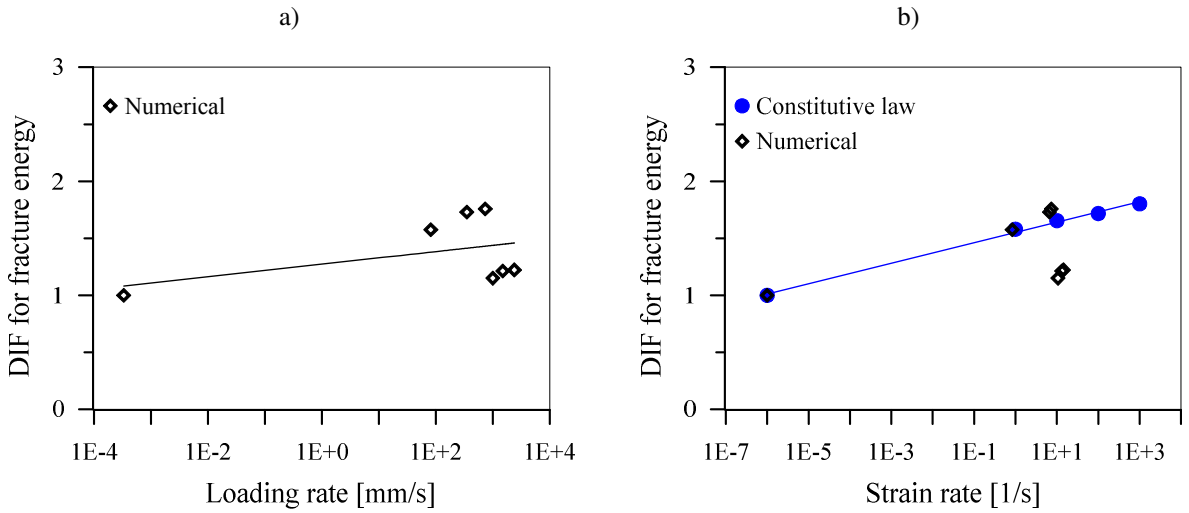

Figure 32. *Numerically obtained DIF for fracture energy as a function of a) loading rate and b) strain rate.*

In Figure 33 is plotted DIF for peak load measured in the analysis and experiment (semi-logarithmic plot). It can be seen that there is very good agreement between numerical prediction and experiment, i.e. for both experiments and numerical simulations, DIF is equal to approximately 40 for the loading rate of 2400 mm/s. Note that static loading rate is taken as 10^{-4} mm/s which corresponds to strain rate of 10^{-6}/s. Figure 33b shows plot of DIF for peak loads in the analysis and experiment as a function of strain rate. Up to the strain rate of approximately 10/s there is linear increase in DIF which nicely follow the rate dependent constitutive law for tensile strength. On the contrary, for strain rates of approximately 10/s and higher, significant increase of peak load is apparent. As discussed previously, at strain rate of approximately 10/s, which correspond to loading rate of approximately 1000 mm/s, various phenomena related to structural inertia are observed, e.g. the crack propagation is changing from horizontal to vertical direction, the main crack branches, amount of small cracks increases. In this range structural inertia becomes dominant, which lead to significant increase of peak load. On the contrary, up to strain rate of approximately 10/s, inertial effects are not dominant and basically rate dependency of the growing microcracks (part of the rate dependent constitutive law) is the influencing factor. Similar was also observed recently for the compact tension specimen (Ožbolt et al. 2013b).

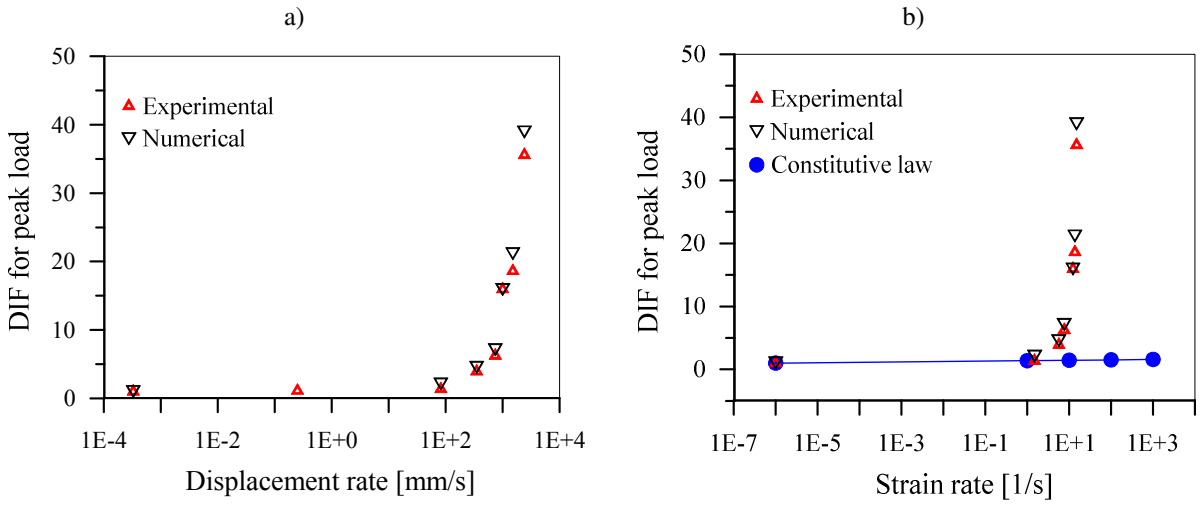

Figure 33. *DIF for peak load as a function of a) loading (displacement) rate and b) strain rate.*

5.1.4 Conclusions

In order to confirm or disconfirm the results of numerical prediction performed by Ožbolt and Sharma (2012) and to verify recently developed computational procedure by Irhan (2014) experiments on L-specimen are numerically simulated. The results of numerical simulations are evaluated and compared with experimental results. In general, the trend and values obtained from the numerical simulation are comparable with those from the experiment.

First, in order to calibrate the model, the effect of viscous damping is studied. The results show that in this model, to achieve a good agreement between experiment and FE analysis, the effect of damping can even be neglected. The numerically obtained load-deflection and load-time curves, for all loading (displacement) rates, are found to be in very good agreement with their experimental counterparts. As expected, experiments and numerical analysis show that peak load increases with increase of loading rate. Moreover, for loading rates higher of approximately 10/s there is progressive increase of load that is controlled mainly by structural inertia.

Both, experiments and numerical analysis show that loading rate significantly influences the failure mode of the L-specimen. Numerically obtained crack patterns correspond remarkably well with the experimentally observed. For relatively low displacement rates there is single crack approximately perpendicular to the loading direction. With the increase of displacement rate structural inertial effect increases and consequently the crack propagation direction

gradually changes from almost horizontal (low displacement rates) to vertical (high displacement rates). Finally, with increase of loading rate and structural inertia the number of cracks increases, i.e. when loading rate reaches approximately 1000 mm/s crack branching occur and for even higher loading rates multiple crack branching. The evolution of experimental and numerical results confirms that crack velocity is rate dependent. The maximum crack velocity is observed before crack branching and it is between 650 and 750 m/s. Used model is capable of simulating crack branching, crack propagation velocity and even the angle of crack branching remarkably good. Hence, it is shown that employed 3D FE code used in simulations is predictive and moreover, capable to reproduce the experimental results very well.

Finally, to gain more insight into behaviour of concrete under dynamic loading influence of the loading rate on specifically chosen parameters such as fracture energy and tensile strength is investigated employing numerical procedure. The evolution of numerical results shows that tensile strength and fracture energy exhibit no progressive increase for high loading rates but follows approximately the rate dependent constitutive law used in the computation. Overall, it can be concluded that for higher strain rates, larger than approximately 10/s, inertial effects dominate and cause progressive increase of load, change of failure mode, crack branching and multiple branching. The same conclusions were obtained by Ožbolt et al. (2013b) on compact tension specimen.

5.2 Notched plain concrete beam under impact load

Zhang et al. (2009, 2010a) performed experiments on notched plain concrete beams under impact loads (see Chapter 3). The results of the experimental measurements show that after reaching certain threshold fracture energy and tensile strength progressively increase with increase of impact velocity. However, experimentally it is difficult to evaluate dynamic fracture energy and tensile strength, i.e. it is difficult to separate the inertial component from the fracture energy evaluated as the area under reaction-displacement curve. Therefore, to bring more light into the problem the experiments performed by Zhang et al. (2009, 2010a) are numerically replicated. First, to validate the numerical results, they are compared with experimental results reported in (Zhang et al. 2009, 2010a). Subsequently the fracture energy is evaluated as suggested by Zhang et al. (2009), i.e. by dividing the area under the reactions versus vertical displacement curve by the cross section area in the region above the notch. Further, for better understanding of the structural effects on fracture energy, the evaluation of fracture energy is performed by considering the stress-strain response of the single finite element in the zone of cracking, i.e. just above the notch. The results are evaluated and discussed in detail to understand the correct evaluation procedure for fracture energy under dynamic loading. Similar procedure is also performed for evaluation of tensile strength.

5.2.1 Finite element model

The geometry, dimensions and finite element mesh of the four bodies (hammer, beam, two roller supports) are shown in Figure 34. Three-dimensional tetrahedral finite elements are used to model the concrete, the impacting hammer and the steel cylindrical supports. The beam is simply supported and the load is applied at the mid span of the beam top surface (Figure 34). Two different material properties of concrete are used in numerical simulations (see Table 4). The typical rate dependent tensile stress-strain curves used in the analysis are plotted in Figure 35. They correspond to the crack band width (element size) of 5 mm. Note that these curves come out from the microplane constitutive law. The impacting hammer and cylindrical roller supports are assumed to be linear elastic. Material properties of steel employed in the analysis are summarized in Table 8.

Table 8. *Mechanical properties of steel used in the analysis.*

Young's modulus, E (GPa)	200
Poisson's ratio, v_s	0.33
Mass density, ρ_s (kg/m^3)	7800

Different impact velocities are employed to study their effect on peak load, strain rate, crack velocity, tensile strength and fracture energy of HSC. The numerical analysis is performed for quasi-static loading condition and for the following impact loading velocities: 1.74×10^1, 8.81×10^2, 1.76×10^3 and 2.64×10^3 mm/s. It is assumed that quasi-static load corresponds to velocity of 5.50×10^{-4} mm/s (Zhang et al. 2009, 2010a). Moreover, in order to separate the effects of strain rate and structural inertia, rate sensitive "static" analysis is also carried out for all loading rates. In the rate sensitive static analysis only inertia effects at the micro scale and the effect of viscosity are accounted for, whereas the other inertia effects, mentioned before, are ignored. Therefore, by comparing the results of rate sensitive static and dynamic analysis it is possible to filter-out the influence of inertia. The rate sensitive static analysis follows the rate sensitive constitutive law (see Figure 35).

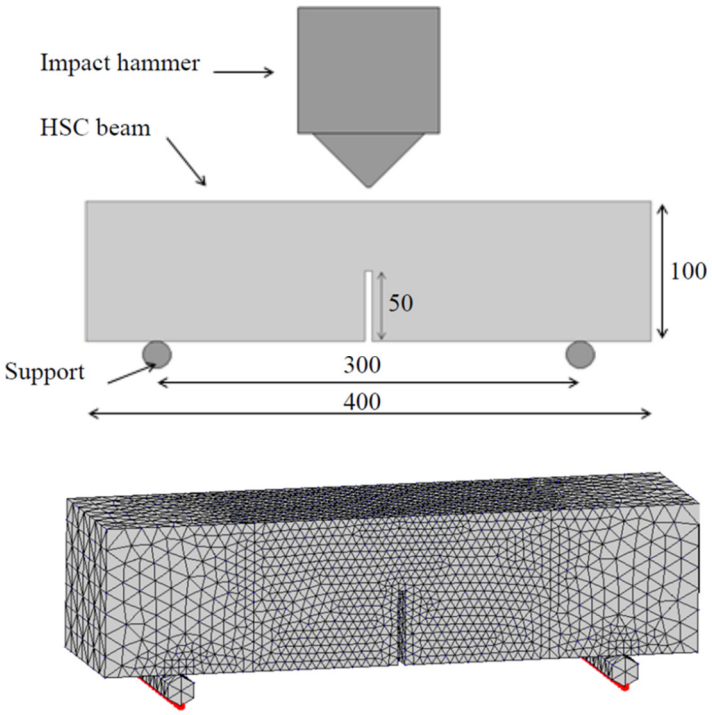

Figure 34. *Geometry and finite element mesh of the model used for the numerical analysis (all in mm).*

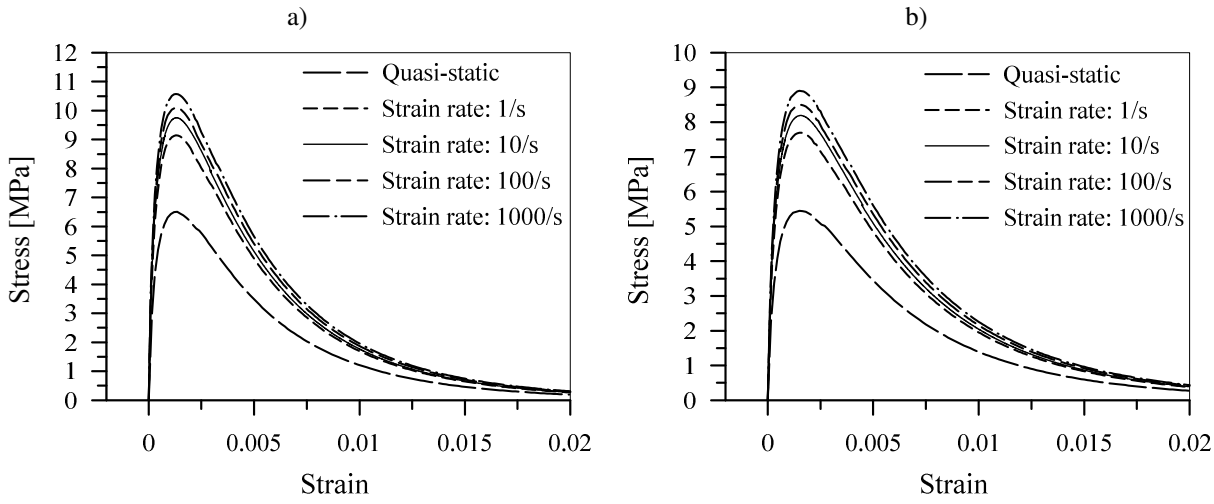

Figure 35. *Rate dependent tensile stress-strain curves (crack band width = 5 mm) at different strain rates for material properties of HSC given in a) Zhang et al. (2009) and b) Zhang et al. (2010a).*

5.2.2 Results and discussion

5.2.2.1 Failure modes

In all investigated cases, including quasi static analysis, the failure mode is due to the mode-I fracture, as expected for plain concrete notched beams. Typical time evolution of crack pattern for the highest impact velocity (2640 mm/s) is shown in Figure 36. The crack (dark zone) is plotted in terms of maximum principal strains that are larger than critical strain, which corresponds to critical crack opening. The critical crack opening w_{cr} is assumed to be 0.1 mm and since the average element size is 5 mm, the critical strain $\varepsilon_{cr} = 0.02$ (smeared crack approach). Note that the critical crack opening of 0.1 mm approximately corresponds to the crack opening at which concrete is fully cracked. Consequently, the used constitutive law is calibrated such that for this crack opening cohesive stress for mode-I fracture approximately reduces to zero. As can be seen from Figure 36, after the initialization crack runs straight from the notch tip to the top surface of the beam. The same failure mode was observed in experiments (Zhang et al. 2010a). As will be shown later, the measured crack velocity in all cases is less than crack branching critical velocity (approximately 800 m/s, see Ožbolt et al. (2013b)). Note that if the impact velocity would increase significantly, the failure mode and crack pattern may change dramatically. To illustrate this, Figure 37 shows failure mode that corresponds to the impact velocity of 50 m/s. As can be seen the failure is due to

the mixed-mode type. In the present paper discussion is limited to the impact velocities which cause only mode-I type of failure.

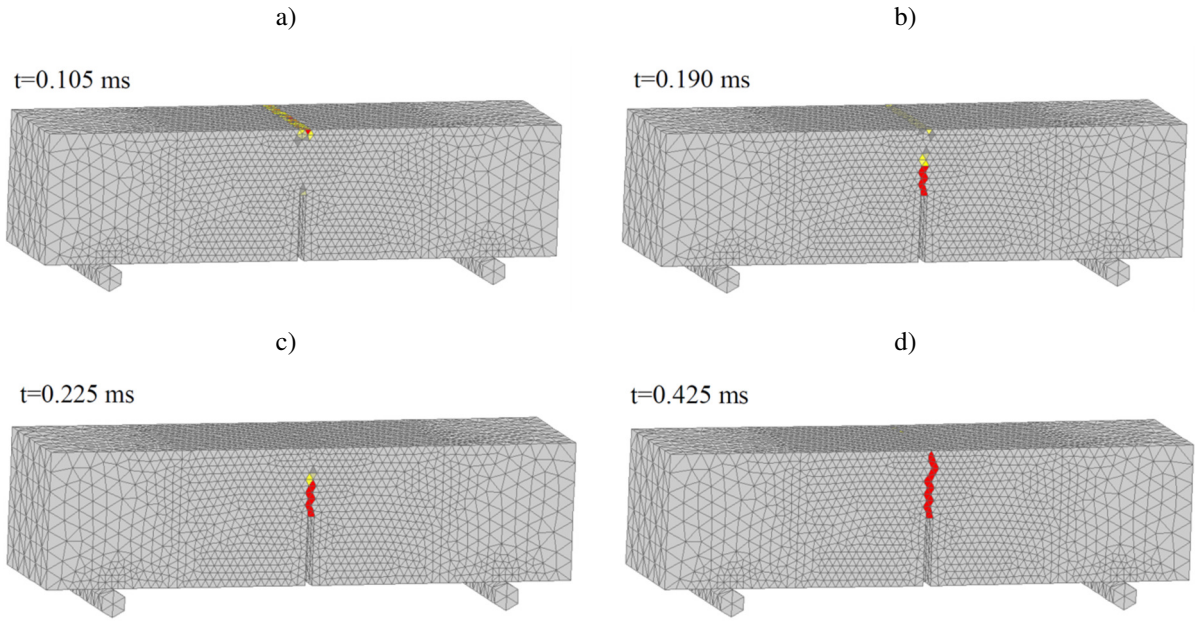

Figure 36. *Failure mode at impact velocity of 2640 mm/s as a function of time a) b) c) d).*

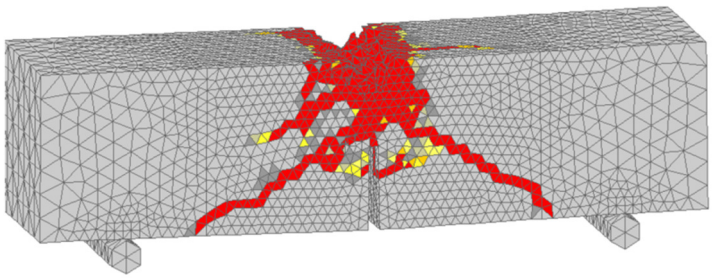

Figure 37. *Failure mode at impact velocity of 50 m/s as a function of time.*

5.2.2.2 Effect of impact velocity on impact load and reaction

Experimentally evaluated results that are reported by Zhang et al. (2010a) are used to validate the capability of the presented FE code in prediction of impact load, reaction forces, strain rates, crack velocity and crack opening velocity. The impact forces versus time for four different impact velocities are plotted in Figure 38. Note that results from Zhang et al. (2010a) are compared for impact velocities of 17.4 mm/s and higher because, as mentioned above, quasi-static load corresponds to velocity of 5.50×10^{-4} mm/s.

As can be seen, peak response and the shape of the curve for the highest impact velocity (2640 mm/s) are in very good agreement with the one obtained from experiment. However, some differences are present for lower impact velocities. For the impact velocities of 1760 and 881 mm/s the analysis overestimates the peaks observed in experiments. On the other hand, for the low impact velocity (e.g. 17.4 mm/s), it can be seen that there is a difference in the initial stiffness of the observed curves. However, having on mind difficulties in exact measurement of impact loads in experiments the agreement is relatively good.

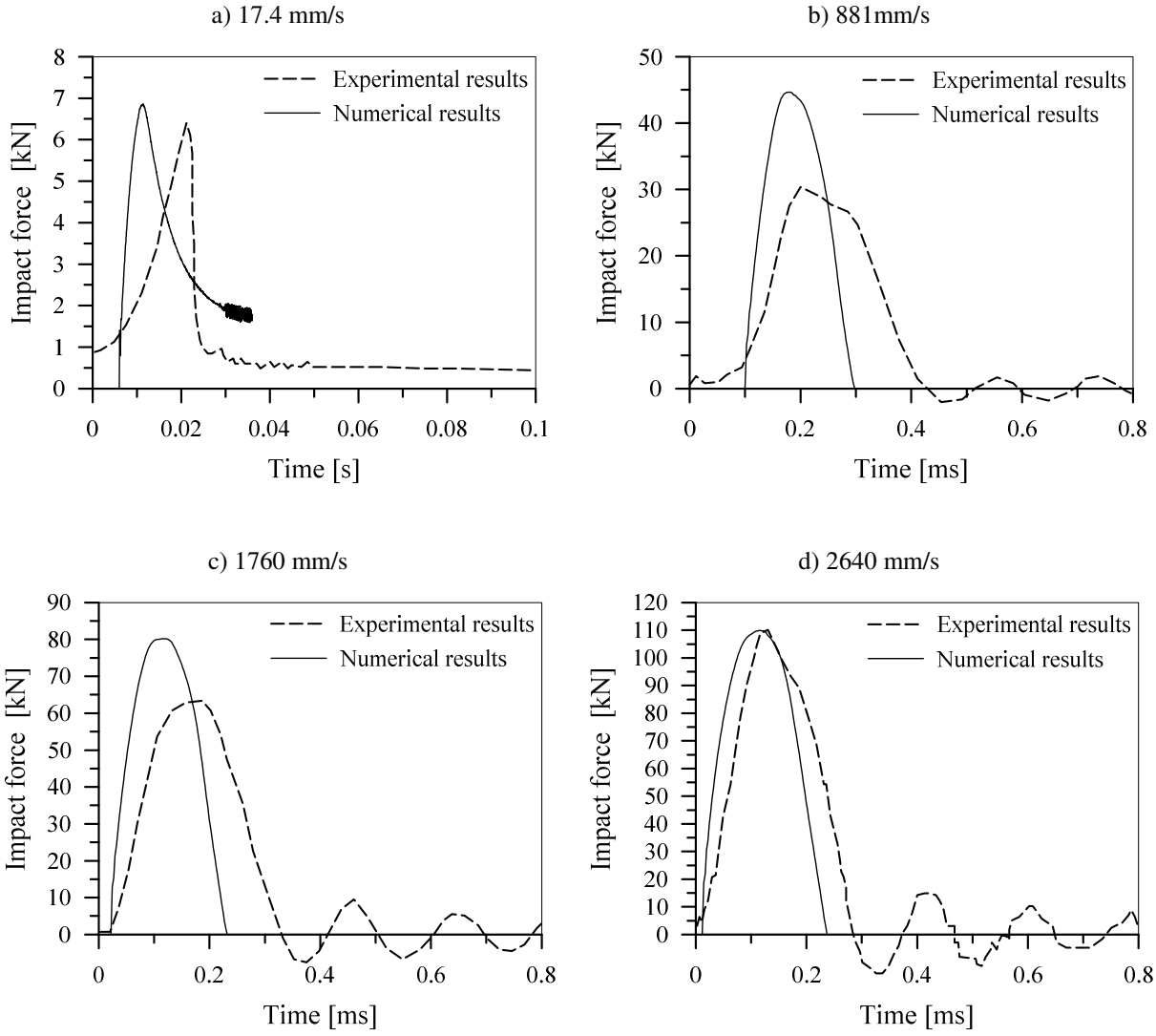

Figure 38. *Comparison of numerical and experimental dynamic impact force (load) versus time history of the concrete beam at different impact velocities.*

Figure 39a shows the comparison between numerical results and experimental data in terms of impact load versus impact velocity (in semi-logarithmic scale). The dynamic increase factor (DIF) for the impact load as a function of impact velocity is plotted in Figure 39b. DIF

is defined as the ratio of impact load and the quasi-static load. As shown in Figure 39, for dynamic analysis the shape of the curves is in very good agreement with the experimental results. In both, experiments and the numerical simulations impact force increases with increase of impact velocity. This increase is very slight for impact velocities below 100 mm/s and from here onwards impact force rises progressively. At impact velocity of 100 mm/s impact force is around 10 kN, whereas it reaches approximately 110 kN for impact velocity of 2640 mm/s. It can be seen that the rate sensitive static analysis for higher loading rates does not exhibit progressive increase in DIF. This indicates that the steep progressive increase observed beyond a certain loading rate is primarily due to the effect of structural inertia.

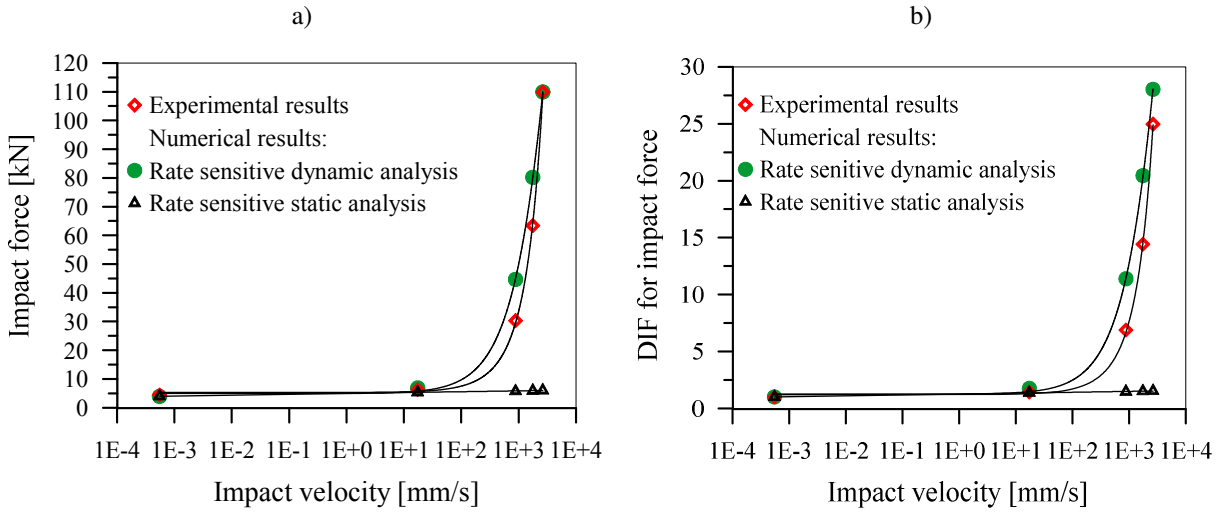

Figure 39. *Comparison of numerical and experimental result at different impact velocities a) impact force (load) and b) DIF for impact force (load).*

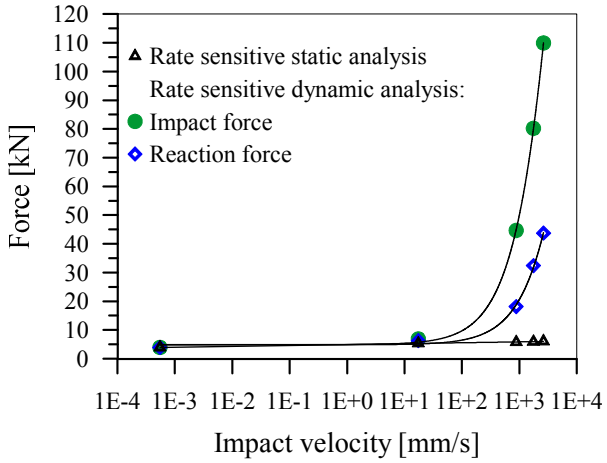

Figure 40. *Numerical results for impact force and reaction force at different impact velocities.*

The experimental data for reactions of high loading rates (impact) were not reported in the experimental study. The results obtained from numerical analysis for impact force and reactions as a function of loading rate are shown in Figure 40. It can be seen that peak reaction increases proportionally to the impact load. Evidently, the impact force and the reaction force exhibit a similar trend for all impact velocities. Under static loading, the total applied load is equal to the total reaction to maintain static equilibrium. However at high loading rates, compared to the impact loads, the reaction forces are relatively small. Beyond a certain threshold of impact velocity (100 mm/s) the effect of inertia becomes more pronounced and a significant difference in the two values is observed. This implies that a significant portion of the impact force is utilized to maintain the balance with the inertia force during loading, while only a small portion of the impact force is actually utilized in deforming and fracture of the specimen. It is worth noting that for rate dependent quasi static analysis, the reaction and load are identical for all loading rates.

By comparing the results of the rate dependent dynamic and rate dependent static analysis, it is not possible to differentiate between the influence of structural inertia and inertia related to material response (i.e. the inertia related to material softening and crack branching) on the impact and reaction force. However, it is possible to filter out the entire inertia effects, except those that are the part of the constitutive law (inertia at micro level: micro-cracking). However, in general, it is well-accepted that for very high loading rates (impact) structural inertia dominates, nevertheless, the inertial effects related to the material response cannot be neglected. On the other hand, for low to moderate loading rates, inertial effects related to the material response (rate sensitivity) are dominant.

The time evolution of numerically evaluated impact force and reactions, for different impact velocities, are shown in Figure 41. It should be noted that in case of low loading rate (17.4 mm/s) the impact force is practically of the same magnitude as the peak load. However, as the loading velocity increases from 881 mm/s to 2640 mm/s, a significant difference between peak load (reaction) and impact force is apparent, i.e. higher the loading velocity larger is the difference between the load and reaction. This difference is attributed to the effect of structural inertia, which is more pronounced for high impact velocities. This is further confirmed by the delay in the rise time of reaction force, which is again attributed to structural inertia.

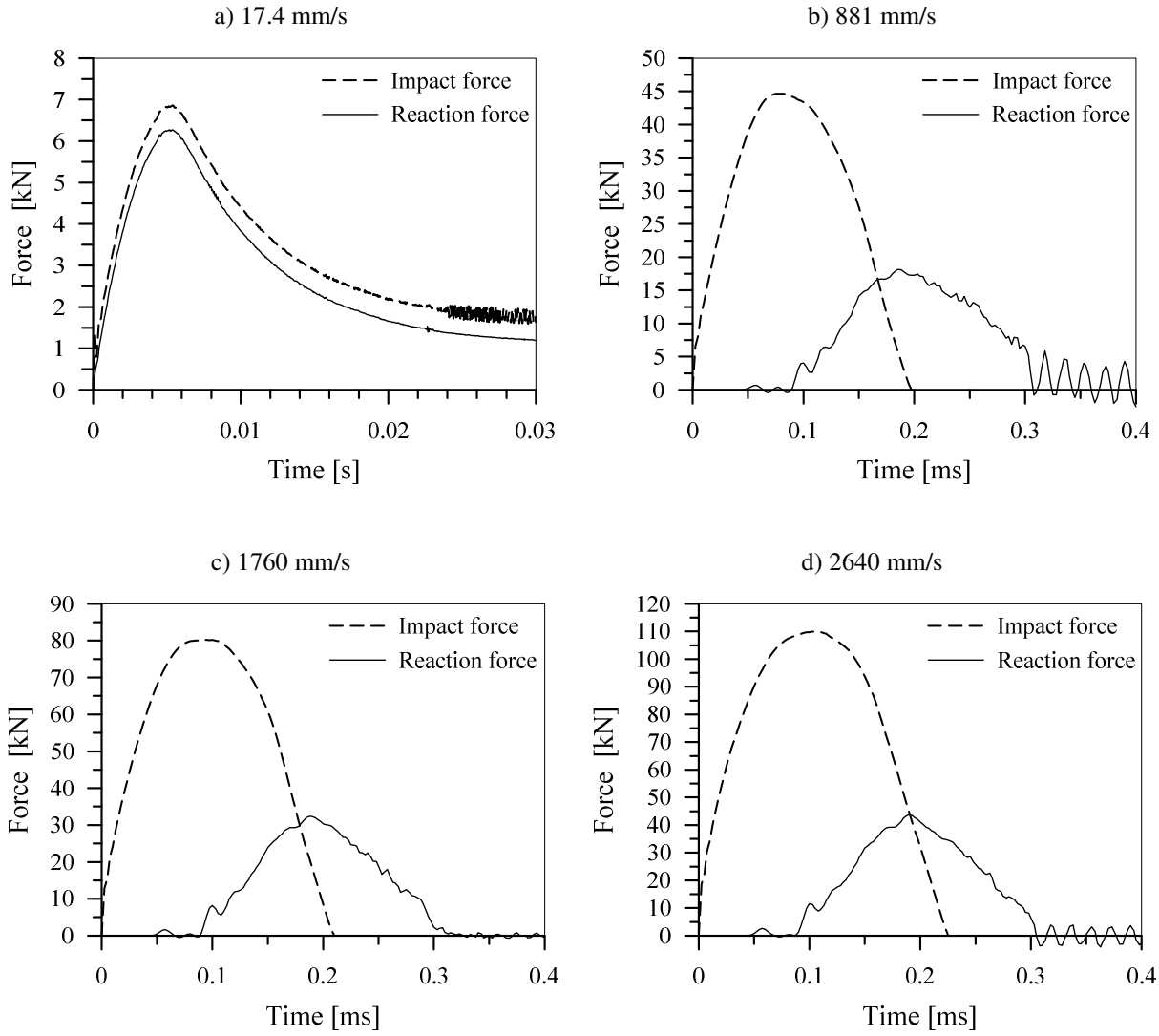

Figure 41. *Numerical comparison of impact force and reaction force versus time for a) low impact velocity b),c),d) high impact velocities.*

5.2.2.3 Effect of impact velocity on strain rates

Principally, with increasing loading rate (impact velocity), the strain rate and strain corresponding to peak stress increase, except in cases where with increase of loading rate failure mode changes, e.g. crack branching. The typical time evolution of strain and stress just above the notch tip, where crack initiates, are numerically evaluated. Figure 42 shows maximum principal strains history and corresponding maximum principal stresses history for different impact velocities in the finite element just above the notch tip. Figures. 42a and 42b show the results obtained for impact velocity of 17.4 mm/s while Figures 42c and 42d show them for higher impact velocities. In general, the curves exhibit a similar trend for all impact velocities. The stress-history curves consist of two regions that can be denoted as pre-peak

and post-peak regions. With the increase in the impact velocity, a slight increase in the peak stress in the element can be observed along with a reduction in the time of its occurrence.

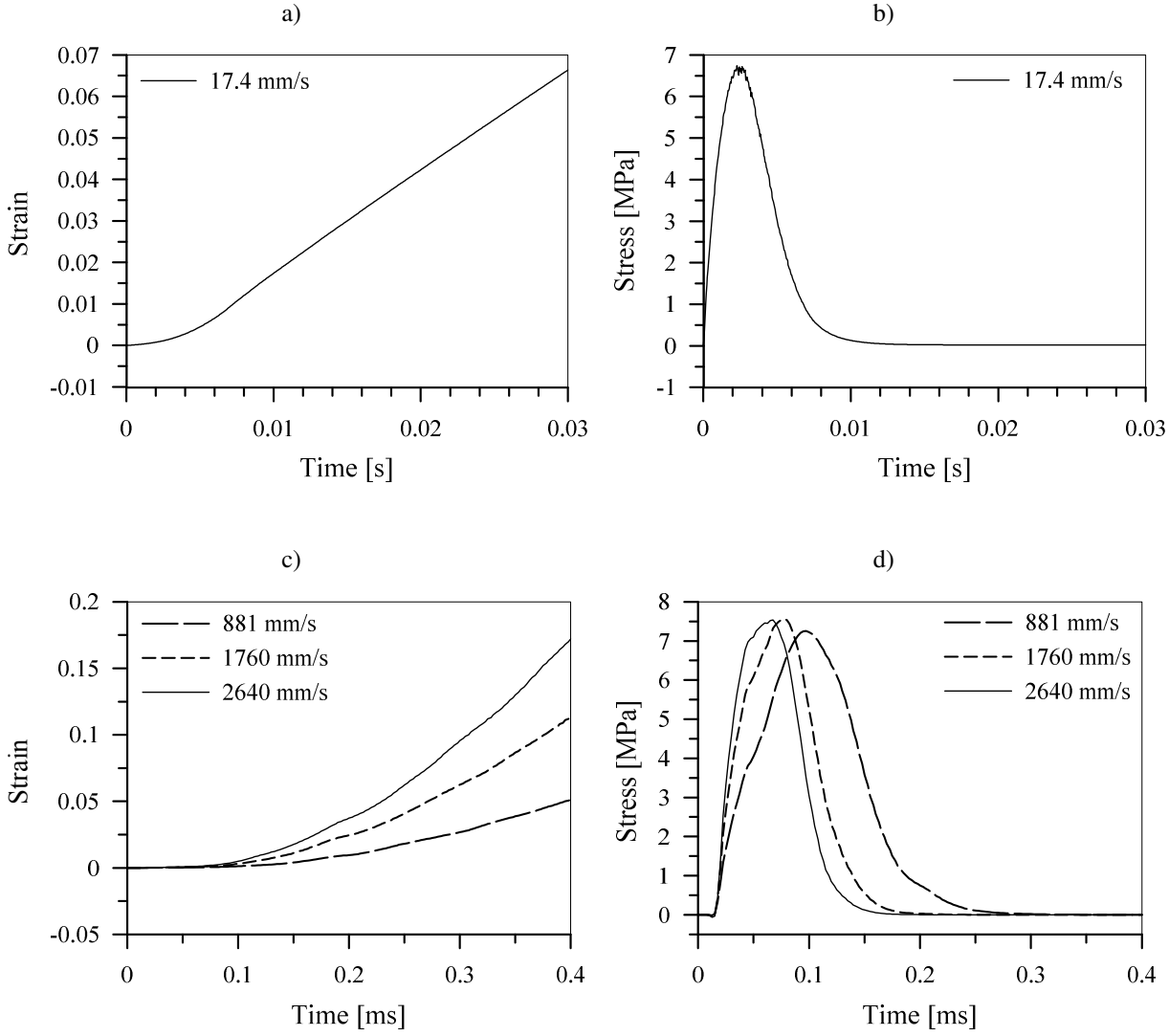

Figure 42. *Numerically predicted strain and stress histories at the center of the beam (notch tip) for a),b) low impact velocity and c),d) high impact velocities.*

The strain in the element just above the notch tip corresponding to the peak stress occurring there is plotted as a function of the impact velocity in Figure 43a. As expected, the strain corresponding to the peak stress rises with the increase in impact velocity. For further evaluation, the stress history for elements at distances of 10, 20 and 30 mm from the notch tip were extracted for the case of highest impact velocity and the information of corresponding strain as a function of distance from notch tip is plotted in Figure 43b. The results indicate that the strain corresponding to peak stress is almost independent of the position of the crack tip.

The strain rate is evaluated as the tangent to the principal strain versus time curve (Figure 42). The evaluation is performed for the time step before the peak stress is reached. The relation between the impact velocity and strain rate measured at the notch tip is shown in Figure 44a. As expected, with increase of impact velocity, strain rate increases and for maximum impact velocity (2640 mm/s) reaches 33.4/s. The results are summarized in Table 9. The distribution of maximum strain rates for different position of crack tip is for low (17.4 mm/s) and the highest impact velocity (2640 mm/s) plotted in Figure 43b. It turns out that for the highest impact velocity (2640 mm/s) the maximum strain rate first slightly increases with the crack propagation (maximum = 47/s) and when the crack approaches the compressive zone, it decreases.

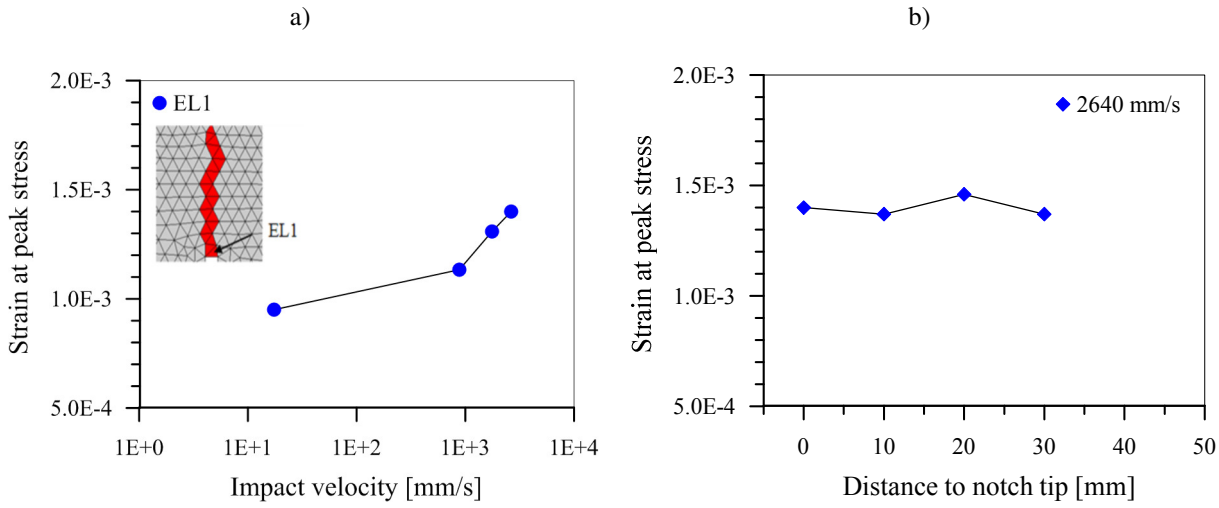

Figure 43. *Numerically evaluated strain at peak stress as a function of a) impact velocity and b) distance to the notch tip.*

Table 9. *Numerically obtained strain at peak stress and strain rate.*

Impact velocity (mm/s)	Strain at peak stress	Strain rate (1/s)
5.50E-04	-	2.34E-06 *
1.74E+01	9.51E-04	5.54E-01
8.81E+02	1.13E-03	2.43E+01
1.76E+03	1.31E-03	3.07E+01
2.64E+03	1.40E-03	3.34E+01

*Zhang et al. (2010a)

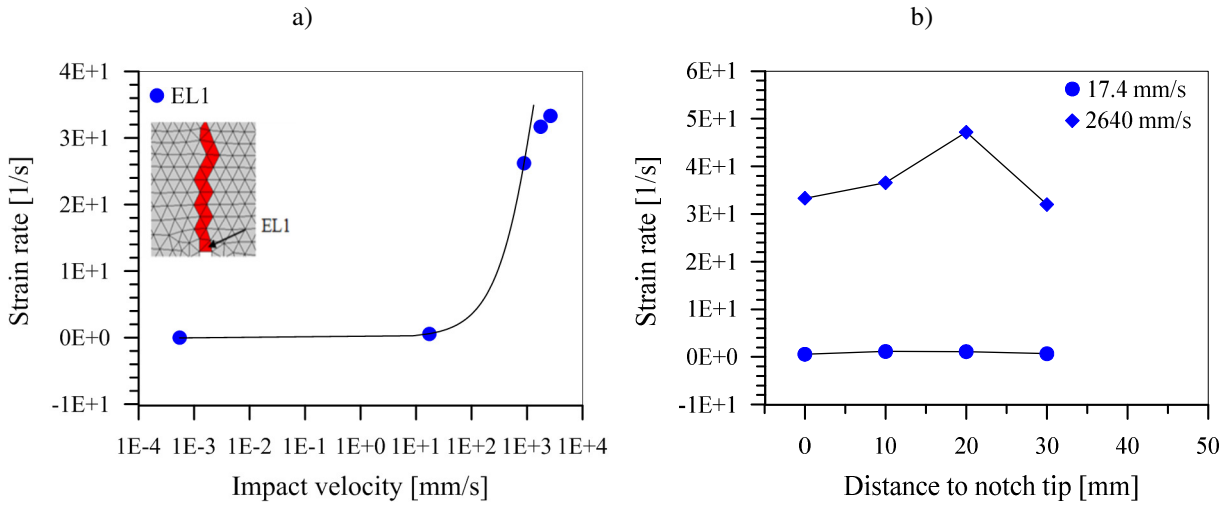

Figure 44. *Numerically evaluated strain rate as a function of a) impact velocity and b) distance to the notch tip.*

5.2.2.4 Effect of impact velocity on crack velocity

In general, with increasing impact velocity, the crack velocity increases. However, as known from the literature (Ožbolt et al. 2011, Ožbolt et al. 2013b) once the crack velocity in concrete reaches critical value (between 600 to 800 m/s) there is crack branching and crack velocity decreases. For the here investigated notched concrete beam, the numerical results are evaluated and compared with available experimental data from Zhang et al. (2010a). The crack propagation velocity is evaluated over the length of cracked beam (see Figure 36), starting from the notch tip. It is calculated by dividing the distance between two observed finite elements (integration points) with the time interval that corresponds to the critical crack openings (0.1 mm) at two measured locations. The calculated velocity is assigned as an average crack propagation velocity. The maximum crack velocities at the notch tip are shown as a function of impact velocities in Figure 45a and summarized in Table 10. The results obtained by the numerical simulation are of the similar order as the experimentally measured crack velocities. Given the difficulties faced in the reliable measurements of such quantities in dynamic experiments, the trends displayed in comparison seem reasonable.

As already stated, the crack opening velocity dw/dt can be calculated from the strain after localization of crack, $dw/dt = (d\varepsilon/dt)\, h$, where h is the width of the crack band (equivalent element size) in the sense of the crack band approach (Bažant and Oh 1983). The detailed information for crack opening velocities above the notch tip are given in Table 10 and plotted in Figure 45b. From Table 10 can be seen that the crack opening velocity approximately

follows impact velocity. As observed earlier this trend is similar to that of the strain rate (Figure 45a), whereas the strain rate increases much slower. Again, this clearly indicates influence of inertial effects on the behaviour.

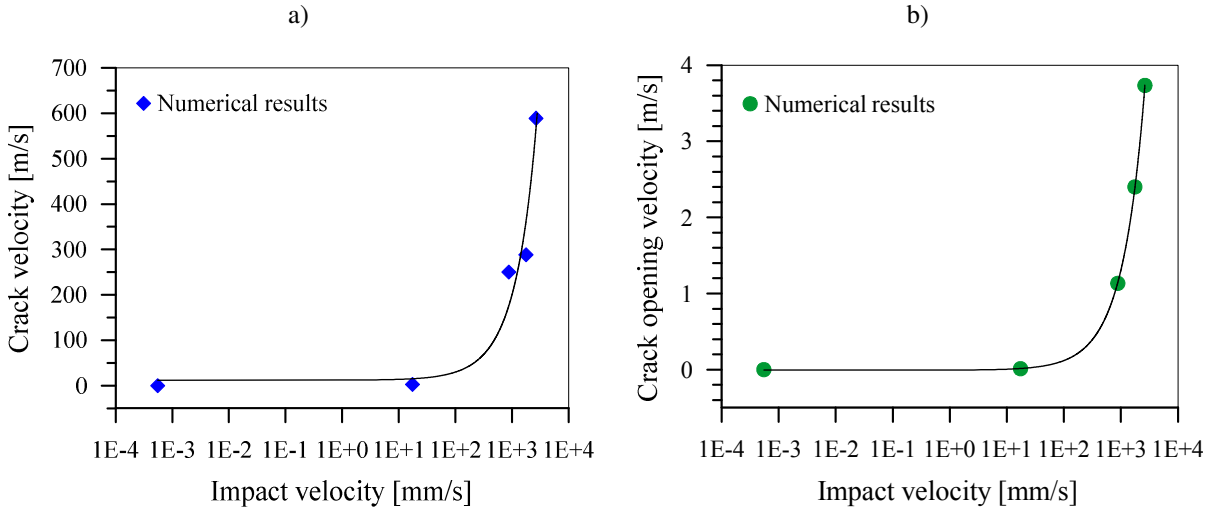

Figure 45. *Numerically obtained a) maximum crack velocity and b) crack opening velocity at different impact velocities.*

Table 10. *Comparison of experimentally and numerically obtained crack velocities.*

Impact velocity (mm/s)	Crack propagation velocity (m/s)								Crack opening velocity (m/s)
	Experimental results (Zhang et al. 2010a)				Numerical results				Numerical results
	Distance to notch tip (mm)								
	0-10	10-20	20-30	30-50	0-10	10-20	20-30	30-50	Notch tip
5.50E-04	1.9E-04	2.7E-04	7.3E-03	2.1E-03	-	-	-	-	-
1.74E+01	11.2	12.6	16	4.2	2.8	1.87	1	-	0.012
8.81E+02	292	250	208	138	250	370	104	82	1.13
1.76E+03	357	278	357	187	288	338	114	101	2.40
2.64E+03	417	417	387	200	589	547	109	81	3.73

5.2.2.5 Rate dependent tensile strength and fracture energy

Currently, no consensus exists within the research community on the correct method to evaluate the dynamic fracture energy of concrete. In this work, to validate numerical results, fracture energy is first evaluated as suggested by Zhang et al. (2009), i.e. by dividing the area under the reactions vs. mid-span vertical displacement curve with the cracked cross section

area of the beam. The fracture energy thus obtained is referred to as apparent fracture energy since it also includes the component of structural inertia and is not true material property. In the context of the present study, the apparent strength contains inertial effects from both sides, i.e. structural and material. However, similar to reaction and impact load, it is not possible to distinguish between the contribution of the structural and material inertia, which are in dynamic analysis coupled and in the rate dependent static analysis decoupled. It should however be noted that the apparent strength in experiments also consists both kind of inertial contributions and therefore can be compared with numerically predicted apparent strength.

To confirm that the numerical analysis replicates experiments reasonably well, the comparison between experimental and numerical reaction-displacement curves for typical load case (impact velocity of 881 mm/s) is shown in Figure 46a. Moreover, in Figure 46b the dynamic increase factor (DIF) for reaction force is plotted against the impact velocity in semi-logarithmic scale. Experimental and numerical results obtained from rate dependent dynamic and static analysis, respectively, are shown. The experimental and numerical results (dynamic analysis) show the same tendency, i.e. the reaction force exhibits a progressive increase in DIF with increasing impact velocity. On the contrary, the results of rate dependent static analysis show linear increase in DIF for the entire range of impact velocity. The difference between static and dynamic analysis is attributed to the inertia effect. DIF for apparent fracture energy is plotted against the impact velocity in Figure 47a. Employing the same evaluation of experimental and numerical results for fracture energy (see Eq. 1), from Figure 47a can be seen that numerical model realistically predicts the behaviour observed in the experiment. Based on the results shown in Figure 47a can be concluded that the fracture energy evaluated from reaction vs. mid-span displacement response exhibits progressive increase with increasing impact velocity. However, this approach accounts also for the effect of structural inertia effects, which should actually be filtered out from the evaluation of results. As mentioned above, in the rate dependent static analysis the entire inertia effects are filtered out. Therefore, the comparison between dynamic and rate dependent static analysis shows the influence of inertia (both structural inertia and inertia from the material side) on the structural response.

Figure 46 and Figure 47confirm the objectivity of the numerical model, because the overall experimental response is replicated realistically. Moreover, based on the comparison between experimental and numerical results it was recently confirmed that the used model is able to

realistically predict complex phenomena in the case of dynamic fracture of concrete in tension dominant problems (Ožbolt et al. 2013b, Ožbolt et al. 2014).

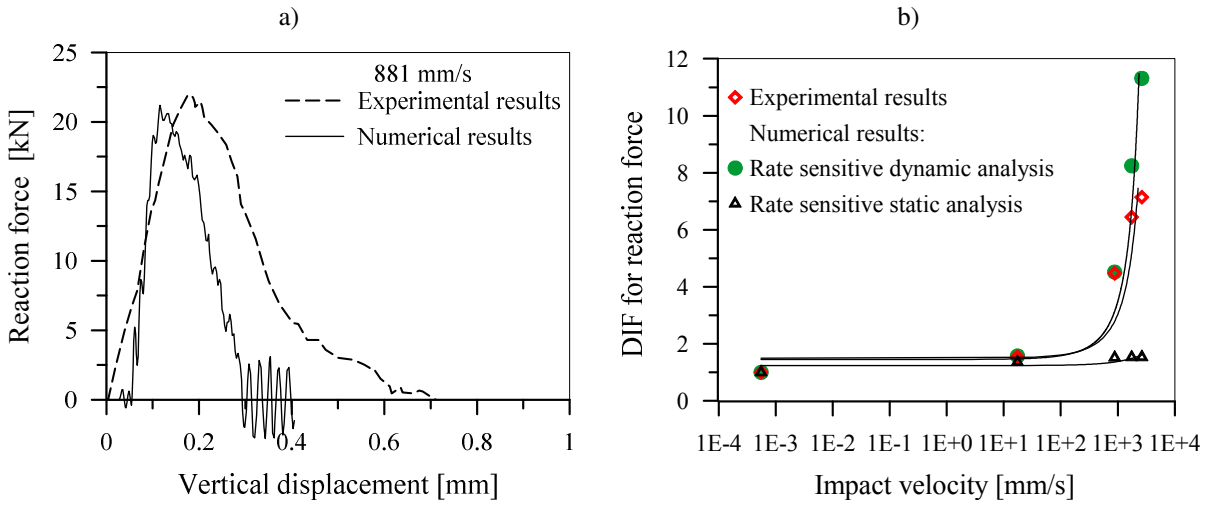

Figure 46. *Comparison between numerical and experimental results for a) typical reaction force vs. displacement curve and b) DIF for reaction force vs. impact velocity.*

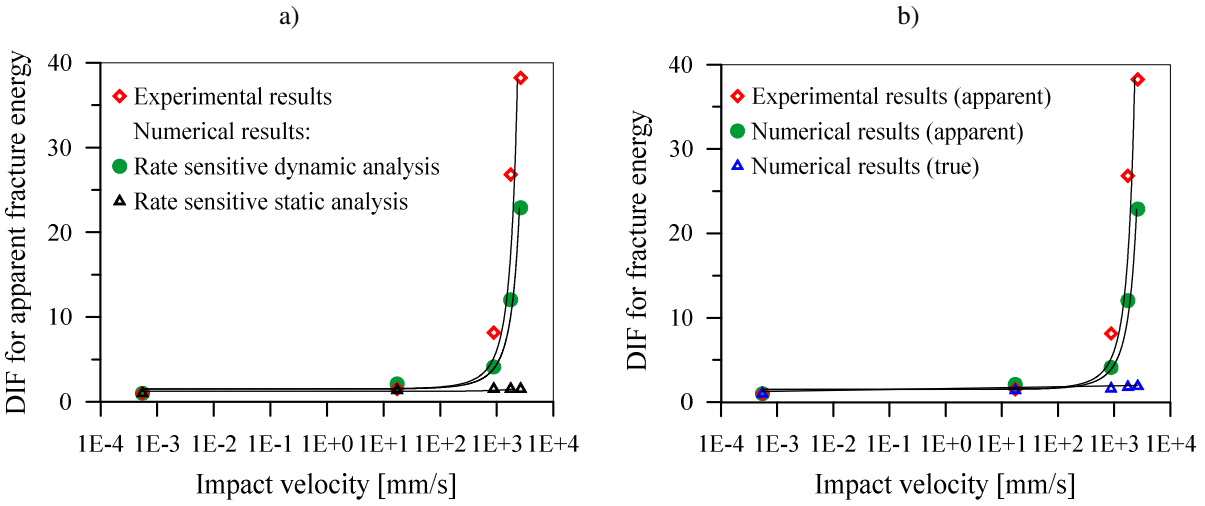

Figure 47. *Comparison between numerical and experimental results for a) apparent fracture energy b) true and apparent fracture energy at different impact velocities.*

To provide more insight in the influence of inertia on fracture energy of the present problem, the evaluation of fracture energy is performed by considering the stress-strain response of a single finite element in the zone of cracking, i.e. just above the notch tip. The numerical results for typical finite element are shown in Figure 47b. These are plotted against the experimental and numerical data shown in Figure 47a. The fracture energy that is calculated

from the single finite element follows exactly the rate dependent constitutive law. Based on the fact that rate dependent dynamic analysis is objective, the difference between the evaluation according to Eq. 1 (apparent fracture energy) and evaluation based on the response of a single finite element (true fracture energy) approximately corresponds to the influence of inertia on the true fracture energy. It should be noted that the exact difference would be obtained by integrating the contribution of all cracked finite elements over the entire cracked cross-section surface. It can be argued that single finite element does not exactly represent the average rate dependent fracture energy over the entire cross section. However, the exact average fracture energy would not significantly deviate from the fracture energy obtained from a single finite element because average fracture energy also follows rate dependent constitutive law which is approximately linear in semi-log scale.

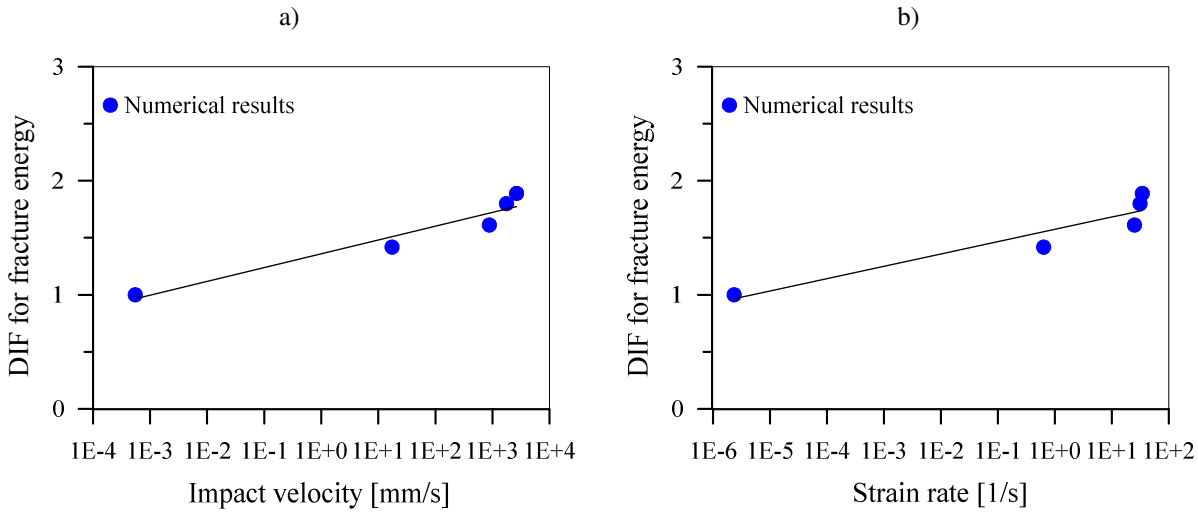

Figure 48. *DIF for the fracture energy as a function of a) impact velocity and b) strain rate.*

It is true that the filtering out of the inertial component from the fracture energy obtained from the experiments is extremely difficult; it can be done relatively easily in numerical analysis. The evaluated true fracture energy from the numerical results is shown in Figure 48a as a function of impact velocity. It can be seen that the true fracture energy of HSC increases as a linear function of impact velocity (semi-log scale), i.e. it approximately follows the rate dependent constitutive law. In Figure 48b true fracture energy is plotted as a function of strain rate. As can be seen, there is a linear increase of fracture energy with increase of strain rate. The increase in fracture energy approximately follows the rate dependent constitutive law of concrete similar to the fracture energy obtained from the rate dependent static analysis (compare Figures 47a and 47b). The fact that dynamic analysis agrees well with the

experimental results indirectly confirm that for the considered range of the strain rates (up to approximately 30/s) fracture energy increases linear in semi-log scale. It needs to be pointed out that in Figure 48 the scale for DIF on fracture energy in the range only up to 3, therefore it may so appear that for strain rates higher than 10/s the slope of the relation gets steeper. However, comparing these data with DIF on apparent fracture energy (compare Figure 47 and 48), it is clear that the increase of apparent strength compared to the increase of true strength is progressive. The differences in DIF for true fracture energies of the three highest strain rates (Figure 48) are most probably caused by the local variation of fracture energy in finite elements due to the 3D effects, e.g. effect of lateral stresses.

The experimental and numerical results are summarized in Table 11. It can be observed that when the numerical results are interpreted in the same way as the experimental ones (apparent strength and fracture energy), they both show same trend of progressive increase, which implies that the analysis is objective. However, the evaluated true strength and fracture energy brings out the fact that this progressive increase is a structural phenomenon, governed by the inertial, and not a material behaviour.

To show the influence of strain rate on tensile strength, the same evaluation approach is used as for the fracture energy, i.e. the strength measured in the finite element above the notch of the beam is plotted against the corresponding strain rate (see Figure 49 and Table 11). It can be seen that, similar as observed for fracture energy, there is linear increase in tensile strength with the increase of strain rate and impact velocity (semi-log scale). It is obvious that tensile strength approximately follows the rate dependent constitutive law. In contrary to the evaluation of experimental results and some recent studies (Zhang et al. 2009, 2010a, 2010b, Lu and Li 2011), which suggest that for strain rates larger than approximately 10/s there is progressive increase of true tensile strength, the numerical results support studies (Cusatis 2011, Ožbolt et al. 2013b, Ožbolt et al. 2014) which confirm that the progressive increase is not due to true tensile strength, but is due to the contribution of inertia. Namely, if one would calculate rate dependent tensile strength from reactions (see Figure 46b), following the same principles as in the case of fracture energy, then is obvious that the tensile strength would increase progressively with increase of strain rate. However, this would be apparent and not true rate dependent tensile strength.

Table 11. *DIF for reaction force, tensile strength and fracture energy at the crack tip.*

Impact velocity (mm/s)	Strain rate (1/s)	DIF for reaction force		DIF for tensile strength	DIF for fracture energy		
	Numerical results	Experimental results* (apparent strength)	Numerical results (apparent strength)	Numerical results (true strength)	Experimental results* (apparent)	Numerical results (apparent)	Numerical results (true)
5.50E-04	2.34E-06	1.0	1.0	1.0	1.0	1.0	1.0
1.74E+01	6.36E-01	1.54	1.57	1.46	1.53	2.10	1.42
8.81E+02	2.50E+01	4.48	4.52	1.60	8.14	4.11	1.61
1.76E+03	3.15E+01	6.44	8.24	1.73	26.81	12.03	1.80
2.64E+03	3.43E+01	7.14	11.31	1.80	38.23	22.89	1.89

*Zhang et al. (2009)

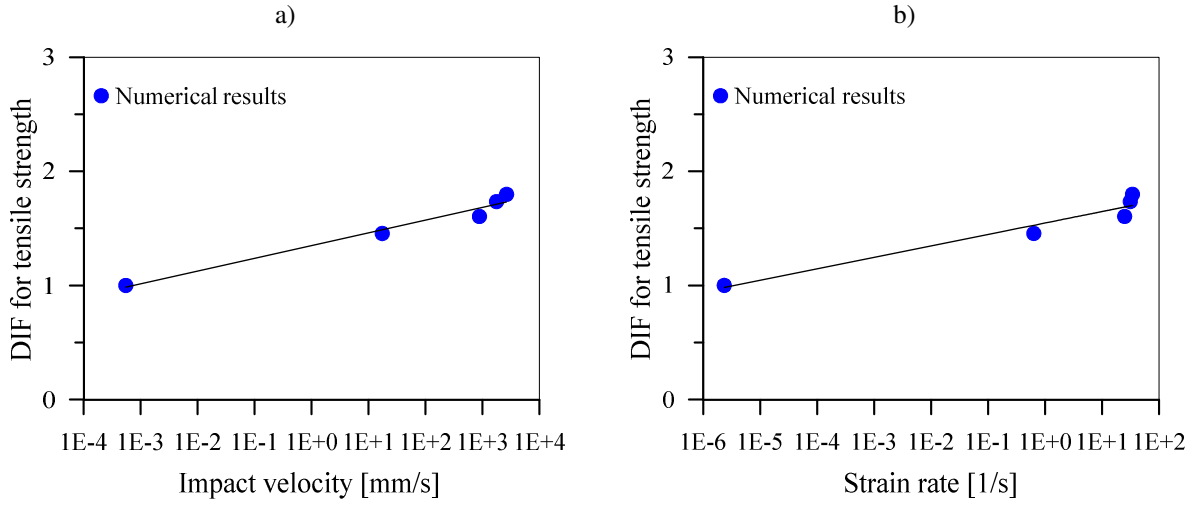

Figure 49. *DIF for the tensile strength as a function of a) impact velocity b) strain rate.*

As mentioned before, to assure mesh objective results in the present study the crack band method is employed. This implies that true fracture energy is consumed within one row of single finite elements. In the present study the size of the elements was chosen in the range of aggregate size. However, in dynamic fracture analysis such approach has some limits. If the resolution of the finite element mesh is too coarse (e.g. very large structure), with elements much larger than the aggregate size, the interaction between rate dependent constitutive law, which because of large elements would need to be elastic-brittle, and inertia could not be properly accounted for. For instance, the crack branching could not be predicted with the consequence that the progressive increase of apparent strength would possibly not be

predicted objectively. Therefore, for such situation (very coarse mesh) the progressive increase of apparent strength needs to be explicitly accounted for in fracture energy and tensile strength, i.e. at the constitutive level. The consequence of such approach would be the correct prediction of resistance, however, in general the failure mode (e.g. crack branching) would not be predicted correctly.

5.2.3 Conclusions

In the present chapter dynamic behaviour of plain notched beam under hammer three-point bending impact load is numerically studied. Rate dependency in numerical analysis is accounted for through the rate dependent microplane model for concrete while explicit dynamic analysis is performed to account for the influence of structural inertia. To model impact of hammer on plain concrete beam, multi body finite element dynamic analysis is performed. Based on the results of the numerical analysis and comparison with experimental results, important conclusions are drawn.

In general, it is found that the numerical results exhibit a good agreement with the experimental counterparts. Comparing impact load with the corresponding reaction force as a function of impact velocity, it is shown that the peak impact force is much greater than that the peak reaction. However, the curves exhibit similar tendency, i.e. for impact velocity greater than approximately 100 mm/s there is a steep progressive increase, which is attributed to the structural inertial effects. Further, it is found that maximum strain rates increase as the impact velocity increases. For the investigated notched beam specimen maximum strain rate of approximately 30/s was obtained. Next, maximum crack velocity is observed at the notch tip and is approximately equal to 500 m/s. Since this is lower than velocity at which there is a crack branching (approximately 600 to 800 m/s), the failure mode for all loading rates was mode-I.

It is demonstrated that both, strain rate dependent fracture energy and tensile strength, evaluated based on reaction forces may be misleading because, there is significant contribution of inertia, which cannot be attributed to material resistance. Consequently, such evaluation of experimental or numerical results leads to their progressive increase when strain rate becomes large than approximately 10/s. Numerical results and their comparison with experiments show that for the investigated range of the strain rate (up to 30/s) the true fracture

energy and tensile strength increase approximately linear with strain rate (semi-log scale) and that approximately follow rate dependent constitutive law used in the computation. These conclusions are indirectly confirmed by the fact that the numerical analysis reasonably well replicates the test results. The progressive increase of rate dependent strength and fracture energy should not be included into the constitutive law, unless a constitutive law employed in the finite element analysis is not able to automatically account for the progressive increase of inertia on resistance or the finite element discretization is too coarse. The consequence of such approach is the correct prediction of resistance, however, the failure mode and crack pattern can be misleading.

6. NUMERICAL PARAMETRIC STUDY

In the previous chapter, a 3D finite element code has been calibrated and verified against experiments. It is shown that the code, based on rate dependent microplane material model, is capable of reproducing the experimental results on concrete structures/specimens under dynamic loading as well as complex phenomena related to dynamic fracture such as crack branching or change of failure mode quite well. Here, the same finite element code as presented in Chapter 4 is employed to assess the influence of contact geometry on dynamically loaded notched beams under different impact velocities. In order to assure different types of failure, i.e. transition from bending to mix-mode failure, loading rates are extended up to 10^4 mm/s.

6.1 Influence of contact geometry

6.1.1 General

From the experiments carried out by various researchers, it can be said that with increase in loading rate the load carrying capacity increases, however, the unfavorable condition may arise from the change in failure mode. Principally, high loading is related with the change of failure mode from mode-I (under static loading) to a mix-mode failure (under dynamic loading), see for example Ožbolt et al. (2006), Travaš (2009), Ožbolt et al. (2011), Ožbolt and Sharma (2011), Ožbolt and Sharma (2012) and Ožbolt et al. (2013b). Moreover, after crack velocity reaches certain threshold, crack branching occurs. The main reason for crack branching are inertia effects at the crack tip which prevents mode-I propagation and force crack to split (branch) into two new cracks (Ožbolt et al. 2013b). Furthermore, it is well known that the behaviour of structure under impact loading depends on size and shape of contact surface, among other factors (Zelinski 1984). In other words, the change of failure mode and response of concrete structures depends on the energy transferred due to impact. Hence, it can be expected that for the same structure, influence of inertia will be stronger in case of larger impact contact surface since the structure has to consume a bigger amount of energy.

From literature survey it is evident that large number of drop hammer experiments are performed to investigate the behaviour of concrete under impact load (Suaris and Shah 1983, Banthia et al. 1989, Sukontasukkul et al. 2004, Zhang et al. 2009, Erdem 2012). Usually, only bending type of failure mode is considered. However, it should be noted that these experiments are conducted under different conditions, such as different impactor (impacting hammer) size and shape, different specimen dimensions and material properties. This makes impossible to directly compare the results since there are many parameters that can affect the impact response of concrete. The most common impactor tip used in these experiments is hemispherical or semi-cylindrical although some researchers have used other impactor shapes such as flat-ended and conical. Obviously, there still remains a need for a systematic study on the influence of contact geometry on the fracture behaviour of notch plain concrete beams loaded by different rates. In the case of civil engineering structures, impact event often consist of a relatively large impactor tip compared to the target (structure). Therefore, it is interesting and important from perspective of engineering design and damage/fracture mechanics to investigate behaviour of concrete beams using varying shape of impactor tip under dynamic loading. Hence, the main objective of this study is to investigate the effect of contact geometry on behaviour of dynamically impacted notched plain concrete beams under different loading rates. In addition, conducted parametric study should assist in understanding previously assumed hypothesis.

6.1.2 Finite element model

As already mentioned, simulations are performed on notched concrete beams using exactly the same finite element model (see Figure 34) and material properties (listed in Table 4) as reported in the Chapter 5 and Chapter 3, respectively. Except velocities listed in Zhang et al. (2009, 2010a): 1.74×10^1, 8.81×10^2, 1.76×10^3, 2.64×10^3, following impact velocities are also employed: 6×10^3, 10×10^3, 30×10^3 and 50×10^3 mm/s. Three types of impactors (impact hammers) with different geometry of the striking head (tip) are used to impact the beam specimen: one with semi-cylindrical tip (6 mm diameter) as already described in previously performed numerical study verified against experiments conducted by Zhang et al. (2009, 2010a) and the other two with the flat-ended tip 6 and 16 mm in size, respectively. Except the shape of the hammer tip, geometrical and material characteristics of impacting hammer are unchanged. Geometry and finite element mesh of the impact hammers used for the numerical analysis are shown schematically in Figure 50.

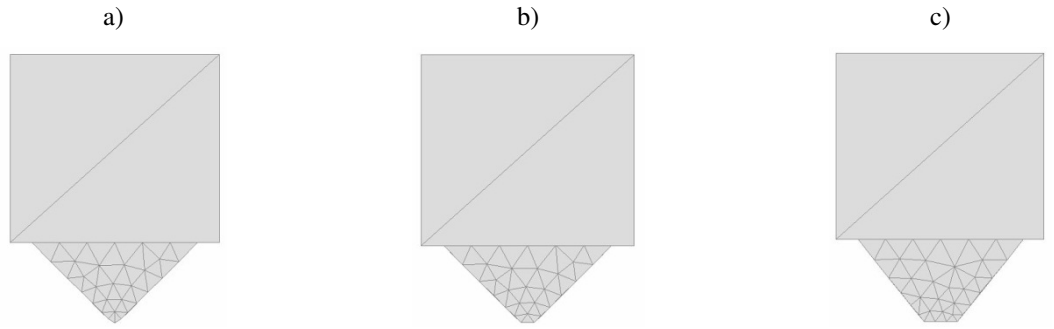

Figure 50. *Geometry and finite element mesh of the impact hammers used for the numerical analysis with a) semi-cylindrical tip (6 mm diameter), b) flat-ended tip 6 mm in size and c) flat-ended tip 16 mm in size.*

6.1.3 Results and discussion

The numerical results obtained for different loading rates and contact geometries are discussed. In the following simulations failure behaviour, crack initiation and propagation, impact load and rebound force are compared. Extra attention is devoted to the change of the failure mode and to the beam resistance.

6.1.3.1 Failure mode and damage area

The failure mechanism and crack patterns for various impact velocities and three types of impactor tip geometry at the time of peak reaction are shown in Figure 51. Clearly, the failure mode of the investigated HSC beam is strongly influenced by the impactor tip geometry as well as the impact velocity (see Figure 51). It turns out that for relatively low loading rates there is only one crack. However, when loading rate reaches approximately 6 m/s there is crack branching. Namely, with increasing loading rate there is a transition of the failure mechanism from bending (mode-I fracture) to shear.

Here, two typical modes of failure are observed. It is found that failure mode of the notched HSC beam is not particularly sensitive to the shape of the impactor tip (loading head of the hammer) for relative low loading rates. For all impact velocities up to approximately 6 m/s different impact hammer tips, e.g. semi-cylindrical or flat-ended tip, produce same failure mechanisms and similar crack patterns, i.e. mode-I type of failure (bending failure) where single crack propagates from notch tip straight to the loading point surface. Beyond this velocity (6 m/s) the failure mode and crack patterns are affected by the shape of impactor tip (contact area), as illustrated in Figure 51. Furthermore, the bending failure mode,

accompanied by considerable localized damage in the vicinity of impacted area, dominates for all impact velocities up to 10 m/s for semi-cylindrical impactor tip (see Figure 51). When using the impactor with flat-ended tip failure mode changes dramatically for impact velocity of approximately 10 m/s, namely the first sign of shear failure occurs. Unlike the beams impacted with the semi-cylindrical tip where damage is concentrated only at the contact area, the amount of localized damage in the vicinity of impacted area decreases and the primary bending failure mode is combined with share where share failure mode predominates.

Figure 52 contains overview of typical crack patterns and failure mechanisms features along the bottom surface of the beam generated by the various impactor shapes. For both flat-ended impactor tips damage initiation of the bottom concrete surface starts at approximately 10 m/s, as shown in Figure 52. On the contrary, for sharp impactor tip there is no visible damage on bottom side surface of the beam. For 50 m/s for semi-cylindrical impactor tip a visible damage is evident at the bottom side surface. On the other hand, for flat-ended imapactors cracks propagates orthogonally to direction of applied loading according supports. Obviously, this difference is due to the shape of the impactor tip. Therefore, both flat-ended impactors produce more extensive bottom-face damage compared to the semi-cylindrical tip for all impact velocities. Moreover, it is observed that both flat-ended impactor tips produce similar failure mechanisms and crack patterns for same range of impact velocity.

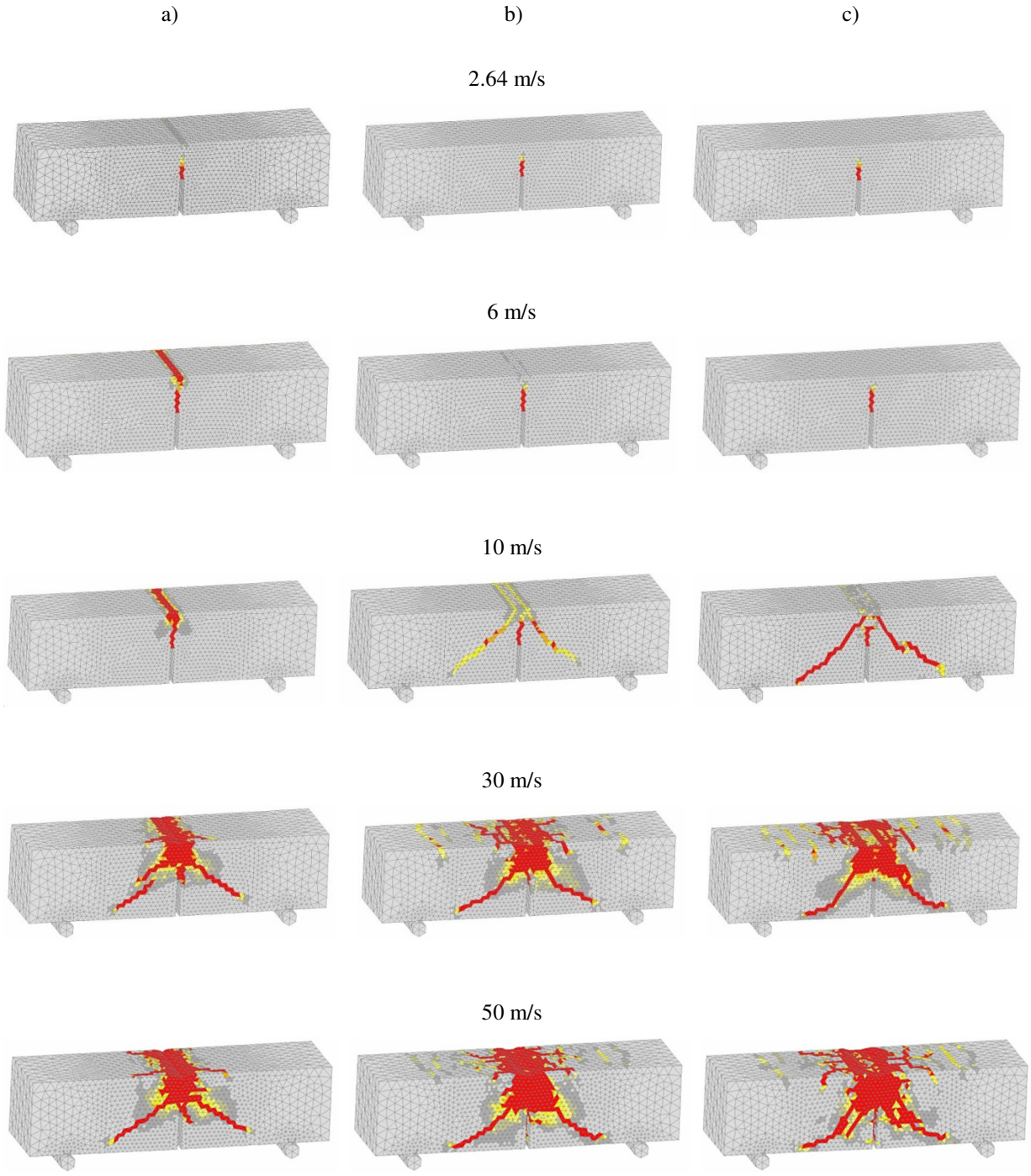

Figure 51. *Failure mode and crack patterns at the peak reaction at different impact velocities for different geometry of hammer tip a) semi-cylindrical tip, b) flat-ended tip 6 mm in size and c) flat-ended tip 16 mm in size.*

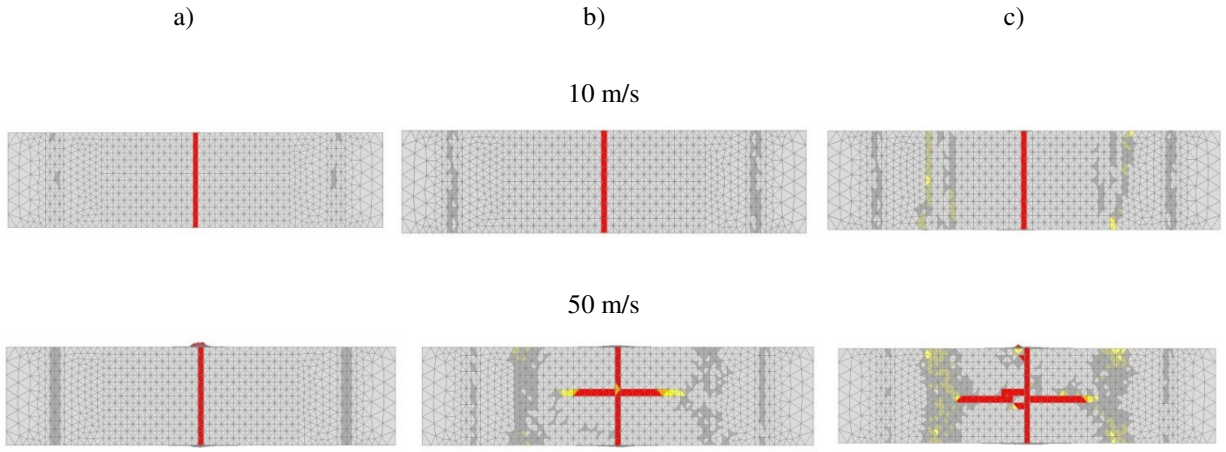

Figure 52. *Crack pattern at the peak reaction at different impact velocities for different geometry of hammer tip a) semi-cylindrical tip, b) flat-ended tip 6 mm in size and c) flat-ended tip 16 mm in size at the bottom surface of the beam.*

Damaged area at the time of peak load for notched beam impacted with different tip of striking head of hammer is illustrated in Figure 53. At the time of impact a certain amount of concrete beam at the impact area becomes damaged immediately. Semi-cylindrical impactor tip shows the most localized damage area followed by the flat-ended in 6 mm and 16 mm size, respectively. As the impact velocity increases damaged area spreads outside the contact region to the ends of the beam. Figure 51 and Figure 53 clearly indicate that damaged area in the vicinity of impacted point is more localized with the decrease of the contact area for all impact velocities. For the same impact velocity semi-cylindrical impactor produces more pronounced damage in the zone of impact point compered to both flat-ended tips. Because contact area of the semi-cylindrical tip is small, the force is highly concentrated at the contact area resulting in considerably high localized damage and first signs of penetration. The first sign of penetration occurs for the semi-cylindrical tip at approximately 6 m/s. By changing the loading head to the flat-ended shape, much larger contact area with greater volume of the beam becomes involved in absorbing of the applied load. As a consequence, the localized damage at the contact surface is reduced. On average, for same impact velocity the flat-ended impactors produce the largest damage area, namely, localized failure is reduced, while sharp impactor produces the most localized damage area and the largest penetration depth.

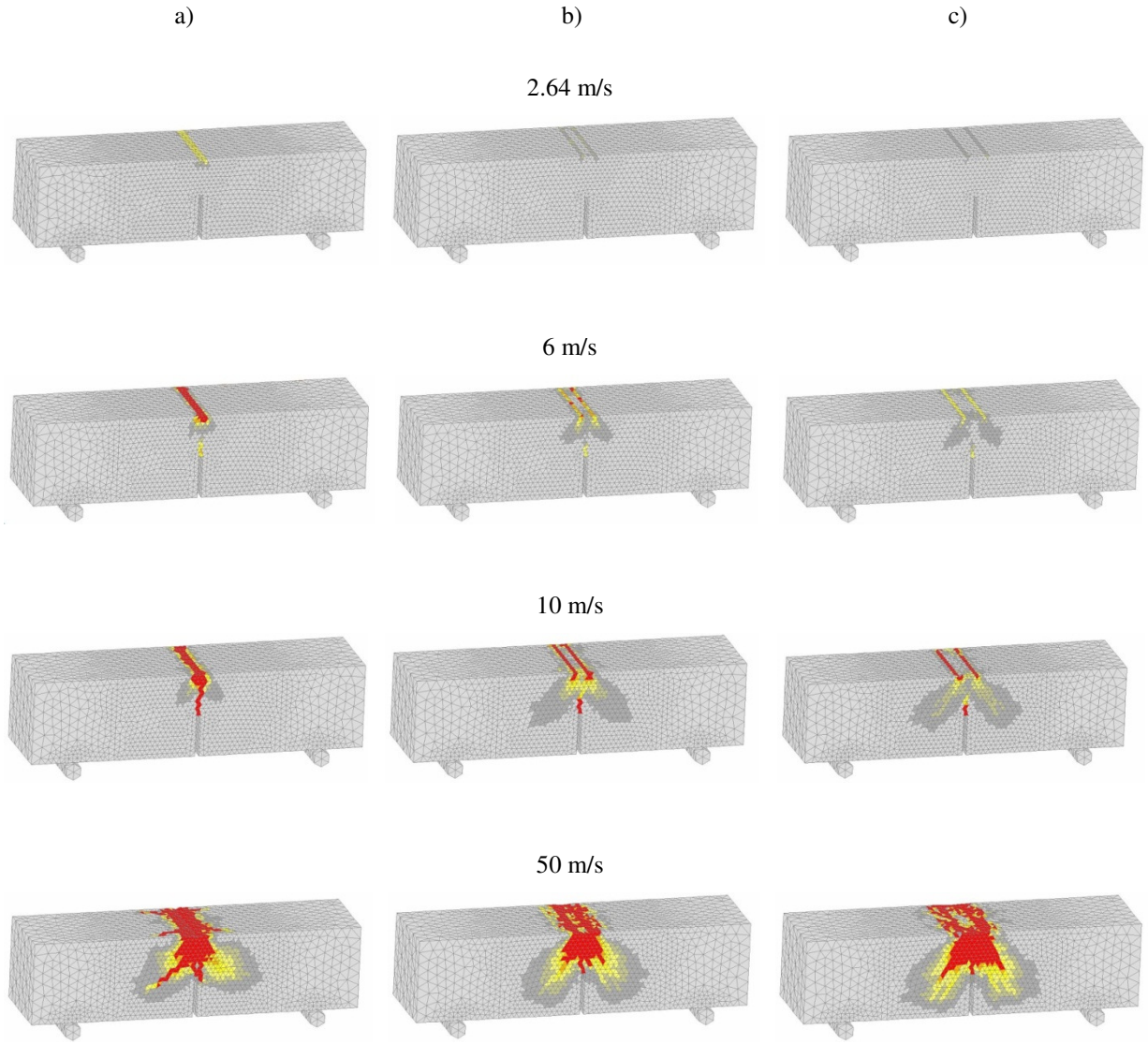

Figure 53. *Crack pattern at the peak load at different impact velocities for different geometry of hammer tip a) semi-cylindrical, b) flat-ended 6 mm in size and c) flat-ended 16 mm in size.*

6.1.3.2 Impact force, reaction force and rebound force

To analyze the resistance of concrete beams against the impact velocity, the impact load and reaction force curves of different impactor shapes are compared for investigated range of impact velocities.

Typical impact force (load) versus time histories produced by the semi-cylindrical and flat-ended impact tips of 6 and 16mm in size, at representative impact velocities of 10 and 30 m/s are shown in Figure 54. It is found that if the contact surface is larger (becomes more blunt), the peak load increases and the impact duration decreases. The bigger penetration depth

realized by the semi-cylindrical tip leads to decrease in the peak force value. Hence, for same impact velocity the semi-cylindrical impactor tip produces the lowest peak load and longest contact duration. On contrary, both flat-ended impactors produce similar peak loads which are higher and shorter in contact duration compared to the semi-cylindrical (see Figure 54). Moreover, it is seen from Figure 54 that the peak force for flat tips is nearly same for same impact velocity, i.e. peak load values for 10 m/s for tip of 6 mm and 16 mm in size are 477 kN and 454 kN, respectively. For the specimens impacted at higher impact velocities, the flat-ended impactors produce cracking over a larger area while bigger penetration depth and much smaller amount of cracking is observed by the semi-cylindrical impactor. Due to that reason, contact duration of flat-ended impact hammer is lower and the peak load higher than for the semi-cylindrical impactor tip.

Figure 55 shows numerical data in terms of impact force (load) versus impact velocity for three different impactor tips, for the semi-cylindrical, flat-ended 6 mm and 16 mm in size, respectively. Beams impacted with semi-cylindrical impactor tip undergo more pronounced damage at the impact point and hence develop lower peak loads than beams that are impacted with flat-ended impactor. The difference is especially pronounced for velocities higher of 6 m/s. The lower peak load produced by the semi-cylindrical impactor is attributed to the bigger penetration depth caused by the sharp tip of impactor. Moreover, this penetration results in bigger friction between the impactor and specimen which increases the contact duration (Figure 54). Hence, it is found that peak impact load is always lower than the one obtained with the flat-ended tip at the same rate of loading (impact velocity) due to the large amounts of localized damage and bigger penetration depth.

It is interesting to observe that this trend is not evident for peak reaction forces. Concrete beam impacted with flat impactor shape 16 mm in size (Figure 50c) indicates highest resistance (Figure 56) for velocity lower of approximately 10 m/s whereas semi-cylindrical impactor tip produces the lowest peak reaction. On the contrary, for velocities higher than 10 m/s semi-cylindrical impactor tip produces the highest peak reaction force while flat impactor shape 16 mm in size, the lowest. In other word, the peak reaction force for semi-cylindrical tip is the lowest for impact velocity at approximately 10 m/s but for higher velocities semi-cylindrical tip gives the highest resistance of the three investigated impactor shapes. To understand the reason of this phenomenon it is interesting to compare failure mode and crack

patterns at the peak load for one typical velocity in more detail, for example for velocity of 10 m/s, see Figure 52 and Figure 53.

In general, at 10 m/s, flat-ended impactors produce more extensive bottom-face damage of beam specimen whereas the semi-cylindrical shows barely visible crack patterns. This overview of results suggests that the back-face damage becomes dependent of impactor shape after a specific level of impact velocity is reached. For tested geometry and concrete properties the first crack branching and bottom surface damage is observed for impact velocity of approximately 10 m/s. From Figure 51 and Figure 52 is evident that decrease of reaction force is a result of the varying failure mechanisms caused by transition of bending to share failure. For the flat-ended impactor tips after bending deformation occurs, the damage zone extends to the edges of the specimen. For this reason, the overall damage zone for this sample is the largest. On the other hand, for the semi-cylindrical tip is the smallest. Therefore, it is supposed that large drop in peak value of resistance (Figure 56) of concrete beams impacted with flat-ended tip is result of the initiation of the overall damage of the beam (see Figure 51 and Figure 52).

Figure 57 shows displacement for various impactors under different impact velocities. It is clearly seen that 16 mm flat-ended impactor produces the lowest deflection, whereas the semi cylindrical impactor produces the highest deflection. Principally, it can be concluded that as the contact surface gets larger, the deflection is smaller.

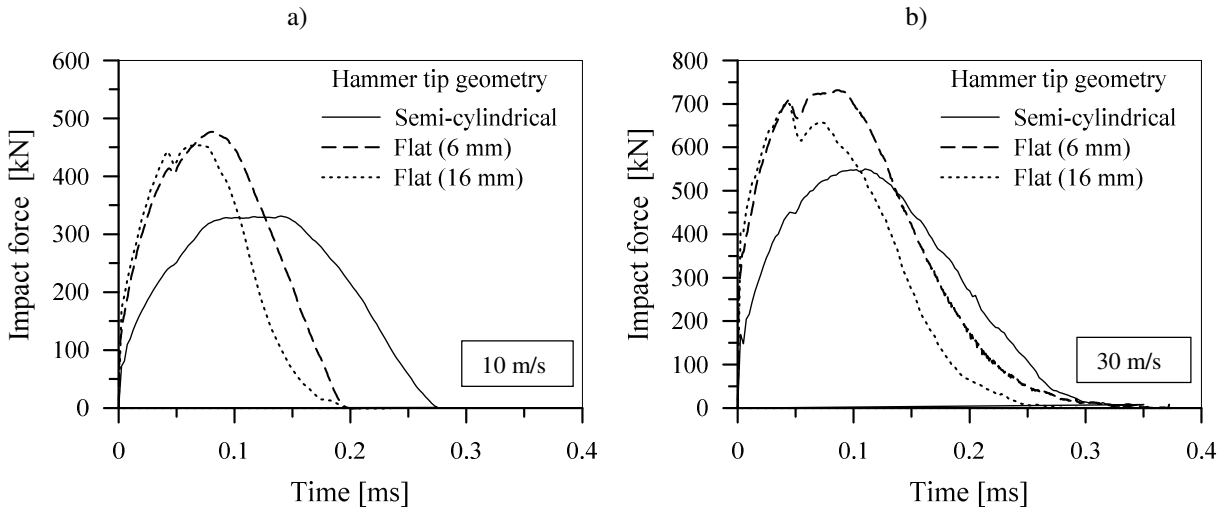

Figure 54. *Typical impact force versus time history produced by the semi-cylindrical and flat-ended impact tips 6 and 16mm in size at different impact velocities a) 10 m/s and b) 30 m/s.*

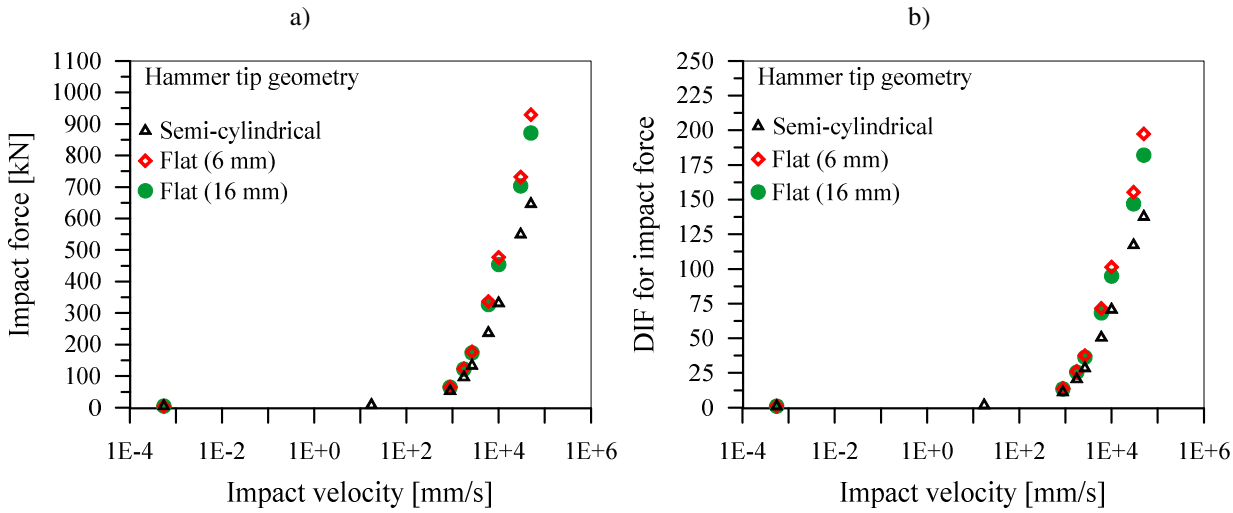

Figure 55. *The effect of impact hammer tip on the a) impact force (load) and b) DIF for impact force (load) at different impact velocities.*

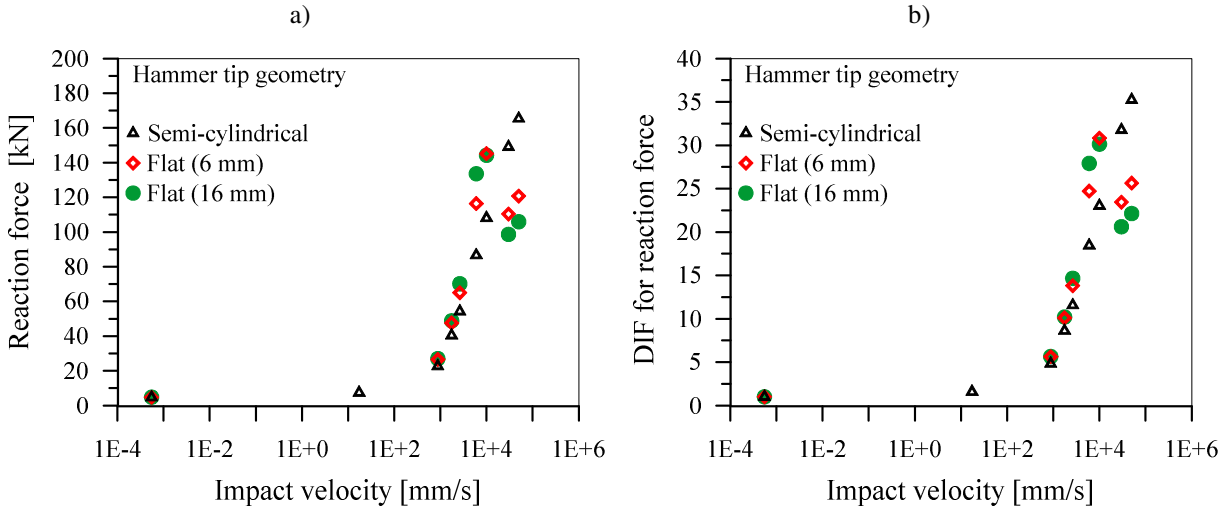

Figure 56. *The effect of impact hammer tip on the a) reaction force and b) DIF for reaction force at different impact velocities.*

The relationship between the rebound forces for different impactor tip shapes against impact velocity is shown in Figure 58. For lower impact velocities barely visible damage at the top surface of the beams in the region of impact are observed (see Figure 53). However, due to the difference of the hammer tip, the damage induced with the semi-cylindrical tip is significantly larger than for the flat-ended. As expected, the sharp tip of semi-cylindrical impact hammer causes the most localized damage and the largest penetration depth. As a result, rebound force is the smallest for the semi-cylindrical shaped impactor and the greatest for the flat-ended 16 mm in size. At the impact velocity of 6 m/s the rebound force is about 25 kN for semi-cylindrical impactor tip, compared to the flat-ended 6 mm and 16 mm in size of

110-140 kN, respectively (see Figure 58b). Due to the fact that the localized damage and penetration depth induced by semi-cylindrical tip are greater than of the flat-ended, consequently, the value of the hammer rebound force is less than the flat-ended one. Hence, when localized damage at the impact point due to penetration starts to increase, rebound force decreases. Consequently, at some critical value of impact velocity, rebound force becomes zero. Here, for example, for semi-cylindrical impactor tip at the impact velocity of 10 m/s and higher as well as for flat-ended impactor tips at the impact velocity of 30 m/s and higher, there is no rebound (see Figure 58b).

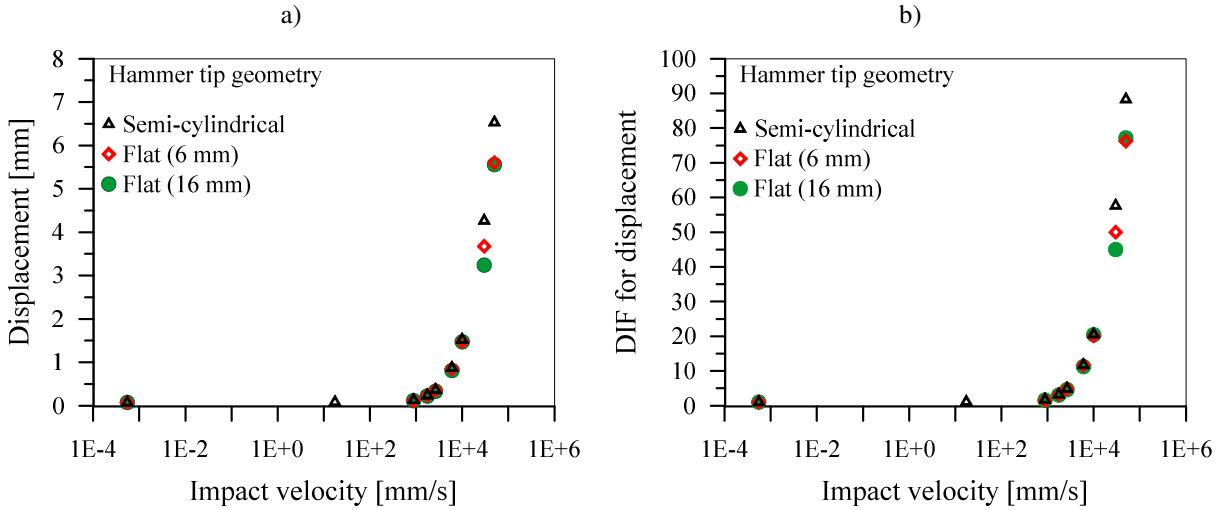

Figure 57. *The effect of impact hammer tip on the a) displacement and b) DIF for displacement at different impact velocities.*

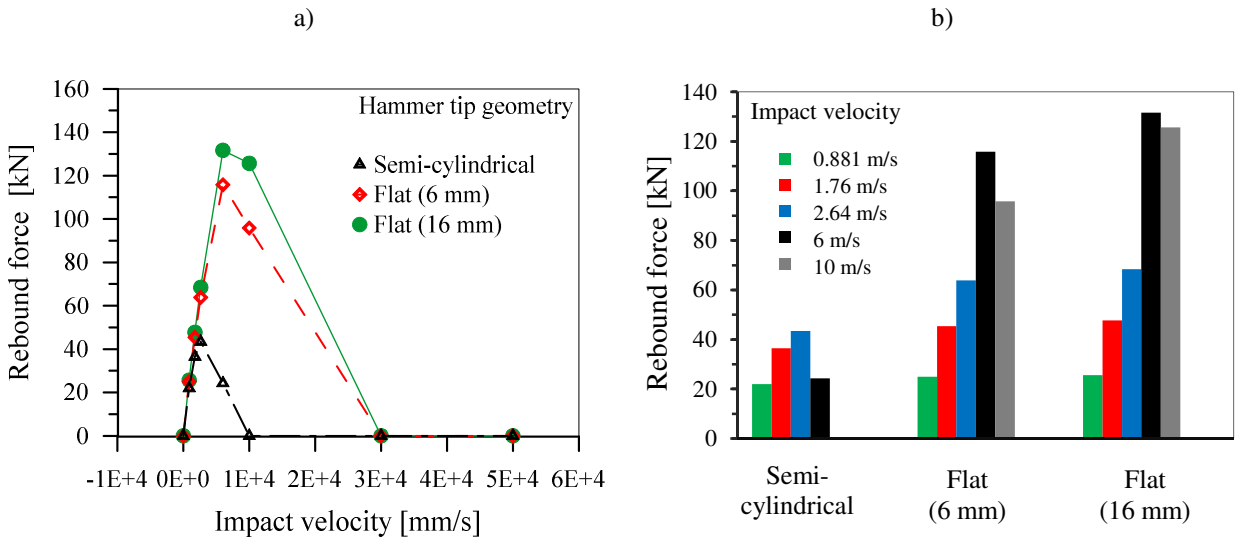

Figure 58. *The effect of impact hammer tip on the rebound force at differenet impact velocities.*

6.1.3.3 Rate dependent tensile strength and fracture energy

Figure 59 presents numerical results for DIF of reaction forces (resistance) compared to the constitutive law as a function of strain rate. With the increase of strain (loading) rate the apparent strength (resistance) increases approximately linear (in semi-log scale) up to the certain strain (loading) rate. As indicated before, in this range of strain (loading) rate the rate dependent constitutive law controls the resistance. For higher strain rates apparent strength exhibits progressive increase clearly dependent on the geometry of impact hammer tip (structural response). This progressive increase occurs exactly at strain rate at which crack branching occurs, approximately 70/s. Moreover, for the flat-ended hammer tips failure mode changes to share mode and resistance drops down. Again, this confirms that increase of apparent strength as well as change of the failure mode is controlled mainly by structural inertia. In contrary to this, the true strength (constitutive law) shows almost no sensitivity on the impact hammer tip geometry (see Figure 60). The evolution of true strength and fracture energy is performed the same as discussed in previous chapter. The results of numerical analysis show increase of DIF with a factor of approximately to 3, which is considerable increase within the investigated range of strain rates (see Figure 60a). The similar trend is observed for fracture energy as a function of strain rate (see Figure 60b). Note that this increase is most probably due to the fact that for strain rates larger than 100/s at the notch tip there is no clear mode-I fracture, i.e. more than one element get damaged. Therefore, most probably the maximum principal strain (crack direction) does not coincide with direction of maximum principal stress (loss of coaxially). Due to this there is an more than linear increase of rate dependent strength and fracture energy. Hence, both fracture energy and tensile strength appeared to deviate slightly at the higher strain (loading) rates from the constitutive law, while progressive increase of resistance, change of the failure mode and crack branching phenomena is due to inertia effects.

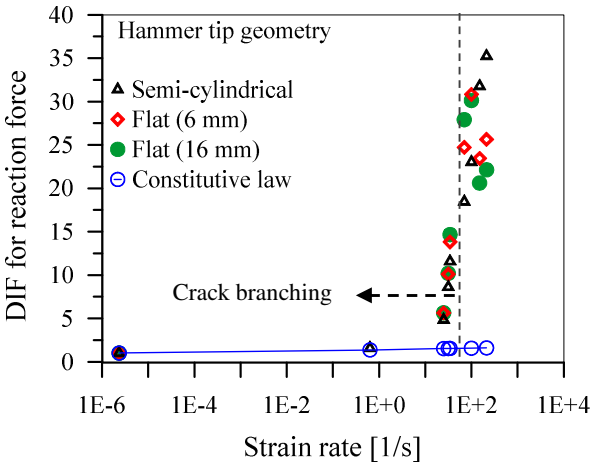

Figure 59. *DIF for reaction force compared with DIF for tensile strength of concrete from rate dependent constitutive law (microplane model).*

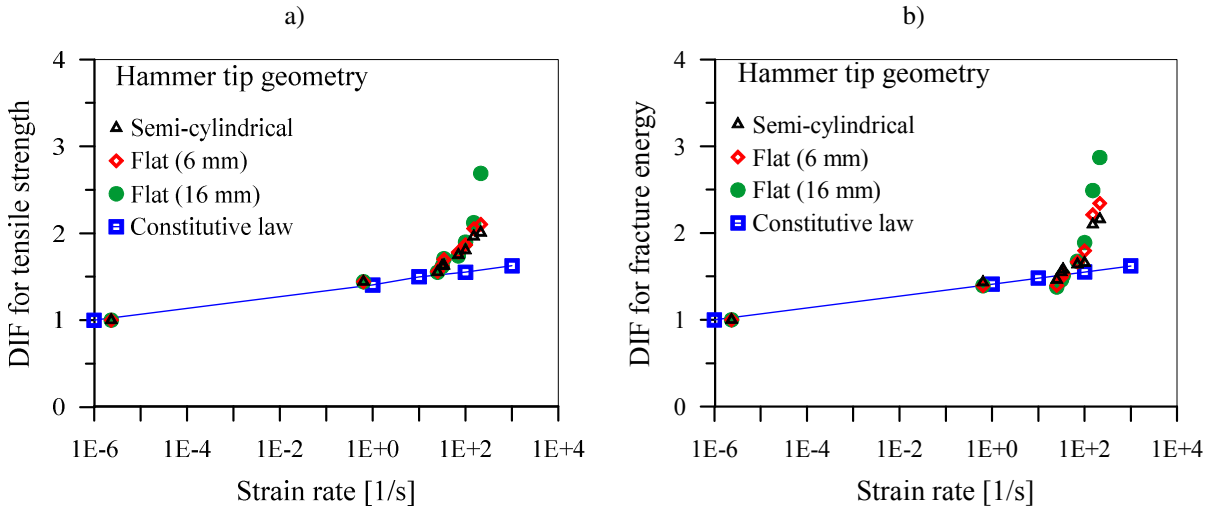

Figure 60. *The effect of impact hammer tip on the a) DIF for the tensile strength and b) DIF for the fracture energy as a function of strain rate.*

6.1.4 Conclusions

In the present chapter, the influence of impactor shape on dynamic fracture of notched concrete beam is investigated numerically for different velocities. Concrete beams are impacted using hammers with different contact area: semi-cylindrical 6 mm in diameter and flat-ended 6 and 16 mmm in size, respectively. A wide range of impact velocities, from low (order of 10^{-7} m/s) and medium (order of 10^{-2} m/s) to high (order of 100 m/s) and very high (order of 10^{1} m/s), are discussed in this study. Based on the numerical results, the mechanisms of cracking and failure have been investigated in detail. It is shown that different impactor shape and impact velocities produce different damage areas and failure mechanisms which

directly affected the beam resistance and load carrying capacity, but do not affect fracture energy and tensile strength of concrete material.

Furthermore, it is shown that under static and low loading rates, less of approximately 70/s, crack patterns and failure mechanisms are not influenced by the various impactor tips. The low velocity impact response of the notched beams is found to be similar for flat-ended and semi-cylindrical tip impactors. However, for higher impact velocities the failure modes and crack patterns are significantly different for different impactor hammer tips. Responsible for this is inertia. Both flat-ended impactor tips of 16 mm and 6 mm in size at approximately 70/s produce transition of bending failure to share failure and fracturing of the bottom concrete surface, leading to a significant drop in reactions compared to semi-cylindrical impactor.

Based on conducted investigation it is clear that apparent strength (resistance) of concrete increases with increase of impact velocity for all impactor shapes. Principally, for the semi-cylindrical impactor tip it is found that, for whole range of investigated velocity resistance increases with increase of impact velocity. Moreover, the concrete cracking initiates at notch tip and vertically propagate to top surface of the beam. For beam impacted with flat-ended tip for velocities higher than 10 m/s resistance (peak reactions) of the concrete beam is reduced due to crack patterns inclined to 45° with respect to applied load. With the flat-ended impactor tips, stress concentration is distributed to greater/wider area and shear crack patterns are found to be the dominant failure mechanism. These results in decrease of peak reaction for higher impact velocities compared to semi-cylindrical tip. The resistance (reaction force), impact load and failure mechanism are found to be very similar for both flat-ended impators for all impact velocities.

For loading velocities higher than 6 m/s both flat-ended impactors produced larger damaged area compared to semi-cylindrical impactor. Hence, for all impact velocities the damaged area is found to be the largest for the flat-ended tip 16 mm in size, followed by the flat-ended tip 6 mm in size and semi-cylindrical impactor, respectively. For semi-cylindrical impactor rebound force is found to be smaller than for the flat-ended impactors for all impact velocities. These conclusions indicate that the local damage increases as the impactor velocity increases and contact area of impactor decreases.

In general terms, the present numerical study has demonstrated the important contribution of contact surface and impactor shape on resulting damage and failure mode of concrete specimens/structures. Therefore, it is found that even if all geometrical and material properties are same but impactor tip is different, the final damage areas and failure mechanism could vary significantly under same impact velocity. On the contrary, true material properties of concrete do not vary with various impactor shape under both static and dynamic loading.

7. CONCLUSIONS AND RECOMMENDATIONS

Conclusions

The study of concrete fracture behaviour under dynamic loading is given through analysis of L-shaped specimen under high loading rate and notched beam under impact load. In order to understand the loading rate sensitivity of concrete, both experimental and numerical techniques are employed. Principally, experimental investigation shows how loading rate influences the overall response of concrete structures, while the numerical results can explain phenomena observed in experimental tests.

In order to confirm the findings of recent numerical predictions and to obtain the experimental evidence on dynamic fracture of concrete, L-shaped concrete specimen under different loading rates is experimentally tested. The relatively simple test setup provides interesting failure mechanism of such concrete specimen at different loading rates. The results show that the response of L-specimen under dynamic load is significantly different than under quasi-static load. As expected, it is found that peak load increases with increase of displacement rate. Beyond a certain critical value of loading rate, peak load is increasing progressively. This is mainly due to the significant increase of inertia effects at high loading rates. Special attention was focused on the change of crack propagation direction. It is shown that direction of crack propagation is strongly influenced by loading rate. Under static loading there is one horizontal crack that is approximately perpendicular to the loading direction. On the contrary, with increase of loading rate the crack becomes more inclined and get closer to the loading zone. Moreover, in most cases with higher displacement rates crack branching occurs and after branching, the crack velocity drops down. This suggests that progressive increase of resistance (apparent strength) beyond certain threshold value of loading rate is due to inertia and is in not related to the true material properties of concrete. The velocity of crack propagation also depends on loading rate. In general, the crack velocities were found to be far lower than the theoretical crack velocities. Experimentally obtained maximal crack speed in concrete is reached before branching and is approximately 650 m/s, which again corresponds well to findings of other researchers.

Although the whole experimental program yields to better understanding of the concrete fracture under dynamic loading, it is limited in analyzing of the inherent material properties of

concrete under dynamic loading. On the other hand, with realistic numerical tools the influence of individual parameters can be studied through extensive parametric studies. Therefore, the numerical methods are particularly important to understand the dynamic fracture of concrete. One of the main objectives of the numerical study is to investigate whether the used relatively simple modeling approach is able to realistically predict complex phenomena related to dynamic fracture of concrete. In order to fully understand the effect of loading rate on concrete fracture as well as to gain more insight into the behaviour at the material level, some relevant parameters that are difficult to observe experimentally are studied by employing numerical model.

The numerical investigations under dynamic loading are performed by employing explicit 3D FE code (Irhan 2014) based on rate dependent microplane material model for concrete. The results from the performed tests on L-specimens under high loading rates and impact loaded notched beams experiments from literature have been used for verification and calibration of the model. The results from the L-specimen tests show that the model is able to accurately capture the influence of loading rate on structural resistance, cracking pattern as well as phenomenon of crack branching. In the example of notched beam under impact, emphasis is stress on the determination of true rate dependent material properties such as tensile strength and fracture energy at the high loading rates. Drop hammer tests show a sudden rise in the tensile strength and fracture energy as a function of loading rate beyond a certain critical value of loading rate. However, it is important to clarify and to understand the reasons for such sudden jumps in the fracture energy and resistance, which are considered as inherent material properties. Based on the numerical results and their comparison with experiments it is demonstrated that the evaluation of the fracture energy from the area under the reaction-displacement curve provides the apparent fracture energy, which consists of true fracture energy and a large inertial component. Similarly, the tensile strength is differentiated as true and apparent tensile strength. Furthermore, the numerical results show that the true fracture energy and tensile strength increase approximately linear in semi-log scale with strain rate and that approximately follow rate dependent constitutive law used in the computation. Hence, in the present work it is emphasized that to evaluate the true rate dependent material properties, such as tensile strength and fracture energy, the inertial component must be filtered out, otherwise, for higher strain rates it leads to a gross overestimation of material properties.

The results of performed numerical parametric study showed that the contact surface has a strong effect on the failure behaviour of dynamically impacted notched plain concrete beams. It is found that although beams impacted with wider contact surface fails by larger loads in contrast to smaller contact surface, the former may experience a brittle share failure mode for the same load intensity. For that reason, besides the peak load, it is also of importance to consider the actual failure mechanism. Namely, it is shown that the failure mode is significantly affected, apart with the applied dynamic impact loading, with the contact surface size and shape. Moreover, progressive increase of applied load is accompanied with the change of failure mode and branching phenomena. The structural inertia is the main reason for the differences found. This confirms that the measured applied load during impact dose not present the true material strength but structural effect.

Finally, it is shown that the numerical approach proposed in this study is able to replicate the experimental behaviour of the L-shaped specimen under high loading rate and the notched plain concrete beams under impact loads very well. Based on the comparison between numerical and experimental results it is demonstrated that the dynamic results need more carful interpretation or it may lead to wrong conclusions. It is pointed out that the progressive increase in dynamic strength and fracture energy is due to inertial effects and it should be interpreted as structural effect rather than material property.

Recommendations

A new experimental investigation on L-specimen is proposed. Investigation has shown that direction of crack propagation is strongly influenced by loading rate. The presented, relatively simple test setup, can be used as a benchmark test for verification and calibration of numerical models for complex fracture behaviour of concrete under high loading rates.

It is found that here used numerical model realistically reproduces all reported experimental observations. Hence, a wide range of numerical parametric studies can be performed as an alternative of high cost and time demanding experiments. It would be interesting to study how different factors such as concrete strength, various geometry and boundary conditions as well as various types of dynamic loads influence on the dynamic fracture response of concrete.

Only little research is available on the complete dynamic fracture of concrete at high loading rates. Hence, much more research is needed to fully understand complex phenomena related to dynamic fracture of concrete, such as rate dependent crack propagation, crack branching or progressive increase of apparent strength.

In order to gain better insight to the fracture behaviour of concrete under dynamic loading and to clarify the rate effect on dynamic material properties further experimental as well as numerical studies are recommended.

BIBLIOGRAPHY

Banthia NP. Impact resistance of concrete. PhD thesis, The University of British Columbia; 1987.

Barpi F. Impact behaviour of concrete: a computational approach. Eng Fract Mech 2004;71(15):2197-2213.

Bažant ZP, Oh BH. Crack band theory for fracture of concrete. Mater Struct RILEM 1983;93(16):155-177.

Bažant ZP, Caner FC, Adley MD, Akers SA. Fracturing rate effect and creep in microplane model for dynamics. J Engng Mech (ASCE) 2000a;126(9):962–970.

Bažant ZP, Adley MD, Carol I, Jirasek M, Akers SA, Rohani B, et al. Large-strain generalization of microplane model for concrete and application. J Engng Mech (ASCE) 2000b;126(9):971–980.

Belytschko T, Liu WK, Moran M. Nonlinear Finite Elements for Continua and Structures. John Wiley & Sons Ltd.; 2001.

Birkimer DL. Critical normal fracture strain of Portland cement concrete. PhD thesis, University of Cincinnati;1968.

Bischoff P, Perry S. Compressive behaviour of concrete at high strain rates. Mater Struct, 1991;24(6):425–450.

Bischoff P, Perry S. Impact behaviour of plain concrete loaded in uniaxial compression. J Eng Mech (ASCE) 1995;121(6):685–693.

Brara A, Camborde F, Klepaczko JR, Mariotti C. Experimental and numerical study of concrete at high strain rates in tension. Mechanics of Materials 2001;33(1):33-45.

Brara A, Klepaczko JR. Fracture energy of concrete at high loading rates in tension. Int J Impact Engng 2007;34(3):424–435.

Carpenter NJ, Taylor RL, Katona MG. Lagrange constraints for transient finite element surface contact. Int J NumerMethods Eng 1991;32(1):103–128.

CEB-FIP Model Code 2010, Chapter 5, Code-type models for concrete behaviour (Draft);2010.

Cotsovos DM, Pavlović MN. Numerical investigation of concrete subjected to compressive impact loading. Part 1: A fundamental explanation for the apparent strength gain at high loading rates. Computers and Structures 2008a;86(1-2):145-163.

Cotsovos DM, Pavlović MN. Numerical investigation of concrete subjected to compressive impact loading. Part 2: Parametric investigation of factors affecting behaviour at high loading rates. Computers and Structures 2008b;86(1-2):164-180.

Cotsovos DM, Pavlović MN. Numerical investigation of concrete subjected to high rates of uniaxial tensile loading. Int J Impact Eng 2008c; 35(5):319-335.

Cusatis G. Strain-rate effects on concrete behaviour. Int J Impact Eng 2011; 38(4):162-170.

Dilger WH, Koch R, Kowalczyk R. Ductility of plain and confined concrete under different strain rates. Detroit: ACI Special Publication;1978.

Elices M, Guinea GV, Planas J. Measurement of the fracture energy using three-point bend tests. 3. Influence of cutting the p-delta tail. Mater Struct 1992;25(6):327–334.

Elices M, Guinea GV, Planas J. On the measurement of concrete fracture energy using three-point bend tests. Mater Struct 1997;30(6):375–376.

Erdem S. Impact load-induced microstructural damage of concrete made with unconventional aggregates. PhD thesis, Department of Civil Engineering, University of Nottingham, 2012.

Guinea GV, Planas J, Elices M. Measurement of the fracture energy using three-point bend tests. 1. Influence of experimental procedures. Mater Struct 1992;25(4):212–218.

Hentz S, Daudeville L, Donze FV. Discrete element modelling of concrete submitted to dynamic loading at high strain rates. Computers and Structures. 2004;82(29-30):2509-2524.

İrhan B. High velocity impact and fragmentation of concrete: Numerical simulation. PhD thesis, Institut für Werkstoffe im Bauwesen der Universität Stuttgart, 2014.

John R, Shah SP. Mixed mode fracture of concrete subjected to impact loading. J Struct Eng 1990;116(3),585–602.

John R, Antoun T, Rajendran AM. Effect of strain rate and size on tensile strength of concrete. In: Schmidt SC, Dick RD, Forbes JW, Tasker DG, editors. Proceedings, 1991 APS topical conf on shock compression of condensed matter. Williamsburg, VA: Elsevier Science Publishers; 1992:501–4.

Karihaloo BL. Fracture Mechanics and Structural Concrete. Longman Pub Group. 1995

Krausz AS, Krausz K. Fracture kinetics of crack growth. Kluwer, Dordrecht, The Netherlands, 1988.

Larcher M. 2009. Development of discrete cracks in concrete loaded by shock waves. Int J Impact Engng 2009;36(5):700–710.

Lu YB, Li QM. About the dynamic uniaxial tensile strength of concrete-like materials. Int J Impact Engng 2011;38(4):171-180.

Löfgren I. Fibre-reinforced Concrete for Industrial Construction. PhD thesis, Department of Civil and Environmental Engineering, Structural Engineering, Chalmers University of Technology, Göteborg, Sweden, 2005.

Malvar LJ, Ross CA. Review of strain rate effects for concrete in tension. ACI Mater J 1998;95(6):735-739.

Mellinger FM, Birkimer DL. Measurement of stress and strain on cylindrical test specimens of rock and concrete under impact loading. Technical Report 4–46, US Army Corps of Engineers, Ohio River Division Laboratories, Cincinnati, Ohio; 1966.

Mihashi H, Wittmann FH. Stochastic approach to study the influence of rate of loading on strength of concrete. HERON, 1980:25(3).

Mindess S, Banthia N, Yan C. The fracture toughness of concrete under impact loading. Cem Concr Res 1987;17(2):231–241.

Mindess S. Crack velocity in concret subjected to impact loading. Can J Phys 1995;73:310-314.

Mohr O. Welche Umstände bedingen die Elastizitätsgrenze und den Bruch eines Materiales, Zeitschrift des Vereins Deutscher Ingenieure 1900;46:1524–1530.

Ožbolt J, Bažant ZP. Numerical smeared fracture analysis: nonlocal microcrack interaction approach. Int J NumerMethods Eng 1996;39:635–661.

Ožbolt J, Li YJ, Kožar I. Microplane model for concrete with relaxed kinematic constraint. Int J Solids Struct 2001a;38(16):2683–711.

Ožbolt J, Mayer U, Vocke H. Smeared fracture FE analysis of reinforced concrete structures - theory and examples. In: Special ASCE publication: Modeling of Inelastic Behaviour of RC Structures Under Seismic Loads. 2001b:234-256.

Ožbolt J, Reinhardt HW. Numerical study of mixed-mode fracture in concrete. Int J Fract, 2002;118(2):145–162.

Ožbolt J, Reinhardt HW. Rate dependent fracture of notched plain concrete beams. In: Pijaudier -Cabot, Gerard, Acker, editor. Proceedings of the 7th international conference CONCREEP-7;2005:57–62.

Ožbolt J, Rah KK, Meštrović D. Influence of loading rate on concrete cone failure. Int J Fract 2006;139:239–252.

Ožbolt J, Sharma A, Reinhardt HW. Dynamic fracture of concrete - compact tension specimen. Int J Solids Struct 2011;48(10):1534–1543.

Ožbolt J, Sharma A. Numerical simulation of reinforced concrete beams with different shear reinforcements under dynamic impact loads. Int J Impact Engng 2011;38(12):940–950.

Ožbolt J, Sharma A. Numerical simulation of dynamic fracture of concrete through uniaxial tension and L-specimen. Eng Fract Mech 2012;85:88-102.

Ožbolt J, Weerheijim J, Sharma A. Dynamic tensile resistance of concrete - split Hopkinson bar test. FraMCos-8; 2013a.

Ožbolt J, Bošnjak J, Sola E. Dynamic fracture of concrete compact tension specimen: Experimental and numerical study. Int J Solids Struct 2013b;50:4270-4278.

Ožbolt J, Sharma A, Irhan B, Sola E. Tensile behaviour of concrete under high loading rates. Int J Impact Eng 2014;69:55-68.

Pedersen RR, Simone A, Sluys LJ. Continuous-discontinuous modelling of dynamic failure of concrete using a viscoelastic viscoplastic damage model. In III European Conference on Computational Mechanics 2006:370–370.

Pedersen RR. Computational modelling of dynamic failure of cementitious materials. Phd Thesis, Delft University of Technology; 2010.

Planas J, Elices M, Guinea GV. Measurement of the fracture energy using three-point bend tests. 2. Influence of bulk energy dissipation. Mater Struct 1992;25(5):305–312.

Rabczuk T, Belytschko T. Cracking particles: a simplified mesh free method for arbitrary evolving cracks. Int J NumerMethods Eng 2004;61(13):2316–2343.

Reinhardt HW. Concrete under Impact Loading, Tensile Strength and Bond. HERON, 1982:27(3).

Rosa AL, Yu RC, Ruiz G, Saucedo L, Sousa JLAO. A loading rate dependent cohesive model for concrete fracture. Eng Fract Mech 2012;82:195–208.

Ross CA, Kuennen ST, Strickland WS. High strain rate effects on tensile strength of concrete. In: Proceedings on the interaction of non-nuclear munition with structures, Panama City Beach; 1989:302–308.

Rossi P, van Mier JGM, Toutlemonde F, Le Maou F, Boulay C. Effect of loading rate on the strength of concrete subjected to uniaxial tension. Mater Struct 1994;27(5):260–264.

Ruiz G, Zhang XX, Tarifa M, Yu RC, Camara M. Fracture energy of high-strength concrete under different loading rates. Anales de Mecánica de la Fractura 2009;26(2):513-518.

Saatci S, Vecchio FJ. Effects of Shear Mechanisms on Impact Behaviour of Reinforced Concrete Beams, ACI Structural Journal, 2009; 106(1):78-86.

Schuler H, Mayrhofer C, Thoma K. Spall experiments for the measurement of the tensile strength and fracture energy of concrete at high strain rates. Int J Impact Eng 2006;32(10):1635–1650.

Suaris W, Shah S. Properties of Concrete Subjected to Impact. J Struct Eng 1983;109(7):1727–1741.

Sukontasukkul P, Mindess S. The shear fracture of concrete under impact loading using end confined beams. Materials and Structures 2003;36:372-378.

Tarifa M, Poveda E, Yu RC, Zhang XX, Ruiz G. Effect of loading rate on high-strength concrete: Numerical simulations. FraMCos-8; 2013:953–963.

Taylor GI. Plastic strain in metals. J. Inst. Metals, 1938;62:307–324.

Travaš V. Three dimensional finite element formulation of concrete failure at high energy impact loadings. PhD Thesis, University of Rijeka; 2009.

Travaš V, Ožbolt J, Kožar I. Failure of plain concrete beam at impact load: 3D finite element analysis. Int J Fract 2009;160(1):31-41.

Vegt I, van Breugel K, Weerheijm J. Failure mechanisms of concrete under impact loading. Fracture Mechanics of Concrete and Concrete Structures, FraMCoS-6, vol. 1, Carpinteri A and Gambarova PG and Ferro G and Plizzari GA (ed.) 2007;1:579–587.

Vegt I, Weerheijm J, Breugel K. The rate dependency of concrete under tensile impact loading - fracture energy and fracture characteristics. In Proceedings of 13th ISIEMS. 2009.

Weerheijm J. Concrete under impact tensile loading and lateral compression. PhD thesis, Delft University of Technology;1992.

Weerheijm J, Van Doormaal JCAM. Tensile failure of concrete at high loading rates: new test data on strength and fracture energy from instrumented spalling tests. Int J Impact Engng 2007;34(3):609–626.

Winkler B, Hofstetter G, Niederwanger G. Experimental verification of a constitutive model for concrete cracking. Proceedings of the Institution of Mechanical Engineers, Part L: Journal of Materials Design and Applications 2001;(215):75-86.

Wittman FH. Crack formation and fracture energy of normal and high strength concrete. Sadhana 2002;27(4): 413–423.

Wriggers, P. Computational Contact Mechanics, Springer 2006.

Yu RC, Zhnag XX, Ruiz G, Tarifa M, Camara M. Evolution of the fracture process zone in high-strength concrete under different loading rates. EPJ Web of Conferences 6;2010.

Zielinski AJ, Reinhardt HW. Stress strain behaviour of concrete and mortar at high rates of tensile loading. Cem Concr Res 1982;12(3):309-319.

Zielinski AJ. Model for tensile fracture of concrete at high rates of loading. Cem Concr Res 1984;14(2):215–224.

Zielinski AJ. Concrete Structures under Impact Loading Rate Effects, Delft University of Technology, Report 5-84-14, Delft, the Netherlands, 1984.

Zhang XX, Ruiz G, Yu RC, Tarifa M. Fracture behaviour of high-strength concrete at a wide range of loading rates. Int J Impact Engng 2009;36:1204-1209.

Zhang XX, Yu RC, Ruiz G, Tarifa M, Camara MA. Effect of loading rate on crack velocities in HSC. Int J Impact Engng 2010a;37(4):359–370.

Zhang XX, Ruiz G, Yu RC. A new drop weight impact machine for studying fracture processes in structural concrete. Strain 2010b;46(3):252-257.

LIST OF FIGURES

LIST OF TABLES